Cu_2O-Based Visible-Light Photocatalysts for Degradation of Organic Pollutants

by

Qiang Zhao

Supervisor: Professor Dr Guoqing Guan

A Dissertation Presented to

the Graduate School of Science and Technology

of the Hirosaki University in partial fulfillment of the requirement

for the degree of Doctor of Philosophy in Safety Science and

Technology

HIROSAKI UNIVERSITY

2020

ABSTRACT

Nowadays, water contamination caused by organic pollutants is one of the main environmental issues. Its degradation over photocatalysts has been regarded as one of efficient and environmentally friendly methods. Among the numerous photocatalysts, Cu_2O is a p-type semiconductor with narrow band gap energy ranging from 2.0-2.2 eV, which could effectively utilize the large amount of visible light in the sunlight. Thusly, the Cu_2O based photocatalysts have been widely applied for the organic-pollutant decontamination nowadays. However, there are still many constraints on its application, such as the instability in oxidizing conditions, the rapid recombination of photo-generated holes and electrons. Therefore, further improvement of the Cu_2O photocatalytic performance is still required.

In this study, to improve the activity and stability of Cu_2O photocatalysts under visible light, a series of Cu_2O based photocatalysts were developed. Firstly, a kind of hyper-cross-linked polymer, named as KAPs-B (Knitting Aromatic compound Polymers-Benzene) with high surface area and special benzene rings structure, was loaded on Cu_2O to form a composite of KAPs-B/Cu_2O by using the precipitation method for the first time. The activities of various KAPs-B/Cu_2O composite photocatalysts with different loading amounts of KAPs-B were tested by methyl orange (MO) degradation. Comparing with the bare Cu_2O, significantly enhanced photocatalytic performances were found for the degradation of methyl orange (MO) over KAPs-B/Cu_2O under visible light. In particular, the 7% KAPs-B/Cu_2O showed the highest photocatalytic performance, by which approximately 92% of MO was decomposed within 60 min. Also, it showed an excellent reusability. It is found that the loading of KAPs-B on Cu_2O can not only effectively enhance the adsorption of organic matter on the catalyst ascribed to its high surface area and meanwhile stabilize the Cu_2O in oxidizing environments, but also enhance the separation rate of the photoinduced electron-hole pairs, leading to the photocatalytic activity and stability enhancement.

These results indicate that it is a feasible method to improve the visible light photocatalytic performance of Cu_2O by compositing with the hypercrosslinked polymer.

Secondly, in order to further improve the performance of Cu_2O based photocatalysts under visible light, a kind of Metal-Organic Framework (MOF) named UiO-66-NH_2 with high surface area, good chemical durability and the adsorption ability for visible light was combined with Cu_2O to form the UiO-66-NH_2/Cu_2O composites with Z-scheme heterojunction. UiO-66-NH_2/Cu_2O composites with different loading amounts of UiO-66-NH_2 were successfully synthesized by using a facile impregnation process. The photocatalytic performances of the composites were measured by the MO degradation. It is found that the developed UiO-66-NH_2/Cu_2O composites possessed better photocatalytic behavior than the pure Cu_2O, and the 20 wt% UiO-66-NH_2/Cu_2O photocatalyst showed the excellent photodegradation activity, by which 98.6% of MO could be decomposed within 50 minutes. In addition, it showed an excellent reusability since the severe photocorrosion issue of Cu_2O was suppressed significantly by combining with UiO-66-NH_2. The excellent photodegradation efficiency of 20 wt% UiO-66-NH_2/Cu_2O should be due to the synergistic effect between Cu_2O and UiO-66-NH_2, in which efficient interfacial charge transfer improved the separation effect of photoinduced electron-hole pairs within the Z-scheme heterojunction The active species trapping experiments indicated that the photo-generated h^+ and $\bullet O_2^-$ radicals were the major active species involved in the MO degradation under visible light.

Meanwhile, in order to further enhance the dispersity of Cu_2O based photocatalysts in the organic pollution, Cu_2O with cubic structure was studied. In addition, for practical applications, tetracycline (TC) antibiotics was used as the degradation target. In the following work, a heterostructured graphitic-carbon-nitride-nanosheets/copper(I) oxide (g-C_3N_4 nanosheets/Cu_2O) composite was successfully prepared using a facile precipitation method and used for the degradation of tetracycline (TC) antibiotics. It is found that this composite had higher photocatalytic activity than the pure Cu_2O as well as the pure g-C_3N_4 nanosheets. Especially, the 30 wt% g-C_3N_4 nanosheets/Cu_2O

composite exhibited the highest photocatalytic activity, by which 92.1% of TC was decomposed within 100 minutes and 83.3% of total organic carbon (TOC) was removed after the reaction for 120 min. In addition, it showed an excellent reusability, and the severe photocorrosion issue of Cu_2O was suppressed significantly by combining it with g-C_3N_4 nanosheets. The high photodegradation efficiency of g-C_3N_4 nanosheets/Cu_2O composite could be ascribed to the efficient interfacial charge transfer at the p-n heterojunction and synergistic effect between Cu_2O and g-C_3N_4 nanosheets, which resulted in the enhanced separation efficiency of photogenerated electron-hole pairs. In addition, the active species trapping experiments confirmed that the photo-generated h^+ and $\bullet O_2^-$ radicals were the main active species involved in the TC degradation under visible light.

All in all, in this work, Cu_2O based photocatalysts were successfully developed for photocatalytic degradation of organic pollutants and the corresponding photocatalytic mechanisms were also proposed. It is expected to give the guidance for the design, fabrication and application of Cu_2O based photocatalyst in the practical degradation processes of environmental pollutants.

ACKNOWLEDGMENTS

I am grateful to all those who have offered me tremendous encouragement and support during the course of my study.

First of all, my heartiest thanks are given to my profound and respectable academic advisor, Professor Dr. Guoqing Guan, who has offered me numerous valuable comments, insightful advice and suggestions with incomparable patience and encouraged me profoundly throughout my Ph. D program. At the same time, I'm sincerely grateful to his help in my everyday life in Japan.

I would like to thank Prof. Abuliti Abudula, Graduated School of Science and Technology, Hirosaki University, for all of his valuable advices and supports of my study.

I would like to thank Professor Dr. Akihiro Yoshida in our group for his kind suggestions and helpful discussion on the design of experiment programs and writing the paper during my Ph. D program.

I would like to thank Prof. Yong Guo, School of Chemistry and Environmental Engineering, Shanxi Datong University, China, for his helps regarding to the photocatalyst characterizations, and encouraging me during my Ph. D program.

I would like to thank all professors and staff at Institute of Regional Innovation (IRI), and at Graduated School of Science and Technology, Hirosaki University, for all of his kind advices and supports of my study.

I would like to thanks all members in our research group for their helps and supports to my research and daily life.

I would like to thanks all members in group of Professor Yong Guo group at Shanxi Datong University, China for their helps and supports to my research.

I would like to thank my loved family for their loving, understanding and great confidence in me all through these years.

Thank you all very much.

Qiang Zhao

October 15, 2020

Aomori, Japan

TABLE OF CONTENTS

LIST OF TABLES

LIST OF FIGURES

CHAPTER 1

Introduction

1.1 General Introduction

Nowadays, environmental pollution and energy crisis are two major problems for human beings. Water contamination is one of the main environmental issues. To solve this problem, photocatalytic degradation over semiconductor-based photocatalysts has been regarded as one of efficient and environmentally friendly methods [1, 2]. TiO_2 was first used for photocatalysis and achieved good results. The major disadvantage of using TiO_2 as a photocatalyst is that it is active only under UV irradiation. So, in order to effectively utilize visible light, many visible light induced semiconductors, such as Cu_2O, $BiVO_4$, Bi_2WO_6, g-C_3N_4, Ag_2CO_3, WO_3, Ag_3PO_4 and CdS have been studied and served as photocatalysts for pollutant degradation [3-10]. Among them, cuprous oxide (Cu_2O) has attracted great interest due to its abundance, low cost, environmental friendliness and safety [11]. It has been used in many fields, such as sensing [12-14], photocatalysis [15], Li-ion batteries [16], CO oxidation [17, 18] and hydrogen production [19]. As an important p-type semiconductor with a direct band gap of 2.00 eV, Cu_2O could absorb most of visible light and its theoretical photoelectric conversion efficiency can reach 18% [20, 21], so, it is a potential photocatalytic material in this field. In particular, Cu_2O, as a photocatalyst for degradation of organic pollutants, has attracted widely attention and been deeply investigated. Fig 1.1 gives a summary of Cu_2O and Cu_2O-based catalysts used for the photocatalytic degradation of organic pollutants. The detailed introductions for them are performed in the following sections.

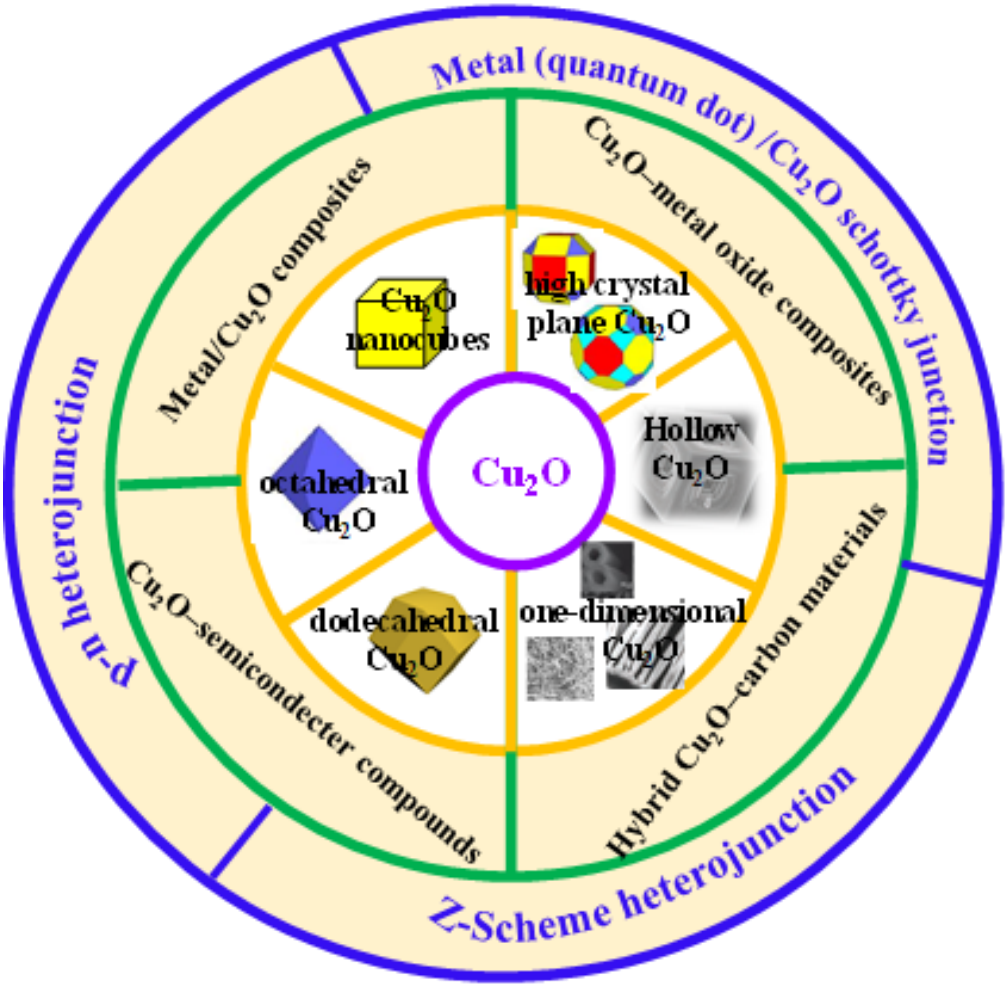

Figuer 1.1 Summary of main Cu_2O-based heterogeneous nanostructures and their mechanisms.

1.2 Cu_2O photocatalysts

In the past several years, various well-defined Cu_2O nanostructures with different shapes and sizes, such as cubes [22,23], octahedrons[24, 25], dodecahedron, star-like structures, hollow nanospheres [26], nanocages [27, 28] and nanowires [29, 30] morphologies, have been synthesized, respectively, by different methods, mainly including wet-chemistry method (liquid reduction, hydrothermal synthesis and solvothermal synthesis), electrodeposition, sputtering, and irradiation technique.

Among them, the wet-chemistry method [31-33] is most widely used to manipulate exposure facets of Cu_2O crystals because of the versatile ability in tailoring the nucleation and growth rates along different orientations. As is well known, shape, size and microstructures are the main factors that determine the chemical and physical properties of nanomaterials.

1.2.1 Cu_2O nanocrystals with regular polyhedral structures

(1) Cu_2O nanocubes

A number of studies are related to the synthesis of Cu_2O nanocubes. Murphy *et al.* have prepared highly uniform and monodisperse cubic Cu_2O nano- and microcubes by using solution-phase synthesis method. The Cu_2O nanocubes were prepared by using a solution of $CuSO_4$, cetyltrimethylammonium bromide (CTAB)surfactant, sodium ascorbate and NaOH at a reaction temperature of 55 ˚C for 15 min. The average edge length of the cubes varies from 200 to 450 nm, as a function of surfactant concentration [34]. Kim *et al.* [35] employed the polyol method to synthesize Cu_2O nanostructures. They found that the polycrystalline colloidal spheres could be prepared by simply reducing copper nitrate with ethylene glycol heated to 140 °C in the presence of poly (vinyl pyrrolidone). After introducing a small amount of sodium chloride, single-crystal nanocubes were obtained. So, they think that chloride plays a pivotal role in controlling the formation of seeds and the growth rates of various crystallographic planes to shape the Cu_2O nanostructures into nanocubes. Monodispersed Cu_2O nanocubes with five different sizes ranged from 40 to 420 nm were achieved by Huang *et al.* [36] using the seed-mediated synthesis approach. Cu_2O seed particle solution was added to a growth solution containing $CuSO_4$, sodium dodecyl sulfate (SDS) surfactant, sodium ascorbate, and NaOH to grow into larger nanocubes. The resultant particle size is very uniform, with the standard deviation of each particle size less than 10%, but the yield is not high. They also found that sodium dodecyl sulfate (SDS) surfactant and SO_4^{2-} are very

important during the preparation process. This seed-mediated method enables the sizes and shapes of nanocubes to be well controlled. Unfortunately, the yield of this method is far from industrially acceptable. Furthermore, Lee group [37] developed a facile one-step nucleation-controlled method for synthesizing uniform sized tunable cubic crystalline Cu_2O with an excellent 87.5% yield. Sodium citrate was firstly added to the Cu^{2+} solution and the Cu^{2+} ions were chelated by citrate ions to form copper-citrate, after that, NaOH was added and the precipitation of $Cu(OH)_2$ was obtained. After adding the reducing agent, the cubic crystalline Cu_2O was prepared. During this process, the Cu^{2+} ions were chelated by citrate ions to form copper-citrate, which can retard the precipitation of $Cu(OH)_2$ during the addition of NaOH. Herein, the pre-capping of Cu^{2+} markedly reduced $Cu(OH)_2$ in the initial stage, resulting in a small amount of Cu_2O seeds which led to the growth of larger sized Cu_2O nanocubes. So, the size of the nanocubes increased with the sodium citrate concentration. Prasad *et al.* [38] developed a single-step protocol to prepare Cu_2O and CuO nanocrystalline particles from the same precursor by microwave irradiation, the pH of the solution was the only variable parameter. Under pH=4.0, the cubic crystalline Cu_2O was prepared and different sizes of the Cu_2O cubes can be obtained in a certain range of pH value. Xu *et al.* [39] also prepared uniform Cu_2O nanoparticles through a facile additive-free aqueous solution route at room temperature and used for the MO degradation under visible light. The size of the nanocubes can be tuned from 20 nm to 500 nm by changing the concentration of the sodium hydroxide solution and the kinds of copper salts. This may be related to the reducing rate of the Cu(II) species, the nucleation rate and growth rate of Cu_2O seeds under different pH values. the photocatalytic experimental results indicated that these Cu_2O nanocubes had good visible-light photocatalytic properties towards MO and the smaller the particle size is, the higher the photocatalystic activity is. After irradiation for 90 min, the concentration of MO decreased to about 6% for the smaller Cu_2O nanocubes and about 22% for the bigger Cu_2O nanocubes. This is because that the size of crystal particle led to different specific surface areas of crystal, which affected the

photocatalytic activity of catalyst. Kumar *et al.* [40] synthesized hierarchically structured Cu_2O nanocubes by a facile and cost effective one-pot solution phase process and used for the methylene blue dye degradation under visible light. During the preparation, self-assembly of 5 nm Cu_2O nanocrystallites induced through reduction by glucose afforded a mesoporous 375 nm cubic architecture. Photocatalytic experiment showed that the hierarchical Cu_2O nanocubes were far more active than conventional nanocubes under visible light irradiation for MB photocatalytic degradation, which is due to the fact that the hierarchical nanocubes offered improved accessible surface active sites and enhanced optical/electronic properties. Karthikeyan *et al.* [41] prepared the well-defined Cu_2O nanocubes with tunable dimensions and physicochemical properties by a simple one-pot reaction. Crystalline Cu_2O nanocubes of between 50 to 500 nm can be obtained by reducing Cu(II) salts by ascorbic acid in the presence of PEG as a structure-directing agent. Its photocatalytic activity was evaluated by aqueous phase phenol degradation under visible light. The greater rate observed for increasing nanocube size from 50 to 500 nm led to the enhanced phenol removal from 36 to 50 % after 6 h. this study implied that despite lower surface area of Cu_2O nanocube, larger Cu_2O nanocubes still offered superior phenol mineralization.

(2) Synthesis of octahedral Cu_2O nanocrystals

The synthesis of octahedral Cu_2O nanocrystals have been also studied by many researchers. Wang *et al.* [42] prepared octahedral Cu_2O crystals with tunable edge length by reducing copper hydroxide with hydrazine without using any surfactants. Firstly, aqueous solutions of $CuCl_2$, NH_3, and NaOH were mixed to form blue $Cu(OH)_2$ precipitate, and then the N_2H_4 was added to prepare the Cu_2O nanocrystals. The experimental results showed that the molar ratios of the reagents (NH_3:Cu^{2+} and OH^-:Cu^{2+}) determined the morphology and size of the corresponding products via affecting the coordination between NH_3 and Cu^{2+} and the edge lengths of octahedra can be easily tuned from 130 to 600 nm by adjusting the molar ratio of OH^- to Cu^{2+}. Authors compared the visible-light photocatalytic properties of octahedral Cu_2O particles with

cubic Cu_2O particles for adsorption and photodegradation of methyl orange, the results demonstrated that Cu_2O octahedra with exposed {111} crystal surfaces possessed much higher activity than Cu_2O cubes. Choi *et al.* [43] prepared the octahedral Cu_2O nanocrystals by electrodeposition in two steps. The defective cubic crystal was obtained firstly by the electrodeposition and then converted into octahedral crystals by second electrodeposition of $Cu(NO_3)_2$ solution containing $(NH_4)_2SO_4$. The role of the second electrodeposition is to fill partial defects in cubic crystals and regulate the growth of {111} crystal faces. Huang *et al.* [44] synthesized cuprous oxide nanocrystals with systematic shape evolution from monodisperse truncated cubic, cuboctahedral, truncated octahedral, to octahedral nanocrystals. This can be realized directly in an aqueous solution of $CuCl_2$, sodium dodecyl sulfate (SDS) surfactant, hydroxylamine ($NH_2OH{\cdot}HCl$) reductant, and NaOH only by simply varying the volume of hydroxylamine added to the reaction mixture. They found that SDS surfactant is very important to precisely control the nanocrystal morphology and the volume of NaOH added affected the particle size. For the octahedral nanocrystals, particles with sizes of 160-460 nm were obtained. Its photocatalytic performance was evaluated by photodegradation of rhodamine B. The experimental results suggested that octahedral Cu_2O nanoparticles with entirely {111} surfaces were more effective at photocatalysis reactions than nanoparticles of other shapes containing partial {100} and {110} surfaces. Lu *et al.* [45] also found that the catalytic activities of Cu_2O were affected by the morphology of the Cu_2O crystals, for photodegradation of rhodamine B, The results showed that octahedron Cu_2O had the strongest photocatalytic activity, followed by Cu_2O cubed with truncated edges and Cu_2O hexagon octahedron. With the as-prepared Cu_2O octahedron as photocatalyst, 80% of the Rhodamine B molecules were degraded after 180 min irradiation. Apart from the size of crystal particle and the crystal morphology, the catalytic activity of Cu_2O was also related to the electrical properties of the organic dyes. Huang *et al.* [46] prepared the cubic, truncated cubic, cuboctahedral, truncated octahedral, octahedral, and short hexapod structures in an aqueous solution

with $CuCl_2$, NaOH, sodium dodecyl sulfate (SDS) surfactant, and hydroxylamine ($NH_2OH \cdot HCl$) reductant only by simply varying the volume of hydroxylamine added to the reaction mixture. For the photodegradation of negatively charged methyl orange, octahedra and the extended hexapods were catalytically active, however, the cubes with only the {100} faces were not active. Authors show that the electrically neutral {100} face cannot interact well with charged molecules and is catalytically inactive. For photodecomposing positively charged methylene blue molecules, both cubes and octahedra were not effective, octahedra and hexapods cannot be well suspended in the methylene blue solution; a significant amount of the crystals gradually moved to the surface of the solution with increasing stirring time. This is because negatively charged molecules can be more effectively adsorbed on the {111} surfaces of the Cu_2O crystals for the photodegradation of the MO. The electrically neutral {100} face cannot interact well with charged molecules and is catalytically inactive. Solutions containing positively charged molecules can repel the crystals with {111} surfaces and make a significant amount of the crystals float to the top surface of the solution. Thus, no catalytic activity was measured.

(3) Synthesis of dodecahedral Cu_2O nanocrystals

The rhombic dodecahedron represents another important Cu_2O nanocrystal morphology because facet-dependent property investigations of Cu_2O crystals can be extended to the {110} faces. Gao *et al.* [47] firstly reported the synthesis of rhombic dodecahedral microcrystals. A series of morphologically different Cu_2O single crystals can be obtained by a facile solution-based one-step reduction method in an alkaline H_2O/ethanol/oleic acid system in the presence of D-(+)-glucose. In the preparation process, oleic acid, as a face selective adsorption additive, can subtly determine the morphology of the final products. Various concentrations of oleic acid can result in a series of morphologies of Cu_2O, such as cube, octahedron, {110} truncated octahedron, and microhombic dodecahedron with {110} surfaces. Yao *et al.* [48] prepared the monocrystal dodecahedral Cu_2O with the size around 100 nm. $Cu(Ac)_2 \cdot H_2O$, n-

hexadecylamine and undecane were mixed firstly and stirred for 10 min under 90 ℃, then the temperature of this solution was increased to 200 ℃ for 15-90 min to obtain the products. They found that n-hexadecylamine used in the present work played multiple roles, as a chelating ligand to form $[Cu(NH_2C_{16}H_{33})_4]^{2+}$ complex precursor, as a phase-transferring agent to transfer divalent Cu^{2+} ions into the organic phase, as a reducing agent to generate monovalent Cu^{+} (i.e., Cu_2O), as a passivating adsorbate to control crystal morphology, and as a surface capping agent to generate self-assemblies of nanocrystals via van der Waals interaction. Huang *et al.* [49] synthesized a series of Cu_2O nanocrystals with systematic shape evolution from cubic to rhombic dodecahedral structures at room temperature by mixing an aqueous solution containing $CuCl_2$, sodium dodecyl sulfate (SDS) surfactant, NaOH, and $NH_2OH.HCl$ reductant. This particle shape evolution can be achieved by a simple adjustment of the amounts of NH_2OH and HCl introduced. The average sizes for the cubes, edge- and corner-truncated octahedra, {100}-truncated rhombic dodecahedra, and rhombic dodecahedra were approximately 200, 140, 270, and 290 nm, respectively. Its photocatalytic performance was evaluated by photodegradation of methyl orange. Results showed that the cubes were essentially inactive as observed before. However, methyl orange was almost completely photodecomposed by Cu_2O rhombic dodecahedra after 90 min of photoirradiation. Due to a high number density of surface copper atoms, the rhombic dodecahedra exposed only the {110} facets which exhibited an exceptionally good photocatalytic activity toward the photodegradation of methyl orange.

(4) Synthesis of Cu_2O with high crystal planes

Nanoparticles with high-index facets were also widely concerned because it could exhibit higher chemical activities in practical applications. Zhang *et al.* [50] successfully synthesized the perfect mixed 26-facet and 18-facet polyhedra of Cu_2O microcrystals by a hydrothermal process with use of stearic acid as a structure-directing agent. In this process, stearic acid served as both a growth directing reagent and reductant. The adsorption and photocatalytic activity of as-prepared 26-facet and 18-

facet Cu_2O polyhedra for decomposition of methyl orange were investigated and compared to those of octahedra and cubes. The results showed that the mixed 26-facet and 18-facet polyhedra with dominant {110} facets had a higher adsorption and photocatalytic activity than Cu_2O octahedra with dominant {111} surfaces and cubes with {100} surfaces. The results showed that both 26-facet and 18-facet Cu_2O polyhedra had higher adsorption and better photodegradation ability than octahedral and cubes. They pointed out that a higher surface energy and a greater density of the "Cu" dangling bonds on {110} facets of 26-facet and 18-facet polyhedra may be ascribed to its higher catalytic activity. Wang *et al.* [51] prepared unusual polyhedral 50-facet Cu_2O microcrystals with a morphological yield higher than 70% by a solution-based approach. In this preparation process, the concentration of OH^- and the volume ratio of polar organic solvent to water in the mixed solvent played crucial roles in controlling the morphology of Cu_2O microcrystals. Wang *et al.* [52] also developed a facile strategy for crystal engineering of Cu_2O polyhedrons with high-index facets in the system of $CuSO_4$/NaOH/ascorbic acid by adjusting the concentration of NaOH. A novel micron-sized Cu_2O 74-facet polyhedrons with high-index {744} and {211} facets were firstly achieved. They pointed out that the formation of a series of different forms of Cu_2O crystals should be controlled by kinetics and the final exposed crystal faces depend on the different growth rates of {100} and {111} faces.

(5) Synthesis of Cu_2O nanocrystals with special structure

Xue *et al.* [53] prepared a series of different forms of Cu_2O nanocrystals, not only including the traditional structure Cu_2O nanocrystals (cubes and rhombic dodecahedra), but also including branching structures and hopper cubes. Results showed that the special structure of Cu_2O nanocrystals can be realized by designed kinetic-control routes instead of traditional thermodynamic control. Liu *et al.* [54] reported a facile synthesis of submicrometer-to-micrometer-sized single-crystalline Cu_2O particles with cetyltrimethyl ammonium bromide (CTAB) as a capping material or template by γ-irradiation under ambient conditions. The eight-pod cubic, six-armed star-like,

octahedral, and spindle-like structures were prepared in high yield by controlling the ratio of the concentration of CTAB to that of copper ions, in this process, CTAB which serves as a nucleation and growth controller is very important. Shang *et al.* [55] proposed a recrystallization induced self-assembly (RISA) process for the construction of 3D Cu_2O superstructures. The results showed that the balancing of the hydrolysis and recrystallization rates of the CuCl precursors through precisely adjusting the experimental parameters was the key to success.

1.2.2 Synthesis of hollow Cu_2O nanostructures

Hollow nanostructures are useful because they have high surface-to-volume ratio and sufficient interior space for potential applications. Generally, there are two major approaches for preparing hollow nanostructures. The most common method involves the use of templates that serve as cores for the subsequent growth of the shells [56-58]. The cores need to be removed by dissolution, etching, or thermal treatment. The procedure is complicated. So, the template-less synthesis by self-construction was proposed by many researchers. This method is based on the ability of spherical nanocrystallites to stabilize certain crystallographic planes as they undergo two-dimensional (2D) and then 3D aggregation. Huang *et al.* [59] successfully developed a facile procedure for the synthesis of truncated rhombic dodecahedral Cu_2O nanocages and nanoframes by using an aqueous solution containing $CuCl_2$, sodium dodecyl sulfate (SDS) as a surfactant, hydroxylamine as a reductant, HCl, and NaOH. Firstly, nanoframes containing just the {110} skeleton faces were prepared by mixing the reagents, then, further crystal growth transformed the nanoframes into nanocages with the formation of the {100} faces. These nanoframes were 300-350 nm in diameter. Acidic etching by HCl via the addition of ethanol to the nanocage solution would result in the formation of another nanocages. Furthermore, by injecting precise volumes of HCl solution to a solution of presynthesized {100}-truncated and all-cornertruncated

Cu_2O rhombic dodecahedra, Huang *et al.* [60] prepared the nanoframes with etched {110} faces and hollow interior. Results suggested that etching rapidly proceeded from the surface {110} faces into the interior regions of the rhombic dodecahedra. Sui *et al.* prepared a well-defined polyhedral hollow structures (PHSs) Cu_2O with hollow interior and high geometrical symmetry by a novel *in situ* oxidative etching method at room temperature. During the preparation process, sodium citrate and glucose were used as the reducing agent. TEM images indicated that the average outer diameter of the nanoframes Cu_2O was about 700 nm with a wall thickness typically in the 60–80 nm range. It had a high degree of geometric symmetry. Hollow Cu_2O nanocubes have also been prepared by the solvothermal synthesis method. Xu *et al.* [61] prepared the single-crystalline Cu_2O hollow nanocubes via a precursor hydrolysis process in an aqueous solution at room temperature. Firstly, a mixture of $CuCl_2 \cdot 2H_2O$, NaOH, and poly(ethylene glycol) 200 (PEG-200) was heated in a Teflon-lined autoclave at 180 ˚C for 6 h, after cooling down to room temperature, the top solution was removed and water was added to this solution with stirring for 30 min. The hollow Cu_2O nanocubes with side lengths of 50-200 nm can be obtained by regulating the concentration of reactants. Results showed that the addition of NaOH and PEG was the key factor responsible for the formation of well-defined single-crystalline hollow structures.

1.2.3 Synthesis of one-dimensional Cu_2O nanocrystals

One-dimensional (1D) nanomaterials such as nanowires [62], nanotubes [63], and nanobelts [64] are highly attractive building blocks for devices because of the inherent anisotropies and efficient transport of electrons and excitons within the smallest dimension.

(1) Cu_2O nanowires

Tan *et al.* [65] developed a novel solution-based synthesis way for the production of single crystalline Cu_2O nanowires with tunable diameter and morphology. Firstly,

0.20 g of $Cu(Ac)_2$ was dissolved in 40 mL of deionized water. 8 mL of an aqueous solution of o-anisidine was added to this solution, dark green solution due to the coordination of Cu^{2+} and *o*-anisidine pyrrole was obtained. Then, the reaction mixture was transferred to a 50 mL autoclave and sealed. The temperature was maintained at 140-180 °C for 5~10 h and subsequently cooled down to room temperature naturally, and finally the Cu_2O nanowires were obtained. The diameter and morphology of Cu_2O nanowires can be easily tuned by the choice of reductant type and synthetic temperature. Wang *et al.* [66] developed a novel reduction route for preparing Cu_2O nanowires in the presence of a suitable surfactant, polyethylene glycol (PEG; Mw 20 000), at room temperature. PEG and $CuCl_2 \cdot 2H_2O$ were firstly dissolved in H_2O, stirring with a magnetic stirrer until dissolved completely, then, NaOH was added into the above solution dropwisely under stirring. A blue precipitate of $Cu(OH)_2$ was obtained. After stirring for 15 min, $N_2H_4 \cdot H_2O$ solution was added. Since N_2H_4 in aqueous solution is a strong reducing agent, the $Cu(OH)_2$ precipitate was gradually reduced into the Cu_2O nanowires with red color. The nanowires obtained by this method are relatively straight and long, resulting in a very large aspect ratio. TEM images showed that the diameters of the Cu_2O nanowires were about 8 nm with the lengths ranged from 10 to 20 μm. Ren *et al.* [67] obtained the porous Cu_2O nanowires from the ordered mesoporous Cu/Cu_2O in ethanol though sinking it for 1 mouth, the diameter of Cu_2O nanowires obtained were 50-100 nm with a length of 5–10 mm.

(2) Cu_2O Nanotubes

Compared with Cu_2O nanowires, there are relatively few reports on Cu_2O nanotubes. In 2003, the synthesis of Cu_2O nanotubes was firstly reported by Cao *et al.* [68] in the presence of a structure-directing surfactant CTAB at room temperature, Cu_2O nanotubes/nanorods were obtained by reducing $Cu(OH)_4^{2-}$ with weak reductant glucose. Jin *et al.* [69] prepared Cu_2O nanowires and nanotubes in aqueous solution by reducing Cu^{2+} to Cu^{+} with glucose or fructose via Fehling's reaction. Results showed that Cu_2O nanotubes was firstly formed at the beginning of crystal growth, however,

with prolonged growth time, the initially hollow NTs could be filled in to become solid NWs. Unlike previous studies, no any surfactant was added in this process, so, another growth mechanism of one-dimensional nanomaterials was confirmed. By imaging the dislocation contrast, the eshelby twist associated with dislocations and the spontaneously formed hollow nanotubes, the screw dislocation-driven growth of Cu_2O nanowires and nanotubes was proposed. Zhong *et al.* [70] prepared the single-crystalline hexagonal Cu_2O nanotube arrays using a two-step solution approach, including the electrodeposition of oriented Cu_2O nanorods and a subsequent dissolution technique to form a tubular structure under the role of NH_4Cl. Soluble $[Cu(NH_3)_4]^{2+}$ was formed from the NH_4Cl and Cu_2O, resulting the dissolution of Cu_2O. In addition, Cl^- ions in solution will also lead to the formation of $CuCl_4^{2-}$ ions in a deposition solution and they will be adsorbed on the surface of Cu_2O nanorods. Because of electrostatic, these adsorbed Cl^- and $CuCl_4^{2-}$ ions provide the electrons to Cu^+ in Cu_2O, and enhance the Cu-O bond. The chemical effect by the specific adsorption of Cl^- and $CuCl_4^{2-}$ ions will lead to the dissolution rate of Cu_2O on the surface of nanorods being much slower than that in the nanorod inner section. So, the selective dissolution affects the center part of the Cu_2O nanorod preferentially along the c axis, leaving the lateral faces and resulting in a tubular structure.

(3) Cu_2O Nanorods

The preparation of Cu_2O nanorods has only been reported in recent years. Guan *et al.* [71] prepared a novel comb-like cuprous oxide nanorod-based structures by an interface etching method with salicylaldehyde as ligand and reducing agent in a water–toluene system. Salicylaldehyde and Cu^{2+} can form a complex compound at the interface of the water/oil, under the solvothermal conditions, the complexes were etched and reduced to cuprous oxide with the special comb-like nanorod-based structure. Musselman *et al.* [72] firstly developed a general technique for producing large-area, free-standing, size-controlled nanorod arrays on conducting substrates by electrodeposition into high-quality anodic alumina templates. Ju *et al.* [73] also

prepared the Cu_2O nanorod on anodic aluminum oxide (AAO) templates under alkaline conditions via electrochemical deposition. The growth rate of Cu_2O nanorods at room temperature reached 360 nm/min. Results showed that Cu_2O nanotubes were in the transition state during the process, that is, Cu_2O nanotubes were firstly formed under constant current, and then Cu_2O nanorods were obtained by filling it. Haynes *et al.* [74] prepared the Cu_2O nanorod arrays via a novel templated electrodeposition process. Firstly, ZnO nanorod films which served as sacrificial templates was firstly formed on the transparent conductive oxide substrates, then ZnO nanorod surface was coated by nitrocellulose and gaps between arrays of nanorods was filling with poly(lactic acid) served as an amorphous pore-filling material. After that, Cu_2O nanorod arrays were obtained by etching process to remove the ZnO and electrodeposition of Cu_2O.

In conclusion, as a promising photocatalyst for degradation of organic pollutants, the physical and chemical properties of Cu_2O were obviously different with different morphology, size and structure. In addition, the catalytic activity of Cu_2O was also related to the electrical properties of the organic dyes. Most studies on photocatalytic degradation of organic pollutants by Cu_2O mainly focus on the application of nanocrystalline with complete crystal face, the research of one-dimensional Cu_2O degradation of organic pollutants is rather little, its photocatalytic properties need to be further studied. Although, with the development of research methods and theories, the morphology, structure, particle size of Cu_2O can be adjusted and controlled at the micro level and has made a great progress. However, the narrow band gap of Cu_2O leads to the rapid recombination of the photogenerated electrons and holes and the photocatalytic activity of Cu_2O is very limit [75]. In addition, Cu_2O has a poor stability in aqueous solution under light irradiation [76], which can easily be oxidized to CuO because of the lower VBM of Cu_2O than the oxidation potential to CuO [77, 78], thereby restricting its photocatalytic efficiency.

1.3 Hybrid Cu_2O-based heterogeneous photocatalysts

To further improve the photocatalytic performance of Cu_2O, coupling it with other semiconductors is regarded as an effective approach to overcome this drawback. It has been reported that Cu_2O can hybrid with some wide-band gap semiconductors and the forming nanocomposites have excellent full-use of sunlight and abundant reactive sites, thus enhance the photocatalytic efficiency of Cu_2O [79, 80]. On the other hand, the hybridization with narrowband materials can effectively suppress recombination of light-induced charge carriers, which contributes to the superior photocatalytic performance of Cu_2O [81, 82]. To date, with the rapid advancements in nanomaterial science and nanotechnology, hybrid Cu_2O-based heterogeneous nanostructures with well-controlled compositions, shapes and sizes have been rationally designed and synthesized, which could bring unexpected property for improving the potential application of Cu_2O.

1.3.1 Metal/Cu_2O composites

It is well known that the photocatalytic efficiency of the Cu_2O semiconductor can be obviously improved by combing with the metal due to the formation of a Schottky barrier at the metal–semiconductor interface which can effectively prevent the recombination of the photo-holes during a photocatalytic process [83]. So, hybrid metal/Cu_2O nanostructures have been extensively investigated.

(1) Cu/Cu_2O composites

Copper is an important metal because of its high electrical and thermal conductivities [84, 85]. Considering the potential applications of copper-based materials, architecture of Cu and Cu_2O has been achieved by using various routes, such as the sol-gel technique, micelles or emulsion method, hydrothermal synthesis, pyrolysis, chemical vapor deposition, etc. [86-88]. Sun *et al.* [89] used a simple solution-phase reduction route for the synthesis of facet-selective growth of low-cost

metal Cu nanoparticles on {111} facets of polyhedral 26-facet Cu_2O architectures and used for the photodegradation of MO. Results showed that the novel Cu–Cu_2O heterogeneous architectures had better adsorption and photodegradation of MO than those of the pure Cu_2O. The density functional theory (DFT) calculations show that the (111) surface of Cu_2O is much more facile to be reduced than the (110) and (100) surfaces, finally leading to the selective growth of Cu nanoparticles on Cu_2O (111) surfaces. The superior photocatalytic performance can be attributed to the introduction of Cu nanoparticles, which exhibited higher adsorption ability and photocatalytic activity for enhancing the degradation of MO dye under the UV light. Chen *et al.* [90] prepared the core–shell heterostructured Cu/Cu_2O nanowires (NWs) using a novel oxidation/reduction process. The core–shell structured Cu/Cu_2O NWs demonstrated superior photocatalytic activity over other counterpart nanostructures in the MB photodegradation under visible-light irradiation. After 120 min irradiation, only 7.9% of the initial dye remained in the solution for Cu/Cu_2O NWs, while nearly 23% and 40% of the initial dye remained after the same period for Cu/Cu_2O NPs and Cu_2O NCs, respectively. In contrast, 90.6% of MB was not degraded after 120 min for CuO NCs. The efficient charge separation induced by the special core–shell heterostructure and the advanced three-dimensional spatial configuration is proposed to be responsible for the superior visible-light activity of Cu/Cu_2O NWs. Ai *et al.* [91] prepared the core-shell Cu@Cu_2O microspheres with an interfacial hydrothermal method. During the preparation process, pure Cu microspheres were firstly formed through the reduction of copper (II) acetylacetonate. Surface Cu was then oxidatively transformed to a Cu_2O shell, resulting in the Cu@Cu_2O core-shell structure. For the degradation of gaseous nitrogen monoxide under visible light irradiation, the as-prepared Cu@Cu_2O core-shell microspheres exhibited enhanced photocatalytic activity as compared to Cu_2O. They pointed out that this enhanced photocatalytic activity could be attributed to the core-shell structure of Cu@Cu_2O, which could favor charge transfer and inhibit recombination of photogenerated hole-electron pairs.

(2) Ag/Cu_2O composites

In order to effectively utilize sunlight, noble plasmonic nanostructured metals, such as Au, Ag, and Pt, are deposited on the surface of semiconductors. The metals act as electron traps that introduce efficient interfacial charge separation in the composites, leading to a drastic improvement in photocatalytic activity over an extended wavelength range [92-95]. Zhang *et al.* [96] prepared the Cu_2O/Ag composite nanospheres (CNSs) based on a one-pot room temperature method. During the preparation process, $AgNO_3$ solution was added to the fresh Cu_2O nanosphere-produced mother solution in various ratios, Ag^+ ions can be reduced by the fresh Cu_2O nanospheres in the acidic solution, and Ag nanoparticles can be directly deposited on the surface of Cu_2O nanospheres. The content of Ag on the Cu_2O nanospheres can be tuned by controlling the volume of $AgNO_3$ solution. The photocatalytic activities of Cu_2O/Ag CNSs and pure Cu_2O were studied by MO photodegradation under visible light. It is found that the obtained Cu_2O/Ag NCSs had superior photocatalytic activity than Cu_2O and Ag nanoparticles enhanced light absorption and electron sink effect. Lee *et al.* [97] synthesized the Ag-Cu_2O core-shell nanoparticles using a very simple co-reduction process and studied the shell thickness of the nanoparticles on its photocatalytic activity and stability. The photocatalytic performance was tested by using MO degradation. It is found that with increasing shell thickness, the activity and the stability were simultaneously improved. The Ag-Cu_2O core-shell nanoparticles showed much broader absorption range of the UV–vis spectrum compared to that of pure Cu_2O. The enhanced activity can be attributed to the high surface area of the bumpy structure and the plasmonic charge transfer from the Ag core. Xiong *et al.* [98] prepared one-dimensional (1D) plasmonic Ag@Cu_2O core-shell hetero-nanowires at room temperature, and found that the resultant 1D Ag@Cu_2O NWs exhibited much higher photocatalytic activity towards degradation of organic contaminants than Ag@Cu_2O core-shell nanoparticles or pure Cu_2O nanospheres under solar light irradiation. The enhancement in photocatalytic activity could be attributed to the surface plasmon resonance and the electron sink effect

of the Ag nanowire core, and the unique 1D core−shell nanostructure. Hu *et al.* [99] prepared Cu_2O coated Au/Ag nanorods (NRs) using a facile wet chemistry method. They pointed out that the transverse plasmon modes of Au/Ag/Cu_2O NR can split into a dipole and an octupole plasmon modes. The core aspect ratio and shell thickness could be used to regulate these two modes for extending the spectral overlap of plasmon resonance and Cu_2O band edge. The photocatalytic activity of the prepared Au/Ag/Cu_2O NRs with different Cu_2O thicknesses was evaluated by MO degradation under visible light (400-750 nm) irradiation. Au/Ag/Cu_2O NRs showed enhanced photocatalytic activity compared to spherical Ag/Cu_2O nanoparticles. In addition, the photocatalytic activity of Au/Ag/Cu_2O NRs was highly dependent on the shell thickness, the optimal thickness of Cu_2O shell is around 20 nm. The enhancement mechanism was ascribed to both dipole and octupole plasmon modes boosting electron-hole separation in Cu_2O via plasmon-induced resonant energy transfer (PIRET) as confirmed by transient absorption measurements. Sharma *et al.* [100] prepared the ternary Ag-Cu_2O/rGO NCs at room temperature by a green and facile route, which is inexpensive, easy to prepare, enabling efficient light harvesting under ambient conditions. Under visible light, the Cu_2O produced photogenerated electrons in the conduction band (CB) and are transferred to Ag and rGO. In Ag-Cu_2O/rGO NCs, the functionalization of reduced sheets significantly alters the Fermi level of rGO which may lead to the enhanced electron injection rate from Cu_2O to rGO, resulting enhanced stability and superior photocatalytic efficiency, compared with that of Cu_2O/rGO and Cu_2O NCs. Wei *et al.* [101] prepared a ternary reduced graphene oxide wrapped octahedral Ag-Cu_2O (Ag-Cu_2O/rGO) photocatalyst by a facile one-pot water bath method. In the composite, Cu_2O octahedral was decorated with the dense Ag nanoparticles and were wrapped with thin rGO nanosheets. For photodegradations of phenol in water under visible light, the ternary Ag-Cu_2O/rGO photocatalyst exhibited much higher activity than pure Cu_2O or binary Cu_2O/rGO or Ag-Cu_2O. This is because that the surrounding of rGO nanosheets prevented the coarsening of Ag nanoparticles and improved the

stability of the octahedral Ag-Cu_2O structure.

(3) Au/Cu_2O composites

As one typical combination of metal and oxide semiconductors, Au@Cu_2O has attracted many attentions for its novel structure and potential applications in many aspects. Liu *et al.* [102] demonstrated that the selective growth of Au nanoparticles on (111) surfaces of truncated octahedral and cuboctahedral Cu_2O crystals can also be achieved. The density and size of Au nanoparticles in the Au/Cu_2O can be controlled by tuning the concentration of the gold precursor. It is found that at lower concentration of $HAuCl_4$, a great number of Au nanoparticles were formed on (111) surfaces of the Cu_2O crystals, but almost none of the Au were formed on (100) surfaces, the Au/Cu_2O core/shell heterostructures can be obtained when the concentration of $HAuCl_4$ was increased. Truncated octahedral Cu_2O-Au nanocomposites have a 10 times higher electrochemically catalytic activity than pure Cu_2O crystals for H_2O_2 reduction. The enhanced catalysis was mainly due to the polarization of Au NPs at the interface, which makes Cu_2O more active for H_2O_2 reduction. Zhu *et al.* [103] developed a strategy of surface-free-energy-distribution induced selective growth of Au nanograins (AuNGs) on specific positions of Cu_2O octahedron surfaces with a series of morphological evolutions. The evaluation of the samples for photocatalytic degradation of MO aqueous solution was performed at room temperature. Photocatalytic degradation experiment showed that Cu_2O–Au heterostructures enhanced the photocatalytic activity and the photo-induced charge separation than the pure semiconductor nanocrystals, leading to enhanced photocatalytic activity. Mahmoud *et al.* [104] prepared Cu_2O–Au nanoframes with different nanolayer thicknesses of Cu_2O and used for the dye degradation. It is found that the hole concentration increased during the activity measurements experiment than Cu_2O and therefore enhancing the dye degradation rate. The plasmonic Au@Cu_2O core/shell heterostructures could bring many advantages, such as effectively protecting the metal nanoparticles from corrosion, maximizing the metal−support interaction through the three-dimensional contact between the metal

core and the semiconductor shell, controlling the center wavelength of the localized surface plasmon resonance. Wang *et al.* [105] prepared the Au–Cu_2O core–shell heterostructures and investigated the effects of polyhedral gold nanocrystal morphology and facets on its formation. Core–shell cubes, face-raised cubes, core–shell octahedra, and face-raised octahedra were obtained by changing the volume of reductant added and were examined for their comparative photocatalytic activity toward the MO photodegradation. It is found that all the cubes were photocatalytically inactive because they were bounded by essentially {100} facets. Face-raised octahedra with more {111} facets showed significantly better photocatalytic performance than the regular Au–Cu_2O core–shell octahedra.

(4) Pd /Cu_2O composites

Pd /Cu_2O nanostructure was also studied by the researchers. Miller *et al.* [106] prepared the Pd /Cu_2O nanostructures via a hydrothermal approach and used for the degradation of polybrominated diphenylethers under visible light. The obtained Pd /Cu_2O demonstrated effective debromination of 2, 2′, 4, 4′-tetrabromodiphenyl ether (BDE-47), one of the polybrominated diphenyl ethers (PBDEs) of greatest environmental concern, under visible light irradiation, approximately 70% of the BDE-47 was debrominated by the Pd /Cu_2O photocatalyst to lower-brominated congeners within the first 10 h of the reaction. This is the first reported case of a non-titania-based metal oxide semiconductor to be used in the photocatalytic degradation of PBDEs. By incorporating Pd nanoparticles on the surface of the Cu_2O, Pd /Cu_2O is able to activate the generated hydrogen to accomplish the reductive hydrodehalogenation of the PBDE.

(5) Zn/Cu_2O composites

Zn-doping not only affects the morphology of Cu_2O crystal, but also significantly influences its photoelectric properties. Zhang *et al.* [107] prepared the Zn-doped Cu_2O with hollow microcube morphology by *in situ* photochemical method with $CuWO_4$ as the precursor. Experimental results showed that the photocatalytic activity was significantly enhanced with an apparent quantum yield of 38.95% when 0.1 wt% Zn

was doped into the Cu_2O. Yu *et al.* [108] prepared the Zn-doped Cu_2O particles by a solvothermal method and used for the photocatalytic degradation of ciprofloxacin, and found that the photocatalytic performance of Cu_2O can be effectively improved by Zn doping. The prepared Zn-doped Cu_2O particles had the preferred orientation of the (1 1 1) crystal planes which can shorten the time for photogenerated carriers to reach the surface, leading to more efficient transport and separation of the photogenerated electrons and holes. In addition, Zn doping can enhance the band gap of Cu_2O, increasing transmission and separation efficiency of the charges.

1.3.2 Cu_2O-metal oxide composites

The electrons of Cu_2O easily undergo excitation by visible light and thus get involved in the processes of degradation of dyes in wastewater. However, the easy recombination of photo-generated electrons and holes could affect its photocatalytic activity. Cu_2O combined with other metal oxides have become an effective means to overcome the above weakness of recombination of photo-generated electrons and holes.

(1) Cu_2O-ZnO composites

Zinc oxide, ZnO, has been recognized as a preferred photocatalyst because of its low cost, high photocatalytic activity and non-toxic nature. However, ZnO can only work in the ultraviolet region of the electromagnetic spectrum because of its wide band gap of 3.2 eV. The Cu_2O, as a p-type semiconductor with a narrow band gap of 2.0 eV, and ZnO, as one of the n-type semiconductors, have a particularly relative position of the energy band, of which the CB of Cu_2O is a little higher than that of ZnO and the VB of ZnO is lower than that of Cu_2O. So, this might promise that the p-n Cu_2O-ZnO heterojunction has valuable applications in photocatalytic field. Ma *et al.* [109] prepared the Cu_2O/ZnO nanocomposites by a coprecipitation method and applied to degrade dye wastewater. It is found that under the optimum conditions, nearly 80% decolorization efficiency of Orange II was achieved by Cu_2O/ZnO nanocomposites

within 2 h of reaction time and this efficiency was much higher than that of either pure Cu_2O or ZnO. When p-type Cu_2O was loaded on n-type ZnO semiconductor's surface, The p–n semiconductor was formed, The conduction band position of ZnO is 0.5 eV lower than that of Cu_2O [110], so the generated electrons in Cu_2O can be transferred to ZnO which makes it possible to separate the electrons/holes in Cu_2O and avoid recombination, thus enhanced photocatalytic activity. Deo *et al.* [111] prepared Cu_2O/ZnO hetero-nanobrush assembly by growing the ZnO nanorods hierarchically on Cu_2O nanoneedles. The photocatalytic activity of Cu_2O nanoneedles and Cu_2O/ZnO hetero-nanobrushes were tested by degradation of methyl orange (MO) dye. As compared to Cu_2O nanoneedles, the photocatalytic properties were enhanced significantly, because of the multiple p–n junctions formed at p-Cu_2O/n-ZnO interfaces and quasi-1-D structures of both the materials, resulting effectively charge separation and transport. After 2 hours, the amount of MO remaining in the case of Cu_2O nanoneedles was around 70% while that in the case of Cu_2O/ZnO nanobrush was only around 7%. Zou *a* [112] prepared the vertically aligned Cu_2O/ZnO hetero-nanorod arrays on indium-doped tin oxide (ITO) glass substrates by a two-step method, namely a hydrothermal method followed by an electrodeposition process. The adsorption and photocatalytic degradation of MO were tested by MO degradation. It is found that under visible light irradiation, the pure ZnO nanorod arrays exhibited a very weak ability for decolorization of MO and the Cu_2O film exhibited an effective ability for decolorization of MO, but the photocatalytic activity was still lower than the Cu_2O/ZnO hetero-nanorod arrays prepared with a Cu_2O electrodeposition time of 20 min which have the highest photocatalytic activity, and the MO concentration can be reduced to around 10% in 5 h. The enhanced photocatalytic activity is attributed to better light scattering for the Cu_2O/ZnO hetero-nanorod array structure and fast charge separation and transport within the heterojunctions of the Cu_2O/ZnO. Kandjani *et al.* [113] also prepared the p-type Cu_2O/n-type ZnO core/shell photo-catalysts, in which monodispersed Cu_2O nanocubes functioned as the core, ZnO nanoparticles having varying morphologies

were coated as the shells. It is found that that the photocatalytic efficiency of the produced core/shell nanoparticles depended not only on the formation of the p/n junction between ZnO and Cu_2O nanoparticles but also on controlling the coverage and morphology of the shell formation. Wu *et al.* [114] prepared the sparse ZnO nanostructures on the surfaces of Cu_2O cubes, octahedra, and rhombic dodecahedra for the examination of their photocatalytic activities to demonstrate the large facet effects on interfacial charge transfer, and found that using pure Cu_2O crystals without surface CuO, ZnO-deposited Cu_2O rhombic dodecahedra showed an enhanced catalytic activity as expected, while ZnO-deposited Cu_2O cubes remained inactive toward photodegradation reaction to illustrate large facet effects on photocatalysis. In addition, photocatalytically active Cu_2O octahedra became totally inactive after ZnO nanostructure deposition, preferential growth of the (101) planes of ZnO over the {111} faces of Cu_2O is believed to cause this abrupt decline in catalytic activity, so, facet-dependent band alignment needs to be taken into account in any design involving charge transport into and out of a semiconductor crystal to maximize its efficiency. Ren *et al*. [115] synthesized the sandwiched ZnO@Ag@Cu_2O nanorod films by successive electrodeposition, magnetron sputtering and the second electrodeposition. Herein, Ag NPs in the composites played the distinct role. Under the visible-light irradiation, active e^--h^+ pairs are generated in the Cu_2O via resonant energy transfer from the plasmon dipole of Ag NPs and are rapidly separated at the ZnO/Cu_2O interface. In addition, the formed Schottky junction (e.g., Ag/ZnO and Ag/Cu_2O) can inhibit the recombination of the photogenerated carriers in ZnO and Cu_2O. So, the sandwiched ZnO@Ag@Cu_2O photocatalysts presented a highly efficient photocatalytic performance in the degradation of the MO solution.

(2) Cu_2O-TiO_2 composites

Titanium dioxide (TiO_2) is a typical n-type semiconductor with excellent photo- and chemical stability, strong oxidizing activity, corrosion resistance and nontoxicity. Unfortunately, the common phases of TiO_2 have wide band gaps, which cannot be

activated effectively under visible light radiation, and the photogenerated electron–hole pairs easily recombine [116]. Both the conduction and the valence bands of Cu_2O are located above those of TiO_2 [117]. Thus, when TiO_2 is coupling with Cu_2O, the photogenerated electrons transfer from the conduction band of Cu_2O to that of TiO_2 to form Ti^{3+} center, which prolongs the lifetime of photogenerated carriers. The merit of the Cu_2O–TiO_2 heterostructures can benefit from the attractive band gap of Cu_2O as well as from the high stability of TiO_2 in aqueous solutions. Huang *et al.* [118] prepared the Cu_2O/TiO_2 nano–nano heterostructures with different concentrations of Cu_2O by an alcohol-aqueous based chemical precipitation method and its photocatalytic efficiency of the Cu_2O/TiO_2 heterostructures was evaluated by degradation of acid Orange II in water under UV–vis light and visible light irradiation. The results showed that the Cu_2O/TiO_2 nano–nano heterostructures had dramatically improved photocatalytic activity comparing with pure TiO_2. The enhanced activity is attributed to the improved optical absorption and the nano–nano heterostructure which favors the separation of photo-introduced electrons/holes pairs in Cu_2O/TiO_2 heterostructures. Wang *et al.* [119] obtained the Cu_2O/TiO_2 p–n heterojunction photoelectrodes by depositing p-type Cu_2O nanoparticles on n-type TiO_2 nanotube arrays via an ultrasonication-assisted sequential chemical bath deposition. It is found that Cu_2O/TiO_2 composite photoelectrodes possessed enhanced absorption in the visible light region and superior photoelectrocatalytic activity and stability in the degradation of Rhodamine B. The largely improved separation of photogenerated electrons and holes in Cu_2O/TiO_2 composite was revealed by photocurrent measurements. The creation of photocatalysts with controlled facets has become an important approach to enhance their activity. Liu *et al.* [120] prepared the $Cu_2O@TiO_2$ core-shell structures by a facile hydrothermal process to coat anatase TiO_2 shell onto three types of Cu_2O crystal cores, namely Cu_2O cubes with exposed {100} facets, Cu_2O cuboctahedra with exposed {100} and {111} facets, and Cu_2O octahedra with exposed {111} facets, respectively. Their photocatalytic activities were tested by the degradation of methylene blue (MB) and 4-

nitrophenol (4-NP) under visible light illumination. Results show that under visible light illumination, Cu_2O@TiO_2 octahedra demonstrated the best photocatalytic performance on MB and 4-NP degradations due to their highest conduction band offset, followed by Cu_2O@TiO_2 cuboctahedra and Cu_2O@TiO_2 cubes. So, the dedicate examination and control of the band alignments formed on exposed facets are critical for the design of composite photocatalysts with heterojunctions formed on exposed facets. Liu *et al.* [121] prepared the ultra-small Cu_2O nanoparticles loaded on TiO_2 nanosheets with {001} facets exposed through a one-pot hydrothermal reaction and used for the degradation of phenol under visible light. The loading of ultra-small Cu_2O nanoparticles on TiO_2 nanosheets led to the formation of heterojunctions which favored the efficient separation of photo-generated electrons and holes, resulting the enhanced photoactivity. Yang *et al.* [122] Cu_2O/TiO_2 prepared the p-n heterojunction network catalyst and used for degradation of p-Nitrophenol under artificial solar light, the network is composed of p-type Cu_2O nanowires on the top surface and Cu_2O nanoparticles on the inner walls of the n-type TiO_2 NT arrays. It is found that The Cu_2O/TiO_2 network had higher degradation rate than the unmodified TiO_2 NTs. The enhanced photocatalytic activity can be attributed to the extended absorption in the visible resulting from the Cu_2O nanowire networks and the effective separation of photogenerated carriers driven by the photoinduced potential difference generated at the Cu_2O/TiO_2 p-n junction interface. Fu *et al.* [123] introduced a dual Z-scheme TiO_2-Ag-Cu_2O photocatalytic system, in which Cu_2O was loaded onto electrospun TiO_2 nanotubes by a facile impregnation calcination method, and Ag was subsequently deposited onto the photocatalyst through a photodeposition method. Under UV-vis light, both TiO_2 and Cu_2O can be excited. The photogenerated electrons in the CB of TiO_2 will transfer to Ag due to the formation of Schottky barrier on the metal-semiconductor interface. Meanwhile, the SPR-induced local electric field will drive the electrons of Ag to combine with the holes on the VB of Cu_2O. So, a dual Z-scheme charge transfer pathway for photocatalytic reactions over TiO_2-Ag-Cu_2O composite was developed,

both resulting in high separation efficiency and high redox ability of photogenerated electrons and holes.

(3) CuO-Cu_2O composites

CuO is a p-type semiconductor with a narrow band gap of 1.3-1.6 eV [124]. Its conduction band and valence band are lower than the corresponding bands of Cu_2O. Jiang *et al.* [125] reported controllable preparation of CuO/Cu_2O heterogeneous by a facile wet chemical method and the different morphologies of CuO, i.e. nanowires (NW), tetrahedra (TH), and nanospheres (NS), have been controllably prepared on Cu_2O cubes/octahedra. The photocatalytic activity and stability of the as-obtained CuO/Cu_2O heterogeneous were tested by photocatalytic degradation of methyl orange (MO) as a model reaction, and found that all the obtained CuO/Cu_2O HCs had significantly improved photocatalytic activity and stability as compared to Cu_2O. Especially, the nanowires CuO/Cu_2O exhibited a specific reaction rate ca. 1.6 μmol min^{-1} g^{-1}, which is 260 times as high as pristine Cu_2O. The reasons for photocatalytic activity enhancements are mainly the result of formation of a type II band structure favoring charge separation and transfer. Yu *et al.* [126] prepared the CuO/Cu_2O composite hollow microspheres by using template-free hydrothermal synthesis method, and found that the synthesized CuO/Cu_2O composite hollow microspheres exhibited higher photocatalytic activity for the photocatalytic decolorization of methyl orange under visible-light illumination than the single phase CuO or Cu_2O samples. [127]. Based on energy band theory, CuO and Cu_2O also can form heterostructures which facilitates charge separation, and thereby improving photocatalytic activity. Liu *et al.* [128] prepared the CuO/Cu_2O hollow microsphere composites with tunable composition and morphology by a facile hydrothermal method and used as highly efficient photocatalysts towards the degradation of methyl orange under visible light irradiation. By changing the amount of soft template Pluronic P123, pH value of the precursor solution, hydrothermal temperature and time, the product was correspondingly transformed from CuO/Cu_2O composite, to Cu_2O and Cu/Cu_2O

composite with tunable morphologies such as bulky particles, polyhedrons, solid and hollow microspheres, etc. Compared with other structures, the CuO/Cu_2O composite hollow microspheres displayed the best visible light photocatalytic activity of 92.2% within 300 min toward the degradation of MO, which can be attributed to their excellent light harvesting capability, unique hollow structure and improved photogenerated charge carrier separation within CuO/Cu_2O heterostructure. Chen *et al.* [129] also prepared the CuO/Cu_2O heterostructured composite hollow microspheres by using a facile soft template assisted hydrothermal method. For methyl orange degradation under visible-light, the CuO/Cu_2O displayed high visible-light photocatalytic activity and reproducibility than the pure Cu_2O, which is due to its high adsorption capacity, enhanced light scattering effects, high throughput hollow reaction regions within the hollow structures and decreased recombination of photogenerated electrons and holes. Yurddaskal *et al.* [130] prepared Cu_2O/CuO structures by thermal oxidation of electroplated copper (Cu) coatings on titanium substrates and its photocatalytic activities were examined by the degradation of methylene blue (MB) under UV light irradiation. The results showed that the microstructure and surface morphology of the samples changed considerably at different annealing temperatures and the sample annealed at 500°C exhibited the highest photocatalytic activity. The needle-like CuO structures on the surface of photocatalyst could increase the interfacial charge transfer and inhibit the recombination of electron–hole pairs. The construction of Z-scheme photocatalyst has been verified to be an effective route to develop high-efficiency visible-light composite photocatalysts. Wang *et al.* [131] designed a highly efficient Z-scheme Cu_2O-rGO-CuO composite photocatalyst by a facile two-step method, including the initial grafting of rGO on the Cu_2O surface and then *in situ* deposition of CuO nanoparticles on the Cu_2O-rGO surface. It was found that all as-prepared Cu_2O-rGO-CuO photocatalysts showed a much higher photocatalytic activity than the Cu_2O, Cu_2O-rGO and Cu_2O-CuO, and the Cu_2O-rGO-CuO (0.5 wt%) showed the highest performance. The enhanced photocatalytic activity can be ascribed the efficient electron

transfer in Cu_2O-rGO-CuO Z-scheme system via rGO as a new and effective electron mediator. Ma *et al.* [132] prepared the copper heterostructure composites (Cu-Cu_2O-CuO/AC) by simple carbothermal reduction procedure using $CuSO_4$ as a single precursor and the activated carbon played both a reducing agent and support role. In the composites, the Cu–Cu_2O–CuO composites with size less than 10 nm dispersed well on the surface of activated carbon. The photocatalytic activities of the catalysts were tested by degrading reactive brilliant blue KN-R under visible-light irradiation. It is found that the Cu–Cu_2O–CuO/activated carbon heterostructure composites showed excellent photocatalytic activity compared with other catalysts, the synergistic effect between the AC and photoactive copper species, and the presence of interfacial structures such as a Cu_2O/CuO heterostructure, Cu/Cu_2O (or CuO) Schottky barrier, and Cu_2O/Cu/CuO ohmic heterojunction are all responsible for its excellent performance. Li *et al.* [133] developed a new kind of free-standing and flexible visible-light photocatalyst Cu/Cu_2O/CuO heterojunction net which can be easily recycled by one-step calcination in air using low-cost Cu net as the matrix. Since both CB and VB of Cu_2O are situated below those of CuO, the photoexcited electrons from Cu_2O transfer to the CB of CuO under visible light irradiation, whereas the photoexcited holes from CuO transfer to the VB of Cu_2O. In addition, Cu framework also acts as good electron acceptors, accepting the photoexcited electrons from CB of Cu_2O, so, the mixing narrow band gaps of the Cu/Cu_2O/CuO heterojunction ensured its wide absorption band in visible region and effective electron/hole separation, and consequently led to markedly photocatalytic activity under visible light irradiation. Ajmal *et al.* [134] prepared the non-noble metal supported Cu_2O-CuO/TiO_2 catalysts and used for the photodegradation of textile dyes, and found that photocatalytic degradation of commercial dyes in general and RB 49 in particular could effectively be achieved using 4 wt.% Cu_2O-CuO/TiO_2. Such enhanced dye degradation ability of Cu deposited catalyst can be ascribed to the immediate electron trapping property of Cu present in Cu_2O-CuO/TiO_2. TEM and XPS results confirmed the presence of Cu in its oxide form

(Cu_2O-CuO).

(4) Fe_2O_3-Cu_2O composite

Recently, the mixed metal oxides composed Cu_2O with iron oxide has gained considerable attention for various applications due to their narrow band gaps, suitable band edge potentials, earthly abundant and non-toxicity [135]. Lakhera *et al.* [136] prepared α-Fe_2O_3/Cu_2O mixed oxide photocatalysts by one step facile hydrothermal method. The reduced photoluminescence intensity of α-Fe_2O_3/Cu_2O photocatalysts implied that the loading of α-Fe_2O_3 on Cu_2O augmented the charge carrier separation and transfer at the interface. 5 wt% α-Fe_2O_3 loaded Cu_2O showed the highest photodegradation activity and exhibited nearly 30% and 95% increase in the photodegradation rate of methyl orange (MO) compared with bare Cu_2O and α-Fe_2O_3, respectively. Herein, the excellent photodegradation activity of α-Fe_2O3/Cu_2O photocatalyst is mainly attributed to the enhanced visible light absorption, efficient charge carriers separation and transfer. Tian *et al.* [137] developed a unique ternary single core-double shell heterostructure consisted of α-Fe_2O_3@SnO_2@Cu_2O with a tube-like morphology. During the preparation, authors used an anion-assisted hydrothermal route for deposition of α-Fe_2O_3, a seed-mediated deposition strategy for SnO_2, and finally an aging process to deposit a Cu_2O layer to complete the tube-like ternary heterostructures. These ternary heterostructures exhibited enhanced photocatalytic performance on the photodegradation of the organic dye of Rhodamine B (RhB) under simulated sunlight irradiation. Herein, the enhanced photocatalytic activity is due to the efficient charge separation of photogenerated electron–hole pairs facilitated through the p–n heterojunction. Li *et al.* [138] synthesized a novel Z-scheme Cu_2O/graphene/α-Fe_2O_3 nanotube arrays (Cu_2O/G/FNA) composite by a facile electrochemical process for the first time. Its photoelectrochemical performance was evaluated by degradation of methylene blue under visible-light irradiation, and found that compared to single- or two-component system, the Cu_2O/G/FNA composite showed the enhanced photoactivity and photostability due to the efficient

photogenerated electron-hole separation as well as the sufficient redox potential via directly quenching between the weak oxidative holes and reductive electrons. The Z-scheme photocatalytic mechanism was confirmed. Shen *et al.* [139] synthesized the all-solid-state Z-scheme system of rGO-Cu_2O/Fe_2O_3 composites and used for the simultaneous hydrogen production and tetracycline degradation to test its photocatalytic performance. The obtained rGO-Cu_2O/Fe_2O_3 composites exhibited more excellent photocatalytic performance than the single Cu_2O or Fe_2O_3 on the H_2 production and TC degradation. This is because that the reduced graphene oxide (rGO) as a solid-state medium can efficiently transport photogenerated electrons from the conduction band of Fe_2O_3 to valence band of Cu_2O, which played a key role in the introduction of tetracycline (TC) degradation during H_2 production.

(5) Other metals oxide - Cu_2O composites

Apart from the above discussed Cu_2O–metal oxide composites, the diverse mixed metal oxides composed by Cu_2O and other metals oxide have also been prepared for effective utilization of solar light for various applications. For instance, Luo *et al.* [140] prepared Cu_2O–modified Bi_2O_3 nanospheres via a two-step method. In the composite, Cu_2O was dispersed on the surface of Bi_2O_3 nanospheres and all of Cu_2O–modified Bi_2O_3 nanospheres showed uniformly nanospheres with the size of 80–150 nm. For the degradation of Rhodamine B, the composite exhibited enhanced photocatalytic activity compared with Cu_2O and Bi_2O_3. The excellent performance is due to the higher BET surface area, the band gap narrowing, and the interfacial charge transfer effect in the Cu_2O–modified Bi_2O_3 nanospheres. Shen *et al.* [141] prepared the rGO-Cu_2O/Bi_2O_3 composite photocatalysts by depositing Cu_2O and Bi_2O_3 nanocrystals on the surface of rGO via an *in situ* precipitation method. In the composite, the Cu_2O and Bi_2O_3 nanocrystals distributed uniformly and separately on rGO. For photodegradation of tetracycline (TC) under visible light irradiation, the photocatalytic performance of three-component rGO-Cu_2O/Bi_2O_3 composites was improved obviously. This is due to the construction of a Z-scheme photocatalytic system where the rGO served as a solid-

state medium for the transfer of the photogenerated electrons from the conduction band of Bi_2O_3 to the valence band of Cu_2O. Wei *et al.* [142] fabricated WO_3/p-Cu_2O composite films on titanium (Ti) substrates with a consecutive cathodic electrode position route. The photocatalytic activity was evaluated by decomposition of Orange II under simulated natural light illumination. The results indicated that WO_3/p-Cu_2O exhibited higher photocatalytic activity compared to both WO_3 and p-Cu_2O alone. This is because that in this p–n heterojunction, the majority electron in WO_3 and the majority hole in p-Cu_2O would combine by transfer through the interface between the two semiconductors, but the recombination of photogenerated charges in the respective semiconductors would be suppressed, resulting high photocatalytic activity. Li *et al.* [143] prepared magnetically recoverable Cu_2O/Fe_3O_4 composite photocatalysts in large quantities by a fast and simple route and its photocatalytic performance were tested by using methyl orange (MO) degradation reaction under visible light irradiation. 90% degradation rate was achieved within 90 min for all the photocatalysts and the optimal weight ratio of Cu_2O/Fe_3O_4 was 4:6, after 5 consecutive used, it retained over 95% of its initial activity, suggesting high reusability. More important, this catalyst was easily isolated from the solution by an external magnet and subsequently reused in competitive photocatalysis with good recyclability.

1.3.3 Cu_2O-other compounds

(1) Cu_2O/Ag-based compounds

Since Ag_3PO_4 was reported to be an outstanding visible light-driven photocatalysis in water oxidation and organic pollution treatment fields by Ye's group [144], this novel semiconductor has attracted much attention, due to its suitable band gap position, safety and high photocatalytic ability. Li *et al.* [145] synthesized a novel Z-scheme octahedral Cu_2O/Ag_3PO_4 composites by a facile chemical method at low temperature. Its photocatalytic performance was evaluated by methylene blue (MB) degradation under

visible light. 90% of MB was degraded by Cu_2O/Ag_3PO_4 after 8 min, however, only 63% and 24% was reached by Ag_3PO_4 and Cu_2O, respectively. The Z-scheme mechanism was used to explain this process. Hou *et al.* [146] fabricated a novel $Ag_3PO_4@Cu_2O$ core@shell heterojunction photocatalysts through liquid phase reduction and chemical deposition method. In the composite, Cu_2O with flower-like structures was loaded on the surface of Ag_3PO_4 nanorods. The $Ag_3PO_4@Cu_2O$ composites exhibited the highest visible-light driven catalytic activity, degrading nearly 97% of MB (100 mL, 20 mg L^{-1}) after 20 min of irradiation.

AgBr is an n-type semiconductor with the band gap of 2.6 eV [147], which has been extensively studied in photocatalysis and exhibited the outstanding photocatalytic activity. To overcome the disadvantages of Cu_2O, small amount of AgBr/Ag was used to modify the surface of Cu_2O. Liu *et al.* [148] prepared a new composite photocatalyst $Ag@AgBr/Cu_2O$ by loading Ag@AgBr on (1 1 1) facts of octahedral Cu_2O substrate via a facile precipitation *in situ* photoreduction method. In the composite, Ag@AgBr nanoparticles were well-dispersed on Cu_2O nanoparticles with narrow size distributions and controllable sizes from 10 to 30 nm. Its photocatalytic activity was evaluated by degradation of methylene blue (MB) under visible-light irradiation. Compared with pure Cu_2O, The $Ag@AgBr/Cu_2O$ composite showed stronger visible light absorption capacity and higher photocatalytic activity and the Ag@AgBr (15 wt.%)/Cu_2O sample presented the best photocatalytic activity, degrading 93.28% of MB after irradiation for 90 min. Hu *et al.* [149] prepared a plasmonic photocatalyst Cu_2O–Ag–AgBr supported on mesoporous alumina (Cu_2O–Ag–AgBr/Al_2O_3) by deposition–precipitation methods. The coupling of Cu_2O with Ag NPs and AgBr accelerated interfacial electron transfer processes, leading to the fast photoreduction of the dissolved Ag^+ and the photostability of Cu_2O. So, for the degradation of toxic persistent organic pollutants, the catalyst showed high photocatalytic activity and stability under visible light irradiation. He *et al.* [150] prepared the Cu_2O/Cu/AgBr/Ag photocatalysts by a redox procedure followed by

photo-assisted deposition. In this composite, Cu nanoparticles (NPs) could be controllably grown in between Cu_2O and AgBr. Under visible light irradiation for 50 min, only a low photocatalytic degradation of MO (-51%) was observed without Cu NPs between Cu_2O/AgBr. However, in the presence of Cu NPs, ~98% MO can be degraded. This is because introducing Cu NPs assisted in accelerating excited carrier transfer at the interface between Cu_2O and AgBr, and the Z-scheme mechanism ca proposed for this process.

Among various wide band gap semiconductor photocatalysts, AgCl is an n-type semiconductor and its direct band gap and indirect band gap are 5.15 eV and 3.25 eV, respectively [151]. Besides, AgCl has a smaller electronic effective mass (AgCl 0.25 me) due to its three-dimensional d10-d10 interaction and shorter Ag-Ag bonds, leading to higher electron mobility and longer photogenerated carrier lifetime [152, 153]. Thus, AgCl coupled with Ag nanoparticles possesses outstanding photocatalytic performance, and it is mainly attributed to surface plasmonic effect of Ag nanoparticle and effective charge transfer [154-157]. To overcome the shortcomings of the charge recombination of Cu_2O, AgCl/Ag was also used to modify the Cu_2O. Lou *et al.* [158] prepared the hierarchical Cu_2O/Ag/AgCl microcubes by a facile method at room temperature using Cu_2O/Ag microcube as a template and $CuCl_2$ as an oxidant. Its photocatalytic performance was evaluated by the degradation of MO and under optimal conditions, 93% of MO can be degraded in 16 min. This is due to the fact that the Cu_2O prevent the recombination of the electrons from the AgCl back to the metal Ag through the interface and promote the separation of the photogenerated carrier, resulting the improved photocatalytic performance.

(2) Cu_2O/Bi-based compounds

Recently, much attention has been given to a series of visible light active Bi-based photocatalysts [159]. Many Bi^{3+}-containing compounds have been found to possess a narrow band gap and exhibit high visible light photocatalytic activity because of the hybridized O_{2p} and Bi_6S_2 valence bands.

$BiVO_4$ with monoclinic structure is an n-type semiconductor with a discrete band gap of ca. 2.3 eV, which has been tested by many groups for applications in the heterogeneous photocatalysis field. The conduction band (CB) and valence band (VB) edges of $BiVO_4$ are located at 0.11 V and 2.65 V vs. NHE, respectively [160]. Both CB and VB potentials are more negative in Cu_2O than in $BiVO_4$. The relative position of the energy bands of these semiconductors indicates that it is possible for the formation of a p-n heterojunction between them. In recent studies, p-n $Cu_2O/BiVO_4$ composite photocatalysts have been synthesized by different methods [161-163]. For example, Wang *et al.* [164] prepared the p-n junction $Cu_2O/BiVO_4$ heterogeneous nanostructures through coupling a hydrothermal process with polyol strategy. Its photocatalytic performance was evaluated by the degradation of model dyes methylene blue and colorless organic phenol under visible light irradiation. The photogenerated electrons and holes can be separated effectively by the p–n junction formed between the p-type Cu_2O and n-type $BiVO_4$ interface, and the recombination of electron-hole pairs can be substantially reduced, resulting an enhanced photocatalytic activity. Deng *et al.* [165] prepared the dual Z-scheme $BiVO_4/Ag/Cu_2O$ nanocomposite via simple wet impregnation of Cu_2O particles coupled with a subsequent photo-reduction pathway for the deposition of metallic Ag on the surface of $BiVO_4$ and used for the degradation of tetracycline (TC) under visible light irradiation ($\lambda > 420$ nm). Under the optimum coating contents of Cu_2O and 2% Ag, nearly 91.22% TC removal efficiency was obtained based on ternary $BiVO_4/Ag/Cu_2O$ nanocomposites, higher than that of pure $BiVO_4$ (42.9%) and binary $BiVO_4/Cu_2O$ (65.17%) and $BiVO_4/Ag$ (72.63%) nanocomposites. The enhanced photocatalytic activity of $BiVO_4/Ag/Cu_2O$ was attributed to the synergistic effect of Cu_2O, Ag and $BiVO_4$, especially the surface plasmon resonance effect and the established local electric field brought about by metallic Ag. The dual Z-scheme charge transfer pathway has been proposed to explain this photocatalytic reaction.

According to the literature [166, 167], upon photoexcitation of the three-

dimensional Bi_2WO_6 flower, charge could be transferred from its O2p Bi6s hybrid orbitals to empty W5d orbitals. Additionally, the Bi_2WO_6 unique flower structure with a large specific surface area could provide a large number of reactive sites and effectively improve the utilization of visible light due to light scattering effect [14–16]. Liu *et al.* [168] prepared the Cu_2O nanodots decorated flower-like Bi_2WO_6 via an interfacial self-assembly method. In the composite, the Cu_2O nanodots with an average diameter of 20 nm, were dispersed on the surface of Bi_2WO_6 uniformly. The 3 wt% Cu_2O/Bi_2WO_6 composites showed the highest degradation rate for MB, which was 2.14 and 12.25 times higher than those of the pure Bi_2WO_6 and Cu_2O. This enhanced photocatalytic activity was attributed to the enhancement of visible light absorption efficiency as well as the efficient photo-generated charge separation originated from a strong interaction in the intimate contact interface. Li *et al.* [169] prepared a novel Z-scheme $Cu_2O/Au/BiPO_4$ composite and used for the methyl orange degradation. In the photocatalytic reaction, metallic Au species not only acted as the solid state electron mediator, but also could absorbed photons from incident light and present surface plasmon resonance effect in this hybridization system. As such, this Z-scheme system could improve the separation efficiency of photoinduced carriers and is beneficial to suppress the recombination of electron–holes. So, this composite showed excellent performance and the methyl orange was fully decolorized after 60 min irradiation.

Xia *et al.* [170] designed and synthesized a novel $BiOI/Cu_2O$ composites for the first time by coupling reduction method at low temperature. This $BiOI/Cu_2O$ composites consisted of three-dimensional (3D), hierarchical cauliflower-like structure composed of BiOI nanosheet and Cu_2O cubic submicrometer structure. In $BiOI/Cu_2O$ composites, the synergistic effect between BiOI and Cu_2O at the interface could greatly enhance the separation of photo-generated electron-hole pairs, improve the migration efficiency of photo-generated charge carriers and efficiently prevent recombination of photo-induced electrons and holes, resulting an excellent photocatalytic performance. Cui *et al.* [171] reported a highly efficient novel photocatalyst QDs-Cu_2O/BiOBr which

is consist of Cu_2O quantum dots (QDs) incorporated into 3D flower-like hierarchical BiOBr via a simple reductive solution chemistry route and used for the organic contaminant degradation under visible light. The 3 wt% QDs-Cu_2O/BiOBr composite showed the highest degradation rate for phenol and methylene blue (MB), which was 11.8 times and 1.4 times higher than that of pure BiOBr. By incorporating Cu_2O QDs with BiOBr, the visible light absorption efficiency as well as the efficient separation of photogenerated charge carriers originating from the intimately contacted interface and the well-aligned band-structures were enhanced.

(3) C_3N_4-Cu_2O composites

Graphitic carbon nitride (C_3N_4), a novel metal free polymeric material, possesses a smaller band-gap of 2.7 eV, which can make it absorb more natural sunlight. Moreover, C_3N_4 is extremely stable with respect to thermal, chemical, and photochemical attack otherwise than the photocatalysts of sulfide and oxynitride semiconductor. Therefore, C_3N_4 should be an ideal photocatalytic material. The formation of heterojunction by combination of C_3N_4 and Cu_2O semiconductors with different band-gaps is an effective route to promote the separation of charges and the subsequent collection of electrons and holes at the interfaces of two semiconductors, thus reducing their recombination. Tian *et al.* [172] prepared the p-n heterojunctions of C_3N_4-Cu_2O by a hydrothermal method via simply depositing Cu_2O to the surface of C_3N_4. The visible light photocatalytic tests showed that the present C_3N_4-Cu_2O heterojunctions possessed excellent photocatalytic activity for degrading MO under visible light irradiation, much higher than those of individual C_3N_4 or Cu_2O. This enhancement was proven to be attributed to the high separation and easy transfer of photogenerated electron–hole pairs at the interface of heterojunctions, which can be reasonably ascribed to the p–n junction structures of C_3N_4 and Cu_2O. Li *et al.* [173] also prepared the g-C_3N_4−Cu_2O with a p-n heterojunction structure in the presence of glutamate by hydrothermal synthesis and high-temperature calcination. By adding the glutamate, the specific surface area and the reaction sites in the composites were all increased. In addition, the charge

recombination rate of the heterojunction was reduced, and the absorption band was red-shifted to 460 nm, leading to stronger heterostructure contact interfaces, thus the visible-light utilization efficiency was enhanced. Liu *et al.* [174] prepared the Cu_2O@g-C_3N_4 core@shell composites by a combined solvothermal and chemisorption method, in which g-C_3N_4 was successfully coated onto Cu_2O nanospheres via a spontaneous adsorption process. The results showed that the g-C_3N_4-coated Cu_2O nanospheres possessed significantly improved activity for photocatalytic hydrogen production, which is due to the synergistic effects of large contact area, specific energy band structure, and enhanced charge separation at the interface of Cu_2O and g-C_3N_4. Yan *et al.* [175] fabricated a highly efficient visible-light-region Cu_2O/g-C_3N_4/rGO composite 3D aerogel photocatalyst by a facile self-assemble method. The Cu_2O/g-C_3N_4 heterojunction loaded on reduced graphene oxide sheets resulted in increasing absorption in the visible light range and improving photodegradation activity, and the ternary composite aerogel exhibited 96% (Methylene Blue) and 83% (MO) degradation efficiency within 80 min. Liang *et al.* [176] synthesized a porous g-C_3N_4/Ag/Cu_2O composite by chemical adsorption of Ag-doped Cu_2O on porous g-C_3N_4 and used for the degradation of rhodamine B under visible light irradiation. When the content of Ag/Cu_2O was 15 wt%, nearly 85% of RhB in a suspension disappeared after irradiation with visible light for 50 min, the enhanced visible-light photocatalytic activity was achieved. This enhanced photocatalytic performance is due to the enhanced utilization of visible light, increasing separation and transfer of photogenerated electron–hole pairs at the interface and the enlarged specific surface area by introducing a porous structure to the composite. Zuo *et al.* [177] prepared a high-performance photocatalyst, attapulgite/Cu_2O/Cu/g-C_3N_4 by a one-pot redox strategy under anoxic calcination. In the preparation process, ultra-fine CuO nanoparticles on the surface of rod-like attapulgite were *in-situ* reduced by NH_3 gas to generate Cu and minority Cu_2O during the pyrocondensation of melamine. Meanwhile, the generated g-C_3N_4 membrane was uniformly encapsulated on the surface of attapulgite/Cu_2O/Cu to assemble Z-scheme

Cu_2O/Cu/g-C_3N_4 heterostructure. The resulting ATP/Cu_2O/Cu/g-C_3N_4 catalysts exhibited excellent photocatalytic performance for the degradation of chloramphenicol. Kumar *et al.* [178] prepared a novel magnetic quaternary BiOCl/g-C_3N_4/Cu_2O/Fe_3O_4 (BGC-F) nano-heterojunction by a facile co-precipitation method. The BGC-F ($0.2\ g\ L^{-1}$) exhibited high photocatalytic activity with 99.5% of 100 μM sulfamethoxazole (SME) degraded in 60 min under visible (Xe) lamp and 92.1% in 120 min under natural sunlight, which was 7.2, 6.8 and 4.2-fold higher as compared to C_3N_4/BiOCl/Fe_3O_4, Cu_2O/BiOCl/Fe_3O_4 and Cu_2O/BiOCl/C_3N_4 junctions respectively. This is due to the formation of an effective p-n-p junction (BiOCl-C_3N_4-Cu_2O) which leads to shifting of energy bands and rising of an in-built electric field and charge separation.

(4) CdS/Cu_2O composites

CdS is an n-type semiconductor with a band gap of about 2.4 eV and can be excited by visible light. It has a wide range of applications, including photocatalysts [179], solar cells [180], biological labeling [181], and environmental sensors [182]. Liu *et al.* [183] synthesized CdS/Cu_2O heterostructural materials by a solvent-thermal process followed by a chemical bath deposition process. In the composite, the surface of CdS nanowires (NWs) was decorated with spherical Cu_2O whose diameter ranges from 100 to 200 nm. Its photoactivity was investigated by MO photodegradation and around 96% of the degradation rate was achieved after 120 min irradiation in the presence of CdS/Cu_2O composites. Under visible light, the photogenerated electrons in the conduction band (CB) of Cu_2O had a tendency to transfer to the CB of CdS, whereas the photogenerated holes transferred in the opposite direction from the valance band (VB) of CdS to that of Cu_2O, resulting in the efficient separation of photo-generated electrons and holes. So, the special heterojunction structure of CdS/Cu_2O composites plays an important role in the photocatalytic degradation process.

(5) Cu_2O/$ZnWO_4$ composites

Recently, $ZnWO_4$ received widespread attention due to its excellent performance

in degrading organic pollutants under ultraviolet light [184]. Meanwhile, the $ZnWO_4$ photocatalyst also has the advantages of stable chemical properties and is easy to develop. The match between the level structure and the intimately contacted interface of $ZnWO_4$ and Cu_2O are beneficial for accelerating the separation of the photogenerated charge carriers, which improves the photocatalytic activity. Tian *et al.* [185] decorated the surface of $ZnWO_4$ nanorods with Cu_2O nanoparticles ($Cu_2O/ZnWO_4$) through a precipitation method. In the composite, the Cu_2O nanoparticles were tightly deposited on the $ZnWO_4$ surface with an average diameter of 20 nm. For MB degradation under visible light, the 5 wt % $Cu_2O/ZnWO_4$ photocatalyst displayed the highest degrade efficiency and was 7.8 and 2 times higher than pure $ZnWO_4$ and Cu_2O, respectively. This is because the nanoparticles not only promoted the absorption and utilization of visible light but also facilitated the separation of photogenerated charge carriers.

(6) Cu_2S/Cu_2O composites

Cuprous sulfde (Cu_2S) is a well-known semiconductor with a band gap of 1.2 eV. The conduction band (CB) of Cu_2O is more positive than that of Cu_2S, the photo-generated electrons in the CB of Cu_2O have a tendency to transfer to the CB of Cu_2S, whereas the photo-generated holes transfer in the opposite direction. So, Yue *et al.* [186] synthesized the Cu_2S-decorated Cu_2O nanocomposites by a facile co-precipitation and calcination method, and used for the removal of organic pollutants, including Congo red (CR), MO and tetracycline (TC). Compared with the previously reported studies, Cu_2O/Cu_2S nanocomposite (O/S molar ratios is 9:1) possessed the much superior photocatalytic performance, and it could remove about 99.8% CR, 90.1% MO and 84.8% TC molecules within 120 min. The enhanced adsorption ability was mainly attributed to the electrostatic interaction and complexation between the nanocomposite and organics. In addition, appropriate amount of Cu_2S could not only increase specific surface area of nanocomposites, but also effectively enhance visible-light absorption and suppress the recombination of light-induced electrons and holes.

(7) $NiFe_2O_4/Cu_2O$ composites

$NiFe_2O_4$ is a narrow band gap (-2.19 eV) semiconductor material, which has magnetic separability, chemical stability and photocatalytic property [187]. Sohrabnezhad *et al.* [188] prepared the $NiFe_2O_4$@AlMCM-41core-shell by solvo- and hydro- thermal methods. In the preparation process, the magnetic $NiFe_2O_4$ core was prepared by solvothermal method, the intermediate AlMCM-41 shell was prepared by the method of liquid crystal templating mechanism and subsequently Cu_2O nanoparticles (NPs) were synthesized in $NiFe_2O_4$@AlMCM-41core-shell via colloidal chemistry approach. In the composite, the $NiFe_2O_4$ as core was regular sphere with a diameter of 68 nm, and the average thickness of AlMCM-41 shells was ~35 nm. The particles size of Cu_2O incorporated in core-shell was less than 5 nm. This composite showed excellent performance and the removal rate of MB achieved up to 90% after 60 min under visible light irradiation since the $NiFe_2O_4$@AlMCM-41 core-shell reduced recombination of electro-hole in Cu_2O. He *et al.* [189] prepared a magnetically separable $NiFe_2O_4/Cu_2O$ composites by a two-step method and used for the MB degradation under simulated solar light illumination. The $NiFe_2O_4/Cu_2O$ composites exhibited higher photocatalytic activity than those of pure Cu_2O and $NiFe_2O_4$, the photocatalytic efficiency of $NiFe_2O_4/Cu_2O$ composite was nearly 98% under simulated solar light irradiation for 60 min. This attribute to co-catalytic effect of $NiFe_2O_4$ and Cu_2O, which caused the effective separation of photo-generated electron-holes pairs and effective transfer of photogenerated electron from $NiFe_2O_4$ to Cu_2O. In addition, the composite could be easily separated by an external magnetic field.

(8) $SrTiO_3$/ Cu_2O composites

$SrTiO_3$ is an important n-type semiconductor with a cubic perovskite structure with a band gap of approximately 3.2 eV [190], which draws extensive interest because of its ant iPhoto chemical corrosion properties, thermal stability, good heat resistance, corrosion resistance, and so on [191，192]. When combing the Cu_2O with $SrTiO_3$, the p-n heterojunction $SrTiO_3$/ Cu_2O composites may be obtained. Xia *et al.* [193] prepared the n-$SrTiO_3$/p-Cu_2O heterojunction composites for the first time via a two-step route

and used for the degradation of pollutant MB. The obtained $SrTiO_3/Cu_2O$ composites exhibited much higher photocatalytic activity than Cu_2O and $SrTiO_3$ and the catalytic efficiency was nearly 90.4% under simulated solar light irradiation for 60 min, which was ascribed to the synergistic effect between $SrTiO_3$ and Cu_2O by forming the p-n heterojunction.

1.3.4 Hybrid Cu_2O-carbon materials

Since the discovery of fullerenes and carbon nanotubes, carbon materials have received research interest because of their potential applications in gas separation as molecular sieves, photonic band gap crystals, catalyst supports and electrode materials. The incorporation of carbon materials into Cu_2O semiconductor photocatalysts has been proved to be an effective strategy to improve their photocatalytic performance.

(1) Cu_2O/carbon sphere (CS)

Among the various structure forms of carbon materials, carbon sphere (CS) has attracted a great deal of attention in different areas owing to their excellent physical and chemical properties, and it also can be used as a support material to synthesis a variety of materials. Zhou *et al.* [194] prepared the Cu_2O/CS heterostructure in which Cu_2O nanospheres were deposited on the surface of the CS via a relatively facile chemical reduction method, using a single-source molecule (cupric acetate) as precursor and CS as a support material. Its photocatalytic performance was evaluated via using MO degradation. The photocatalytic activity of Cu_2O/CS composites was improved comparing with pure Cu_2O, which is attributed to the good adsorption ability of the composites and the separation of photogenerated electrons–holes pair between Cu_2O and CS.

(2) Cu_2O/ Carbon Nanotubes (CNTs)

Recently, several studies have demonstrated that the combination of Cu_2O NPs with CNTs can improve the photocatalytic performance remarkably, because CNTs

facilitate the dispersion of Cu_2O NPs as well as electron transport [195]. Cu_2O/CNTs composites have been prepared by several methods [196]. Yang *et al.* [197] prepared a novel Cu_2O/CNTs hierarchical chrysanthemum-like nanocomposite which is made of three-dimensional (3D) ordered structures with an average diameter of about 80-120 nm by a facile wet chemical method for the first time. Its catalytic performance was evaluated by the degradation of phenol under visible light irradiation. The Cu_2O/CNTs chrysanthemum-like nanocomposites exhibited outstanding photocatalytic properties when compared with other as-prepared Cu_2O/CNTs, which is because that this structure enlarged the range of absorbed light, improved the connection of Cu_2O NPs with CNTs and enhanced the absorption intensity of light.

(3) Cu_2O/ EG

Because the unique 2D p-conjugation structure of exfoliated graphite (EG) can provide a three-dimensional environment for photocatalytic reaction which can separate the photo generated charge pairs resulting in low recombination rate and endowed a high adsorption capacity for the sample, thus, the photocatalytic degradation efficiency of Cu_2O can be enhanced by combing with EG. Zhao *et al.* [198] firstly prepared the Cu_2O/EG by the precipitation method and its photocatalytic activity of the material was evaluated using the decolorization of MO solution as model reaction. In the composite, Cu_2O was deposited on the worm-like flakes of EG in the form of nanocrystals. Compared with pure Cu_2O, the photocatalytic performance of Cu_2O/EG composites was enhanced obviously and the decolorization efficiency of MO for 60 min can reach 96.7%.

(4) Cu_2O/GO

Graphene oxide (GO), one of the most important derivatives of graphene, is characterized by a layered structure with oxygen functional groups bearing on the basal planes and edges. GO attracts the most attention of researchers due to the following aspects. First, GO can be thought as a semiconductor material because of the presence of the local sp2 hybridization structure. If Cu_2O particles are assembled on the GO

surface, the photo-generated electrons that are induced in Cu_2O can easily migrate to GO, which avoids the surface recombination of the photogenerated electron-holes pairs in Cu_2O [199]. Second, there are many oxygen-containing groups on the surface of GO nanosheets, which is favorable for the adsorption of organic dyes on the surface of GO and consequently, enhancing the photocatalytic degradation efficiency of the composite photocatalysts [200, 201]. Tu *et al.* [202] prepared a visible-light photocatalysts by *in situ* synthesizing Cu_2O in the micropores of regenerated cellulose (RC)/GO composite films. In the composite, Cu_2O nanoparticles were immobilized and evenly distributed in the RC matrix to excite and generate free photoelectrons and electron holes, GO sheets transferred the yielded photoelectrons to prevent local high potential zone generation and to induce the chain degradation reaction at more points, leading to the high photodegradation efficiency against methyl orange dye under visible-light irradiation.

Foams belong to a well-known porous materials with extremely low density but very high porosity, and they exhibit great potential applications in various fields. The highly porous structure is very usable for the penetration of organic dyes and the exposure of photocatalysts. So, Nie *et al.* [203] prepared a novel composite foam that composed of the regenerated microcrystalline cellulose (MCC) fibers and Cu_2O/GO composite photocatalysts and its photocatalytic performance was measured by MB degradation. The composite foams exhibited the typical porous structure and, in addition, due to the hydrogen bonding interaction between Cu_2O and GO, the dispersion of Cu_2O in the composite foam was promoted. The MCC/Cu_2O/GO composite foams exhibited excellent photocatalytic degradation ability toward MB, which is much higher than those reported in literature using the other Cu_2O-based photocatalytic degradation materials. This is mainly attributed to the porous structure of the foam and the formation of the composite structure of Cu_2O and GO, which shows the role of ‘micro-reactor’ during the photocatalytic degradation process of MB. The photocatalytic mechanism of MB degradation over the MCC/Cu_2O/GO composite foams was shown in Figure 1.

(5) Cu_2O/rGO

Reduced graphene oxide (rGO) which is a promising material with a range of unique properties, such as superior mobility of charge carriers, extremely high specific surface area and excellent conductivity [204], has recently received people's considerable concern. It is also used as a flexible conducting support to encapsulate Cu_2O nanocrystals in many fields. Abulizi *et al.* [205] prepared the Cu_2O-reduced graphene composites (Cu_2O-rGO) using a simple sono-chemical route without any surfactants or templates. The Cu_2O sphere which is approximately 200 nm in diameter composed of nanoparticles with approximately 20 nm in diameter uniformly dispersed on both the graphene surface and the interlayers and no agglomeration was observed in the Cu_2O-rGO sheet. The as-synthesized Cu_2O-rGO composites were evaluated by MO degradation. The Cu_2O-rGO composites showed a remarkable photocatalytic degradation efficiency of MO compared with pure Cu_2O spheres. Under UV light illumination for 60 min, 96.6% of the initial MO dyes were decomposed using the Cu_2O-rGO composites, however, only 52.6% of the initial dyes were decomposed for pure Cu_2O spheres under the same conditions. The increase in the photocatalytic degradation efficiency can be attributed to the fact that rGO acts not only as a charge acceptor to promote the separation and transfer of photo-generated carriers but also as a support to stabilize Cu_2O and adsorb MO molecules in the aqueous solution. Pu *et al.* [206] prepared Cu_2O-rGO nanoheterostructures through a facile and green preparation of photochemical reaction. With a suitable amount of rGO, a fluent electron transfer from Cu_2O NCs to rGO sheets was achieved, resulting an increasingly pronounced charge separation in the samples. The photocatalytic activity of the Cu_2O-rGO nanoheterostructures was found to surpass that of pristine Cu_2O NCs, commercial Cu_2O powder and N-doped P-25 TiO_2 powder. Zou *et al.* [207] synthesized the Cu_2O-rGO composites with tunable Cu_2O crystal facets ({1 1 1}, {1 1 0} and {1 0 0} facets) and used for the degradation of MB under visible light. The results indicated that the catalytic behaviors of composites were related to the electronic structures and

interfacial connections. *In-situ* ESR study showed that the larger amount and longer lifetime of superoxide radicals ($O_2^{\bullet -}$) were present over o-Cu_2O-rGO composite. So, the degradation performance of MB under visible light was ranked as: o-Cu_2O{1 1 1}-rGO > d-Cu_2O{1 1 0}-rGO > c-Cu_2O{1 0 0}-rGO. Zhang *et al.* [208] prepared the cubic Cu_2O-rGO and used for the removal of MO under visible light. Compared with pure cubic Cu_2O particles under similar preparation conditions, the as-prepared cubic Cu_2O-rGO nanocomposites demonstrated enhanced photocatalytic activity for MO dye with a 100% degradation rate in 100 min, which is mainly attributed to the increased charge transportation, effective separation of photoelectrons from vacancies, and the improved contact area. For practical applications, it is ideal to immobilize the nano-structured photocatalysts on certain solid surfaces for separation and recycling. Cai *et al.* [209] synthesized the Cu_2O/rGO composite aerogel by a one-pot hydrothermal method using glucose as a reducing agent and cross-linker. It is found that in the presence of Cu_2O/rGO composite aerogel, nearly 70% of MO was degraded after irradiated for 5 h, while only less than 30% of MO was degraded in the presence of Cu_2O nanoparticles. This improved activity can be attributed to the following factors. Firstly, rGO is a material with good electrical conductivity, and the incorporation of rGO can promote the charge transfer and help to separate the photogenerated charge carriers on Cu_2O. Secondly, the floating of Cu_2O/rGO composite aerogel on the surface of the aqueous reaction system can ensure it to absorb more visible light than Cu_2O powder. In addition, the as-prepared Cu_2O/rGO showed a higher adsorption toward the pollutants which is a prerequisite for superior photocatalysis.

1. 4 The photocatalytic mechanism of Cu_2O based photocatalysts

As stated above, Cu_2O is a kind of p-type semiconductor and its band gap is 2.2 eV. Compared with traditional photocatalytic materials (TiO_2 and ZnO), the band gap of Cu_2O is much narrower and could cause the photocatalytic reaction under visible light. Valence band, conduction band and forbidden band are three indispensable elements of

semiconductor materials. When semiconductor is stimulated by light, the electrons transfer from the valence band to the conduction band, forming photogenerated electrons in the conduction band and photogenerated holes in the valence band. By using the reducibility and oxidability of photogenerated e^--h^+ pairs, the O_2 or H_2O molecules can be changed into $\bullet O_2^-$ or •HO with strong oxidation, which can degrade organic pollutants in the environment without causing secondary pollution. The photocatalytic mechanism of Cu_2O-based photocatalysts are summarized as follows.

1.4.1 p-n heterojunction mechanism

The p-n heterojunction is an effective structure for charge collection or separation. Usually, when the p-type semiconductor combines with n-type semiconductor, due to the movement of the e^- and h^+, the p-n heterjunction would be formed at the interface, the built-in potential will be generated to guide the e^- and h^+ flow in opposite directions and the e^- and h^+ will be separated quickly, e^- is transferred to the CB of n-type semiconductor and h^+ is transferred to the VB of p-type semiconductor. For p-n heterostructure, there are following advantages: more efficient charge separation, quick transfer of the charge to the surface of the catalyst and longer life of the charge carriers.

Zou group [112] indicates that after the combination of Cu_2O and ZnO, the band gap of Cu_2O becomes narrow and the absorption range of the solar spectrum can be expanded. In addition, the formation of the p-n junction helps to separate photoinduced e^--h^+ pairs under visible light irradiation and avoid charge recombination. As shown in Fig. 2a, photogenerated electrons in the conduction band (CB) of Cu_2O can migrate to the CB of ZnO nanorode, while photogenerated holes migrate in the opposite direction from the valence band (VB) of ZnO nanorode to the Cu_2O. After separation, due to the one-dimensional structure and single crystal characteristics, photogenerated electrons are rapidly transferred to the surface of ZnO nanorods, which is conducive to the degradation of dyes. Xia *et al.* [193] pointed out that after the n-$SrTiO_3$ particle is combined with the p-Cu_2O cube [Fig 2. b], according to the formation theory of the p-

n heterojunction, the charge carriers will diffuse and transfer between Cu_2O and $SrTiO_3$ due to the concentration difference of the charge carriers. Finally, a p-n heterojunction is formed at the interface of the two semiconductors. A large number of photogenerated charge carriers are generated under simulated sunlight. Photogenerated electrons formed in Cu_2O are transferred to $SrTiO_3$ through the interface, and the photogenerated holes are transferred from $SrTiO_3$ to Cu_2O, further improving the separation of photogenerated electron-hole pairs, thus increasing the lifetime of photogenerated charge carriers.

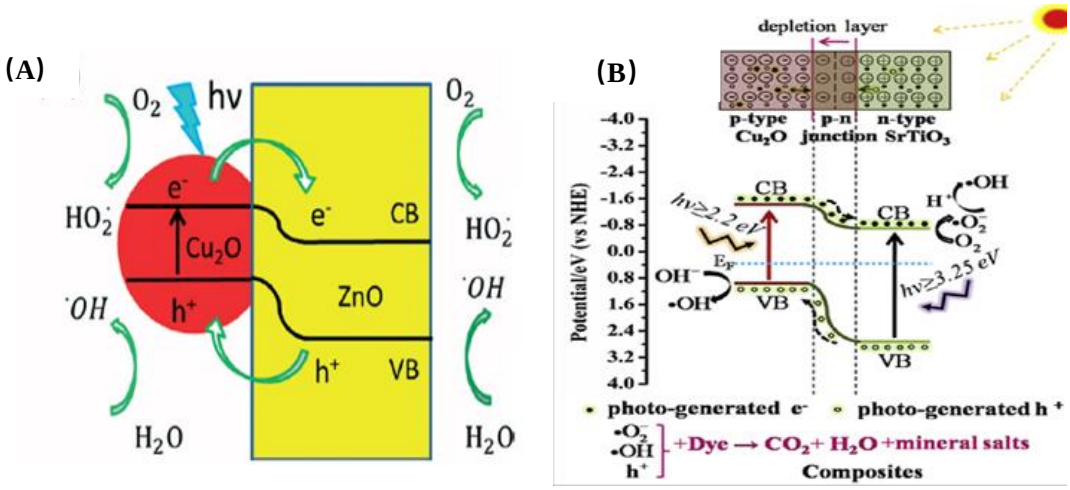

Figuer 1.2 p-n mechanism of (a) Cu_2O/ZnO Reprinted with permission from ref. 112, copyright 2014, The Royal Society of Chemistry. and (b) $SrTiO_3$/Cu_2O composites. Reprinted with permission from ref. 193, copyright, 2018, Elsevier.

In addition, the photocatalytic degradation mechanisms of heterojunction such as Cu_2O/TiO_2[119], Cu_2O/Fe_2O_3[137], WO_3/Cu_2O[142], Cu_2O/AgCl[147], Cu_2O/AgBr [151], Cu_2O/C_3N_4[172] and CdS/Cu_2O [183] can also be explained by the above mechanism.

1.4.2 Metal (quantum dot) /Cu_2O schottky junction mechanism

Another effective way is to form metal/semiconductor junctions. For the metal /Cu_2O composite, at the interface of the two materials, electrons would flow from one material to the other (from higher to lower Fermi levels) to align with the Fermi levels. The

formation of schottky barrier leads to excessive negative charges in the metals and excessive positive charges in the semiconductors. Thus, electron-hole recombination was suppressed and the photocatalytic performance was enhanced. Zhang *et al.* [210] explains the photocatalytic mechanism of Au/Cu_2O, as shown in Fig 1.3. When Au combined with Cu_2O, due to the formation of Schottky junction at the interface, electrons would migrate from Au to Cu_2O to balance Fermi levels. Under visible light, the photoinduced electrons in the CB of Cu_2O would move quickly to the Au nanoparticles, and the hole is left on the VB of Cu_2O. Thus, photogenerated electrons and holes are effectively separated. The separated electrons are captured by the adsorbed O_2 to produce $\bullet O_2^-$, and the separated holes are captured by the surface hydroxyl group to produce ·OH. Thus, the organic pollutants are effectively degraded by the two radicals.

In addition, the photocatalytic mechanism of Cu/Cu_2O[91], Ag/Cu_2O[96] and Zn/Cu_2O[108] can be also explained by the above mechanism.

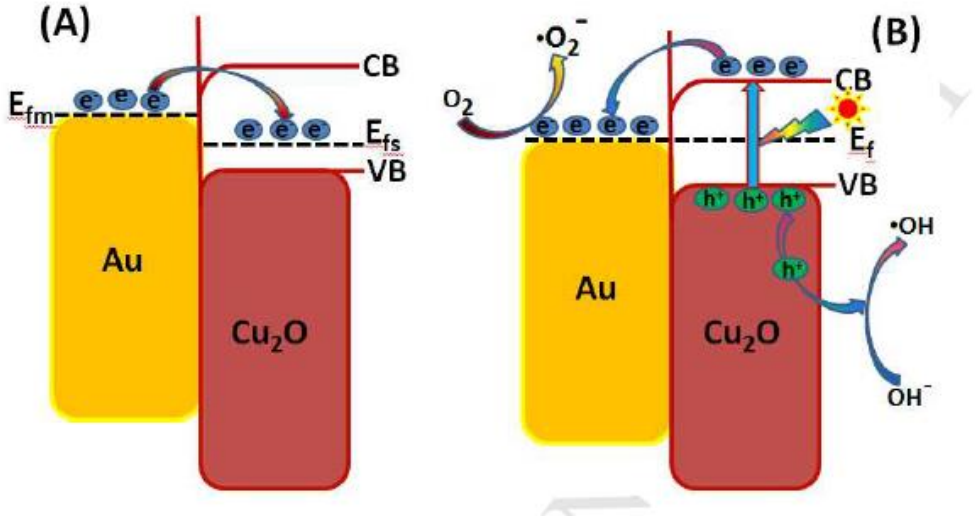

Figuer 1.3 Schottky junction mechanism of Au/Cu_2O heterostructure. Reprinted with permission from ref. 210, copyright, 2019, Elsevier.

1.4.3 Z-Scheme heterojunction

Compared with p-n heterojunction, the photocatalyst of Z-scheme composite material not only separates photogenerated electron-holes efficiently, but also has excellent redox capability.

Li *et al.* [145] reasonably explained the electron-hole separation of Cu_2O/Ag_3PO_4 composite by Z-scheme mechanism, as seen in Fig. 4. The CB potential of Ag_3PO_4 is lower than the standard reduction potential of $\bullet O_2^-/O_2$, and photoexcited electrons cannot reduce O_2 to $\bullet O_2^-$. The VB position of Ag_3PO_4 is more positive than $\cdot OH/OH^-$ and $\cdot OH/H_2O$. The photogenerated holes in VB of Ag_3PO_4 can react with H_2O and OH^- to form hydroxyl radical ($\cdot OH$). For Cu_2O/Ag_3PO_4 composites, under visible light irradiation, the photoinduced e^- at the CB of Ag_3PO_4 would be quickly quenched by the h^+ at the VB of Cu_2O. As a consequence, the holes can be enriched in VB of Ag_3PO4, while the electrons can be enriched in CB of Cu_2O, and the photogenic carriers can be easily separated. Therefore, the prepared Cu_2O/Ag_3PO_4 composite showed high photocatalytic efficiency through Z-scheme mechanism.

Similarly, photocatalytic degradation activities of Cu_2O/CuO[131], RGO-Cu_2O/Bi_2O_3[141], $Cu_2O/Ag/BiVO_4$[165] and $Cu_2O/Cu/g\text{-}C_3N_4$[177] can be also explained by the Z-scheme mechanism.

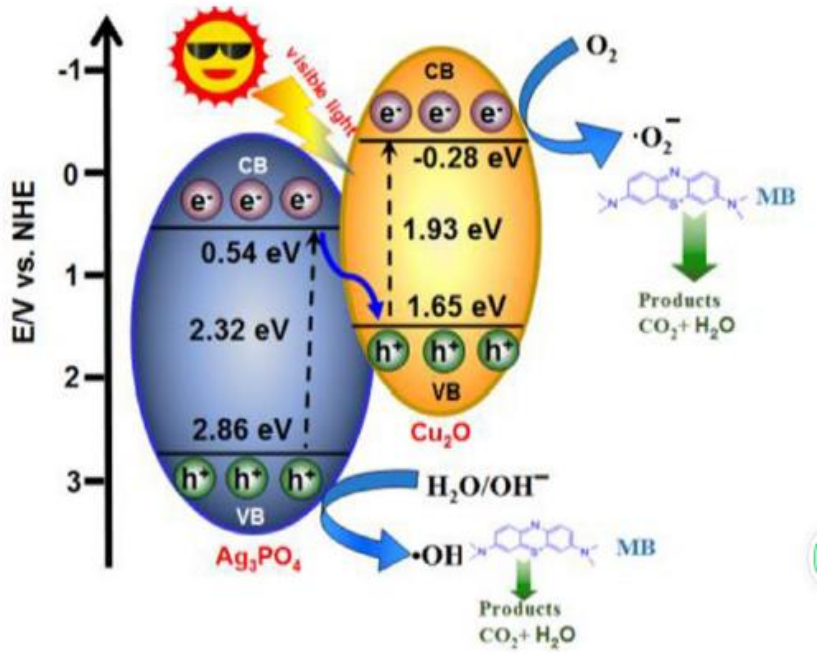

Figuer 1.4 Z-scheme mechanism of Cu_2O/Ag_3PO_4 photocatalyst. Reprinted with permission from ref. 145, copyright, 2017, Elsevier.

By combined with precious metals, metal oxides and carbon materials to form the semiconductor heterojunction, Schottky junction or Z-scheme structure, the light utilization was enhanced and the photogenerated electron-hole pair recombination rate was reduced, resulting in higher photocatalytic performance of Cu_2O.

1.5 Objectives of this study

As reviewed above, to suppress the recombination of photogenerated electron-hole pair is the crucial factor to increase the catalytic performance of Cu_2O based photocatalyst. Various efficient tactics have been considered to enhance its performance. For example, loading on the carrier with large surface area to increase the active sites and adsorbability, coupling with conductive material to separate effectively the electron in the Cu_2O, compositing with other semiconductor to form heterojunction to reduce the recombination of photogenerated electron-hole pair in the Cu_2O. Although many achievements on Cu_2O based photocatalyst have been reported, the activity and stability

of Cu_2O based photocatalysts still suffer some serious issues: instability in oxidizing conditions, the rapid recombination of photo-generated holes and electrons. Hence, the objectives of this study are to develop the efficient and stable Cu_2O based photocatalysts by forming the heterojunction with other semiconductor to realize the fast separation of photogenerated electron-hole pair in the catalyst. Furthermore, the photocatalytic reaction mechanisms of degradation process will be also discussed. It is expected to obtain novel Cu_2O based photocatalysts for the degradation of organic pollutants.

1.6 Scope of this dissertation

The introduction is considered as **Chapter 1**, in which the crystal structure of Cu_2O, Cu_2O based photocatalysts, catalyst classification, photocatalytic performance and the degradation mechanism are presented.

Chapter 2 presents the synthesis, photocatalytic performance and the related mechanism of KAPs-B/Cu_2O composite. KAPs-B (Knitting Aromatic compound Polymers-Benzene) which is a kind of Hyper-cross-linked polymers (HCPs) is a porous polymer with a structure that benzene rings are connected with methylene linkers. The excellent adsorption ability of KAPs-B could enhance the catalytic performance of Cu_2O and meanwhile stabilize the Cu_2O in oxidizing environments. In this chapter, KAPs-B was loaded on Cu_2O with various amounts by a one-step precipitation method. The composition and microstructures of the obtained composite are measured by X-ray diffraction (XRD), scanning electron microscopy (SEM), transmission electron microscopy (TEM), X-ray photoelectron spectroscopy (XPS), FT-IR spectrum and Brunauer-Emmett-Teller (BET). In addition, its photoelectric properties are measured by UV-vis diffuse reflectance spectroscopy (UV-vis DRS), the photocurrent response and electrochemical impedance spectroscopy (EIS). The photocatalytic ability of the as-obtained catalyst was tested by degradation of methyl orange (MO) as the pollutant under visible light. The active species trapping analysis and the photocatalytic

mechanism was also analyzed.

Chapter 3 demonstrates the preparation and photocatalytic performance of UiO-66-NH_2/Cu_2O composite. UiO-66-NH_2/Cu_2O composites with different loading amounts of UiO-66-NH_2 were firstly synthesized by using a facile impregnation process. The composition, structure and its photoelectric properties are analyzed and characterized by means of several analysis methods. The higher surface area which can be seen in the BET will be favorable for the increasement of the active sites and the adsorbability for MO. The photocatalytic performances of the composites were measured by the methyl orange (MO) degradation. The photocatalytic performance was improved obviously. The study on the photocatalytic mechanism indicate that the Z-scheme heterojunction was formed in the composite and thus improve the efficient separation of photoinduced e^--h^+ pairs, resulting in the excellent photocatalytic performance.

Chapter 4 is about the synthesis and photocatalytic performance of graphitic-carbon-nitride-nanosheets/copper(I) oxide (g-C_3N_4 nanosheets/Cu_2O) composite. In order to further enhance the dispersity of Cu_2O based photocatalysts in the organic pollution, Cu_2O with cubic structure was studied. In addition, for practical applications, tetracycline (TC) antibiotics was used as the degradation target. The g-C_3N_4 nanosheets with a high surface area were firstly obtained by an expansion method. Then, the g-C_3N_4 nanosheets/Cu_2O composite was successfully synthesized by using a facile precipitation method and used as a visible light photocatalyst for the degradation of tetracycline (TC) antibiotics. The effects of g-C_3N_4 nanosheets amount on the photocatalytic activity of composite are investigated in details. The g-C_3N_4 nanosheets/Cu_2O composite are characterized by XRD, SEM, TEM, FTIR, UV/Vis Spectrophotometer, XPS, EDS and BET surface area measurement. The photocatalytic performance of g-C_3N_4 nanosheets/Cu_2O composite are compared with the corresponding pure material. The excellent photocatalytic degradation activities of g-C_3N_4 nanosheets/Cu_2O composite was explained by the p-n type heterostructure

mechanism.

Finally, the general conclusions of this research and suggestions for future work are summarized in **Chapter 5**.

References

[1]. X. Meng, Z. Li, J. Chen, H. Xie, Z. Zhang, Enhanced visible light-induced photocatalytic activity of surface-modified BiOBr with Pd nanoparticles, Appl. Surf. Sci., 2018, 433, 76-87.

[2]. Z. Yu, F. Li, Q. Yang, Nature-mimic method to fabricate polydopamine/graphitic carbon nitride for enhancing photocatalytic degradation performance, ACS Sustain. Chem. Eng., 2017, 5, 7840-7850.

[3]. S. Yoon. M. Kim. I. S. Kim. J. H. Lim. B. Yoo, Manipulation of Cuprous Oxide Surfaces for Improving Their Photocatalytic Activity. J. Mater. Chem. A. 2014, 2, 11621-11627..

[4]. Z. Wei.T. Xinyue. W. Xiaomeng. D. Benlin. Z. Lili. X. Jiming. Z. Fengxia, Novel pn heterojunction photocatalyst fabricated by flower-like $BiVO_4$ and Ag_2S nanoparticles: Simple synthesis and excellent photocatalytic performance. Chem Eng J., 2019, 361,1173-1181.

[5]. S. Zhong. C. Lv. M. Shen. L. Wu. C. Li, Synthesis of Bi_2WO_6 photocatalyst modified by SDBS and photocatalytic performance under visible light. J Mater SCI-Mater EL, 2019, 30, 4152-4163

[6]. R. Dadigala. R. Bandi. B. R. Gangapuram. V. Guttena, Construction of in situ self-assembled $FeWO_4$/g-C_3N_4 nanosheet heterostructured Z-scheme photocatalysts for enhanced photocatalytic degradation of rhodamine B and tetracycline. Nano Adv, 2019, 1, 322-333.

[7]. R. Li, F. Zhang, D. Wang, J. Yang, M. Li, J. Zhu, X. Zhou, H. Han and C. Li, Spatial separation of photogenerated electrons and holes among {010} and {110} crystal facets of $BiVO_4$, Nat. Commun., 2013, 4, 1-7.

[8]. J. Zhang, H. Ma and Z. Liu, Highly efficient photocatalyst based on all oxides WO_3/Cu_2O heterojunction for photoelectrochemical water splitting, Appl. Catal. B, 2017, 201, 84-91

[9]. T. Cai. L. Wang. Y. Liu. S. Zhang. W. Dong. H. Chen. S. Luo, Ag_3PO_4/Ti_3C_2 MXene interface materials as a Schottky catalyst with enhanced photocatalytic activities and anti-photocorrosion performance. Appl. Catal. B, 2018, 239, 545-554

[10]. H. Fang. Y. Pan. M. Yin. L. Xu. Y. Zhu. C. Pan. Facile synthesis of ternary Ti_3C_2-OH/ln_2S_3/CdS composite with efficient adsorption and photocatalytic performance towards organic dyes. J. Solid State Chem, 2019,*280*, 120981.

[11]. C. H. B. Ng and W. Y. Fan, Shape evolution of Cu_2O nanostructures via kinetic and thermodynamic controlled growth, J. Phys. Chem. B, 2006, 110, 20801-20807.

[12]. J. T. Zhang, J. F. Liu, Q. Peng, X. Wang and Y. D. Li, Nearly monodisperse Cu_2O and CuO nanospheres: preparation and applications for sensitive gas sensors, Chem. Mater., 2006, 18, 867-871.

[13]. H. Zhang, Q. Zhu, Y. Zhang, Y. Wang, L. Zhao and B. Yu, One-pot synthesis and hierarchical assembly of hollow Cu_2O microspheres with nanocrystals-composed porous multishell and their gas-sensing properties, Adv. Funct. Mater., 2007, 17, 2766-2771.

[14]. J. H. Zhong, G.R. Li, Z.L. Wang, Y.N. Ou and Y.X. Tong, Facile electrochemical synthesis of hexagonal Cu_2O nanotube arrays and their application. Inorg. Chem., 2011, 50, 757-763.

[15]. C. H. Kuo, Y.C. Yang, S. Gwo and M. H. Huang, Facet-dependent and Au nanocrystal-enhanced electrical and photocatalytic properties of Au-Cu_2O Core-shell heterostructures, J. Am. Chem. Soc., 2011, 133, 1052.

[16]. J. Y. Xiang, X. L. Wang, X. H. Xia, L. Zhang, Y. Zhou, S. J. Shi and J. P. Tu, Enhanced high rate properties of ordered porous Cu_2O film as anode for lithium ion batteries, Electrochim. Acta., 2010, 55, 4921-4925.

[17]. B. White, M. Yin, A. Hall, D. Le, S. Stolbov, T. Rahman, N. Turro and S. O'Brien, Complete CO oxidation over Cu_2O nanoparticles supported on silica gel, Nano Lett., 2006, 6, 2095-2098.

[18]. M. Leng, M. Liu, Y. Zhang, Z. Wang, C. Yu, X. Yang, H. Zhang and C. Wang, Polyhedral 50-facet Cu_2O microcrystals partially enclosed by {311} high-index planes: synthesis and enhanced catalytic CO oxidation activity, J. Am. Chem. Soc., 2010, 132, 17084-17087.

[19]. A. Paracchino, V. Laporte, K. Sivula, M. Graetzel and E. Thimsen, Highly active oxide photocathode for photoelectrochemical water reduction, Nat. Mater., 2011, 10, 456-461.

[20]. J.N. Kondo，Cu_2O as a photocatalyst for overall water splitting under visible irradiation, Chem. Commun., 1998, 3, 357-358.

[21]. A. Roos, B. Karlsson, Properties of oxidized copper surfaces for solar applications, Sol. Energ. Mater., 1983, 7, 467-480.

[22]. H. Bao, W. Zhang, D. Shang, Q. Hua, Y. Ma, Z. Jiang and W. Huang, Shape-dependent reducibility of cuprous oxide nanocrystals, J. Phys. Chem. C., 2010, 114, 6676-6680.

[23]. C.H. Kuo, C.H. Chen, M.H. Huang. Seed-mediated synthesis of monodispersed Cu_2O nanocubes with five different size ranges from 40 to 420 nm, Adv. Funct. Mater., 2007，17，3773-3780.

[24]. Y. Xu, H. Wang, Y. Yu, L. Tian, W. Zhao, B, Cu_2O. nanocrystals: surfactant-free room-temperature morphology-modulated synthesis and shape-dependent heterogeneous organic catalytic activities, J. Phys. Chem. C, 2011, 15, 15288–15296.

[25]. Y. Zhang, B. Deng, T. Zhang, D. Gao, A.W. Xu. Shape effects of Cu_2O polyhedral microcrystals on photocatalytic activity, J. Phys. Chem. C, 2010, 114, 5073-5079.

[26]. L. Zhang, H. Wang, Interior structural tailoring of Cu_2O shell-in-shell nanostructures through multistep Ostwald ripening, J. Phys. Chem. C, 2011, 115, 18479-18485.

[27]. C. Lu, L. Qi, J. Yang, X. Wang, D. Zhang, J. Xiand J. Ma, One-pot synthesis of octahedral Cu_2O nanocages via a catalytic solution route, Adv. Mater. 2005, 17, 2562-2567.

[28]. C. H. Kuo, M. H. Huang. Fabrication of truncated rhombic dodecahedral Cu_2O nanocages and nanoframes by particle aggregation and acidic etching, J. Am. Chem. Soc., 2008, 13, 12815-12820.

[29]. Z.C. Orel, A. Anžlovar, G. Dražić, M. Zigon, Cuprous oxide nanowires prepared by an additive-free polyol process, Cryst. Growth. Des., 2007, 7, 453-458.

[30]. P. Grez, F. Herrera, G. Riveros, R. Henríquez, A. Ramírez, E. Muñoz and R. Schrebler, Synthesis and characterization of p-Cu_2O nanowires arrays, Mater. Lett., 2013, 92, 413-416.

[31]. Z. Zhang H. Che, Y. Wang, J. Gao, L. Zhao, X. She, F. Su, Facile synthesis of mesoporous Cu_2O microspheres with improved catalytic property for dimethyldichlorosilane synthesis, Ind. Eng. Chem. Res., 2012, 51, 1264-1274.

[32]. E. Ko, J. Choi, K. Okamoto, Y. Tak, J. Lee, Cu_2O nanowires in an alumina template: Electrochemical conditions for the synthesis and photoluminescence characteristics, ChemPhysChem., 2006, 7, 1505-1509.

[33]. L. Gou, C.J. Murphy, Solution-phase synthesis of Cu_2O nanocubes, Nano Lett., 2003, 3, 231-234.

[34]. L. Gou, C.J. Murphy, Solution-phase synthesis of Cu_2O nanocubes, Nano Lett., 2003, 3, 231-234.

[35]. M. H. Kim， B. Lim， E. P. Lee, Y. Xia, Polyol synthesis of Cu_2O nanoparticles： Use of chloride to promote the formation of a cubic morphology, Mater. Chem.， 2008,18, 4069-4073.

[36]. C. H. Kuo, M. H. Huang, Morphologically controlled synthesis of Cu_2O nanocrystals and their properties, Nano Today., 2010, 5, 106-116.

[37]. I. C. Chang, P. C. Chen, M. C. Tsai, C. Y. Lee, Large-scale synthesis of uniform Cu_2O nanocubes with tunable sizes by in-situ nucleation, CrystEngComm., 2013, 15, 2363-2366.

[38]. A. V. Nikam, V. Arulkashmir, B. L. V. Prasad, pH-Dependent single-step rapid synthesis of CuO and Cu_2O nanoparticles from the same precursor. Cryst. Growth. Des., 2014, 14, 4329-4334.

[39]. Y. Y. Cao，Y. Y. Xu，H. Y. Hao，G. Zhang, Room temperature additive-free synthesis of uniform Cu_2O nanocubes with tunable size from 20nm to 500nm and photocatalytic property. Mater. Lett., 2014, 114, 88-91

[40]. S. Kumar, C. M. A. Parlett, M. A. Isaacs, A. F. Lee, Facile synthesis of hierarchical Cu_2O nanocubes as visible light photocatalysts, Appl. Catal. B, 2016, 189, 226-232.

[41]. S. Karthikeyan, S. Kumar, L. J. Durndell, A. F. Lee, Size-Dependent Visible Light Photocatalytic Performance of Cu_2O Nanocubes, ChemCatChem, 2018, 10, 3554-3563.

[42]. H. L. Xu, W. Z. Wang, W. Zhu. Shape evolution and size-controllable synthesis of Cu_2O octahedra and their morphology-dependent photocatalytic properties, J. Phys. Chem. B, 2006, 110, 13829-13834.

[43]. M. J. Siegfried, K. S. Choi. Directing the architecture of cuprous oxide crystals during electrochemical growth, Angew. Chem. Int. Ed., 2005, 44, 3282-3287.

[44]. C. H. Kuo, M, H, Huang. Facile synthesis of Cu_2O nanocrystals with systematic shape evolution from cubic to octahedral structures, J. Phys. Chem. C, 2008, 112, 18355-18360.

[45]. H. Pang, F, Gao，Q. Y. Lu. Glycine-assisted double-solvothermal approach for various cuprous oxide structures with good catalytic activities, Cryst. Eng. Comm.， 201, 12, 406-412.

[46]. J. Y. Ho，M. H. Huang. Synthesis of submicrometer-sized Cu_2O crystals with morphological evolution from cubic to hexapod structures and their comparative photocatalytic activity, J. Phys. Chem. C，2009, 11, 14159-14164

[47]. X. Liang, L. Gao, S. Yang, J. Sun, Facile Synthesis and Shape Evolution of Single-Crystal Cuprous Oxide, Adv. Mater., 2009, 21, 2068-2071.

[48]. K. X. Yao，X. M. Yin，T. H. Wang，H. C. Zeng, Synthe, self-assembly，disassembly， and reassembly of two types of Cu_2O nanocrystals unifaceted with {001} or {110} planes, J. Am. Chem. Soc., 2010, 132, 6131-6144

[49]. W. C. Huang, L. M. Lyu, Y. C. Yang, M. H. Huang, Synthesis of Cu_2O nanocrystals from cubic to rhombic dodecahedral structures and their comparative photocatalytic activity, J. Am. Chem. Soc., 2011, 134, 1261-1267.

[50]. Y. Zhang，B. Deng，T. R. Zhang，A. W. Xu, Shape effects of Cu_2O polyhedralmicrocrystals on photocatalytic activity, J. Phys. Chem. C, 2010, 114, 5073-5079

[51]. M. Leng，M. Z. Liu，Z. Q. Wang，C. Wang, Polyhedral 50-facet Cu_2O microcrystals partially enclosed by {311} high-index planes: Synthesis and enhanced catalytic CO oxidation activity, J. Am. Chem. Soc., 2010, 132, 17084-17087.

[52]. X. P. Wang，S. H. Jiao，D. P. Wu, D. Xu, A facial strategy for crystal engineering of Cu_2O polyhedrons with high-index facets, Cryst. Eng. Comm., 2013, 15, 1849-1852

[53]. K. Chen，C. Sun，S. Song, D. Xue， Polymorphic crystallization of Cu_2O compound, Cryst. Eng. Comm., 2014, 16, 5257-5267.

[54]. H. Liu，W. Miao，Z. Zhang, J. Chen, Controlled synthesis of different shapes of Cu_2O via γ-irradiation, Cryst. Growth Des., 2009, 9, 1733-1740.

[55]. Y. Shang，Y. M. Shao，D. F. Zhang, L. Guo， Recrystallization-induced self-assembly for the growth of Cu_2O superstructures, Angew. Chem. Int. Ed., 2014, 53, 11514-11518.

[56]. S. Jiao, L. Xu, K. Jiang, D. Xu, Well-defined non-spherical copper sulfide mesocages with single-crystalline shells by shape-controlled Cu_2O crystal templating, AdV. Mater., 2006, 18, 1174-1177.

[57]. F. Caruso, R. A. Caruso, H. Mohwald, Production of hollow microspheres from nanostructured composite particles, Chem. Mater., 1999, 11, 3309-3314.

[58]. L. Wang, T. Sasaki, Y. Ebina, K. Kurashima, M. Watanabe, Fabrication of controllable ultrathin hollow shells by layer-by-layer assembly of exfoliated titania nanosheets on polymer templates, Chem. Mater., 2002, 14, 4827.

[59]. C. H. Kuo，M. H. Huang, Fabrication of truncated rhombic dodecahedral Cu_2O nanocages and nanoframes by particle aggregation and acidic etching, J. Am. Chem. Soc., 2008, 130, 12815-12820

[60]. Y. H. Tsai， C. Y. Chiu， M. H. Huang, Fabrication of diverse Cu_2O nanoframes through face-selective etching Fabrication of diverse Cu_2O nanoframes through face-selective etching, J. Phys. Chem. C，2013, 117, 24611-24617.

[61]. Y. Y. Xu，X. L. Jiao，D. R. Chen. PEG-assisted preparation of single-crystalline Cu_2O hollow nanocubes, J. Phys. Chem. C，2008, 112, 16769-16773

[62]. Z. Zhong, Y. Fang, W. Lu, C. M. Lieber, Coherent single charge transport in molecular-scale silicon nanowires, Nano Lett. 2005, 5, 1143-1146.

[63]. C. C. Hu, K. H. Chang, M. C. Lin, Y. T. Wu, Design and tailoring of the nanotubular arrayed architecture of hydrous RuO_2 for next generation supercapacitors, Nano Lett. 2006, 6, 2690-2695.

[64]. M. S. Arnold, P. Avouris, Z. W. Pan, Z. L. Wang, Field-effect transistors based on single semiconducting oxide nanobelts, J. Phys. Chem. B, 2003, 107, 659-663.

[65]. Y. Tan， X. Xue， X. Peng， H. Zhao, T. Wang, Y. Li, Controllable fabrication and electrical performance of single crystalline Cu_2O nanowires with high aspect ratios, Nano Lett., 2007, 7, 3723-3728

[66]. W. Z. Wang，G. G. Wang，X. S. Wang，Y. J. Zhan, Y. K. Liu, C. L. Zheng, Synthesis and characterization of Cu_2O nanowires by a novel reduction route, Adv. Mater., 2002, 14, 67-69.

[67]. Y .Ren，Z. Ma，P. G. Bruce. Transformation of mesoporous Cu/Cu_2O into porous Cu_2O nanowires in ethanol, Cryst. Eng. Comm., 2012，14, 2617-2620

[68]. M. H. Cao, C. W. Hu, Y. H.Wang, Y. Guo, C. Guo, E. Wang, A controllable synthetic route to Cu, Cu_2O and CuO nanotubes and nanorods, Chem. Comm., 2003, 39, 1884-1885.

[69]. S. Hacialioglu，F. Men，S. Jin, Facile and mild solution synthesis of Cu_2O nanowires and nanotubes driven by screw dislocations, Chem. Comm., 2012, 48, 1174-1176.

[70]. J. H. Zhong，G. R. Li，Z. L. Wang，Y. N. Ou, Y. X. Tong, Facile electrochemical synthesis of hexagonal Cu_2O nanotube arrays and their application. Inorg. Chem.， 2011, 50, 757-763

[71]. L. Guan，H. Pang， J. Wang，Q. Lu, J. Yin, F. Gao, Fabrication of novel comb-like Cu_2O nanorod-based structures through an interface etching method and their application as ethanol sensors, Chem. Comm., 2010，46, 7022-7024

[72]. K. P. Musselman, G. J. Mulholland, A. P. Robinson, L. Schmidt-Mende, J. L. MacManus-Driscoll, Low-temperature synthesis of large-area, free-standing nanorod arrays on ITO/glass and other conducting substrates, Adv. Mater., 2008, 20, 4470-4475

[73]. H. K. Ju，J. K. Lee，J. Lee, J. Lee, Fast and selective Cu_2O nanorod growth into anodic alumina templates via electrodeposition, Curr. Appl. Phys., 2012, 12, 60-63.

[74]. K. M. Haynes，C. M. Perry，M. Rivas，T. D. Golden, A. Bazan, M. Quintana, W. J. Youngblood, Templated electrodeposition and photocatalytic of cuprous oxide nanorod arrays, ACS Appl. Mater. Inter., 2015, 7, 830-837

[75]. Y. Zhang, B. Deng, T. Zhang, D. Gao, A. W. Xu, Shape effects of Cu_2O polyhedral microcrystals on photocatalytic activity, J. Phys. Chem. C, 2010, 114 ,5073-5079.

[76]. A. Paracchinol, V. Laporte, K. Sivula, M. Gratzel, E. Thimsen, Highly active oxide photocathode for photoelectrochemical water reduction, Nat. Mater., 2011,10, 456-461.

[77]. H. J. Li, Y. Zhou, W. Tu, J. Ye, Z. Zou, Adv. Funct. Mater. 2015, 25, 998-1013

[78]. L. Liu, S. Lin, J. Hu, Y. Liang, W. Cui, Plasmon-enhanced photocatalytic properties of nano Ag@AgBr on single-crystalline octahedral Cu_2O (111) microcrystals composite photocatalyst, Appl. Surf. Sci., 2015, 330, 94-103

[79]. M.E. Aguirre, R. Zhou, A.J. Eugene, M.I. Guzman, M.A. Grela, Cu_2O/TiO_2 heterostructures for CO_2 reduction through a direct Z-scheme: protecting Cu_2O from photocorrosion, Appl. Catal. B, 2017, 217, 485-493.

[80]. J. Ma, K. Wang, L. Li, T. Zhang, Y. Kong, S. Komarneni, Visible-light photocatalytic decolorization of orange II on Cu_2O/ZnO nanocomposites, Ceram. Int., 2015, 41, 2050-2056.

[81]. A. Kumar, G. Sharma, Aa. H. Al-Muhtaseb, M. Naushad, A. A. Ghfar, F. J. Stadler, Quaternary magnetic BiOCl/g-$C_3N_4/Cu_2O/Fe_3O_4$ nano-junction for visible light and solar powered degradation of sulfamethoxazole from aqueous environment, Chem. Eng. J., 2018, 334, 462-478.

[82]. D. Wang, N.B. Saleh, W. Sun, C.M. Park, C. Shen, N. Aich, W. Peijnenburg, W. Zhang, Y. Jin, C. Su, Next-generation multifunctional carbon-metal nanohybrids for energy and environmental applications, Environ. Sci. Technol., 2019, 53, 7265–7287.

[83]. P. Wang, B. B. Huang, X. Y. Qin, X. Y. Zhang, Y. Dai, J. Y. Wei and M. H. Whangbo, Ag@ AgCl: a highly efficient and stable photocatalyst active under visible light, Angew. Chem. Int. Ed., 2008, 47, 7931

[84]. J. R. Hayes, G. W. Nyce, J. D. Kuntz, J. H. Satcher, A. V. Hamza, Synthesis of bi-modal nanoporous Cu, CuO and Cu_2O monoliths with tailored porosity, Nanotechnology. 2007, 18, 275602.

[85]. Y. Liu, Y. Chu, Y. J. Zhuo, L. H. Dong, L. L. Li, M. Y. Li, Controlled synthesis of various hollow Cu nano/microstructures via a novel reduction route, Adv. Funct. Mater. 2007, 17, 933-938.

[86]. Y. H. Lee, I. C. Leu, M. T. Wu, J. H. Yen, K. Z. Fung, Fabrication of Cu/Cu_2O composite nanowire arrays on Si via AAO template-mediated electrodeposition, J. Alloys Compd., 2007, 427, 213-218.

[87]. J. J. Teo, Y. Chang, H. C. Zeng, Fabrications of hollow nanocubes of Cu_2O and Cu via reductive self-assembly of CuO nanocrystals, Langmuir., 2006, 22, 7369-7377.

[88]. H. M. Zheng, X. H. Liu, S. B. Yang, X. Wang, New approach for preparation of ultrafine Cu particles and shell/core compounds of Cu/CuO and Cu/Cu_2O, J. Mater. Sci., 2005, 40, 1039-1041.

[89]. S. Sun, C. Kong, H. You, X. Song, B. Ding, Z. Yang, Facet-selective growth of Cu-Cu_2O heterogeneous architectures, CrystEngComm., 2012, 14, 40-43.

[90]. W, Chen, Z, Fan, Z. Lai, Synthesis of core–shell heterostructured Cu/Cu_2O nanowires monitored by in situ XRD as efficient visible-light photocatalysts, J. Mater. Chem. A, 2013, 1, 13862-13868.

[91]. Z. Ai, L. Zhang, S. Lee, W. Ho, Interfacial hydrothermal synthesis of Cu@ Cu_2O core− shell microspheres with enhanced visible-light-driven photocatalytic activity, J. Phys. Chem. C, 2009, 113, 20896-20902.

[92]. W. Hou, S. B. Cronin, A Review of Surface Plasmon Resonance EnhancedPhotocatalysis, Adv. Funct. Mater. 2013, 23, 1612-1619.

[93]. P. Wang B. Huang, Y. Dai, M. H. Whangbo, Plasmonic Photocatalysts:Harvesting Visible Light with Noble Metal Nanoparticles, Phys. Chem. Chem. Phys.,2012, 14, 9813-9825.

[94]. S. K. Cushing, J. Li, F. Meng, T. R. Senty, S. Suri, M. Zhi, M. Li, A. D. Bristow, N.Wu, Photocatalytic Activity Enhanced by Plasmonic Resonant Energy Transfer from Metal to Semiconductor, J. Am. Chem. Soc., 2012, 134, 15033-15041.

[95]. F. Xiao, Layer-by-Layer Self-Assembly Construction of Highly Ordered Metal-TiO_2 Nanotube Arrays Heterostructures (M/TNTs, M = Au, Ag, Pt) withTunable Catalytic Activities, J. Phys. Chem. C, 2012, 116, 16487-16498

[96]. Zhang W, Yan g X, Zhu Q, Wang, K., Lu, J., Chen, M., Yang, Z. One-pot room temperature synthesis of Cu_2O/Ag composite nanospheres with enhanced visible-light-driven photocatalytic performance, Ind Eng Chem Res., 2014, 53, 16316-16323.

[97]. C. Lee, K. Shin, Y. J. Lee, C. Jung, H. Lee, MEffects of shell thickness on Ag-Cu_2O core-shell nanoparticles with bumpy structures for enhancing photocatalytic activity and stability. Cata Today, 2018, 303, 313-319.

[98]. J. Xiong, Z. Li, J. Chen, S. Zhang, L. Wang, S. Dou, Facile synthesis of highly efficient one-dimensional plasmonic photocatalysts through Ag@Cu_2O core-shell heteronanowires, ACS appl. mater. inter., 2014, 6, 15716-15725.

[99]. Z. Hu, Y. Mi, Y. Ji, R. Wang, W. Zhou, X. Qiu, X. Wu, Multiplasmon modes for enhancing the photocatalytic activity of Au/Ag/Cu_2O core-shell nanorods, Nanoscale, 2019, 11, 16445-16454.

[100]. K. Sharma, K. Maiti, N. H. Kim, D. Hui, J. H. Lee, Green synthesis of glucose-reduced graphene oxide supported Ag-Cu_2O nanocomposites for the enhanced visible-light photocatalytic activity, Compos Part B-Eng., 2018, 138, 35-44.

[101]. Q. Wei, Y. Wang, H. Qin, J. Wu, Y. Lu, H. Chi, J. Liu, Construction of rGO wrapping octahedral Ag-Cu_2O heterostructure for enhanced visible light photocatalytic activity, Appl. Catal. B., 2018, 227, 132-144.

[102]. X. W. Liu, Selective growth of Au nanoparticles on (111) facets of Cu_2O microcrystals with an enhanced electrocatalytic property, Langmuir., 2011, 27, 9100-9104.

[103]. H. Zhu, M. Du, D. Yu, Y. Wang, L. Wang, M. Zou, Y. Fu, A new strategy for the surface-free-energy-distribution induced selective growth and controlled formation of Cu_2O-Au hierarchical heterostructures with a series of morphological evolutions, J, Mater. Chem. A, 2013, 1, 919-929.

[104]. M. A. Mahmoud, W. Qian, M. A. El-Sayed Following charge separation on the nanoscale in Cu_2O-Au nanoframe hollow nanoparticles, Nano lett, 2011, 11, 3285-3289.

[105]. W. C. Wang, L. M. Lyu, M. H. Huang. Investigation of the effects of polyhedral gold nanocrystal morphology and facets on the formation of Au-Cu_2O core-shell heterostructures, Chem. Mater., 2011, 23, 2677-2684.

[106]. E. B. Miller, E. M. Zahran, M. R. Knecht, L. G. Bachas, Metal oxide semiconductor nanomaterial for reductive debromination: visible light degradation of polybrominated diphenyl ethers by Cu_2O@ Pd nanostructures, Appl. Catal. B, 2017, 213, 147-154.

[107]. B. Heng, T. Xiao, W. Tao, X. Hu, X. Chen, B. Wang, D. Sun, Y. Tang, Zn doping induced shape evolution of microcrystals: the case of cuprous oxide, Cryst. Growth Des. 2012, 12,3998-4005.

[108]. X. Yu, J. Zhang, J. Zhang, J. Niu, J. Zhao, Y. Wei, B. Yao, Photocatalytic degradation of ciprofloxacin using Zn-doped Cu_2O particles: Analysis of degradation pathways and intermediates, Chem. Eng. J., 2019, 374, 316-327.

[109]. J. Ma, K. Wang, L. Li, T. Zhang, Y. Kong, S. Komarneni, Visible-light photocatalytic decolorization of Orange II on Cu_2O/ZnO nanocomposites, Ceram. Int., 2015, 41, 2050-2056.

[110]. T. Jiang, T. Xie, L. Chen, Z. Fu, D. Wang, Carrier concentration dependent electron transfer in Cu_2O/ZnO nanorod arrays and their photocatalytic performance, Nanoscale., 2013, 5, 2938–3944.

[111]. M. Deo, D. Shinde, A. Yengantiwar, J. Jog, B. Hannoyer, X. Sauvage, S. Ogale, Cu_2O/ZnO hetero-nanobrush: hierarchical assembly, field emission and photocatalytic properties, J. Mater. Chem., 2012, 22, 17055-17062.

[112]. X. Zou, H. Fan, Y. Tian, S. Yan, Synthesis of Cu_2O/ZnO hetero-nanorod arrays with enhanced visible light-driven photocatalytic activity, CrystEngComm, 2014, 16, 1149-1156.

[113]. A. E. Kandjani, Y. M. Sabri, S. R. Periasamy, N. ohora, M. H. Amin, A. Nafady, S. K. Bhargava, Controlling core/shell formation of nanocubic p-Cu_2O/n-ZnO toward enhanced photocatalytic performance, Langmuir, 2015, 31, 10922-10930.

[114]. S. .C Wu, C. S. Tan, M. H. Huang. Strong facet effects on interfacial charge transfer revealed through the examination of photocatalytic activities of various Cu_2O-ZnO heterostructures, Adv. Funct. Mate., 2017, 27, 1604635.

[115]. S. Ren, G. Zhao, Y. Wang, B. Wang, Q. Wang, Enhanced photocatalytic performance of sandwiched ZnO@Ag@Cu_2O nanorod films: the distinct role of AgNPs in the visible light and UV region, Nanotechnology., 2015, 26, 125403.

[116]. H. R. Liu, J. H. Yang, Y. Y. Zhang, S. Y. Chen, A. Walsh, H. J. Xiang, Xi. G. Gong and S. H. Wei, Prediction of $(TiO_2)x(Cu_2O)$ y alloys for efficient photoelectrochemical water splitting, Phys. Chem. Chem. Phys., 2013, 15, 1778–1781.

[117]. Y. Hou, X. Y. Li, Q. D. Zhao, X. Quan and G. H. Chen, Fabrication of Cu_2O/TiO_2 nanotube heterojunction arrays and investigation of its photoelectrochemical behavior, Appl. Phys. Lett., 2009, 95, 093108.

[118]. L. Huang, F. Peng, H. Wang, H. Yu, Z. Li, Preparation and characterization of Cu_2O/TiO_2 nano-nano heterostructure photocatalysts, Catal. Commun., 2009, 10, 1839-1843.

[119]. M. Wang, L. Sun, Z. Lin, J. Cai, K. Xie, C. Lin, p-n Heterojunction photoelectrodes composed of Cu_2O-loaded TiO_2 nanotube arrays with enhanced photoelectrochemical and photoelectrocatalytic activities, Energ. Environ. Sci., 2013, 6, 1211-1220.

[120]. L. Liu, W. Yang, W. Sun, Q. Li, J. K. Shang, Creation of Cu_2O@ TiO_2 composite photocatalysts with p-n heterojunctions formed on exposed Cu_2O facets, their energy band alignment study, and their enhanced photocatalytic activity under illumination with visible light, ACS appl. Mater. Inter., 2015, 7, 1465-1476.

[121]. L. Liu, X. Gu, C. Sun, H. Li, Y. Deng, F. Gao, L. Dong, In situ loading of ultra-small Cu_2O particles on TiO_2 nanosheets to enhance the visible-light photoactivity, Nanoscale., 2012, 4, 6351-6359.

[122]. L. Yang, S. Luo, Y. Li, Y. Xiao, Q. Kang, Q. Cai, High efficient photocatalytic degradation of p-nitrophenol on a unique Cu_2O/TiO_2 p-n heterojunction network catalyst, Environ. Sci. technol., 2010, 44, 7641-7646.

[123]. J. Fu, S. Cao, J. Yu. Dual Z-scheme charge transfer in TiO_2-Ag-Cu_2O composite for enhanced photocatalytic hydrogen generation, J. Mater., 2015, 1, 124-133.

[124]. K. Nakaoka, J. Ueyama, K. Ogura, Photoelectrochemical behavior of electrodeposited CuO and Cu_2O thin films on conducting substrates, J. Electrochem. Soc., 2004,151, 661–665.

[125]. D. Jiang, J. Xue, L. Wu, W. Zhou, Y. Zhang, X. Li, Photocatalytic performance enhancement of CuO/Cu_2O heterostructures for photodegradation of organic dyes: effects of CuO morphology, Appl. Catal. B, 2017, 211,199-204.

[126]. H. Yu, J. Yu, S. Liu, S. Mann, Template-free hydrothermal synthesis of CuO/Cu_2O composite hollow microspheres, Chem. Mater., 2007, 19, 4327-4334.

[127]. C. Morales-Guio, L. Liardet, M.T. Mayer, S.D. Tilley, M. Grätzel, X. Hu, Photoelectrochemical hydrogen production in alkaline solutions using Cu_2O coated with earth-abundant hydrogen evolution catalysts, Angew. Chem. Int. Ed., 2015, 54, 664–667.

[128]. X. Liu, J. Chen, P. Liu, H. Zhang, G. Li, T. An, H. Zhao, Controlled growth of CuO/Cu_2O hollow microsphere composites as efficient visible-light-active photocatalysts, Appl. Catal. A, 2016, 52, 34-41.

[129]. J. Chen, X. Liu, H. Zhang, P. Liu, G. Li, T. An, H. Zhao, Soft-template assisted synthesis of mesoporous CuO/Cu_2O composite hollow microspheres as efficient visible-light photocatalyst. Mater. Lett., 2016, 182, 47-51.

[130]. M. Yurddaskal, T. Dikici, E. Celik. Effect of annealing temperature on the surface properties and photocatalytic efficiencies of Cu_2O/CuO structures obtained by thermal oxidation of Cu layer on titanium substrates, Ceram. Int., 2016, 42, 17749-17753.

[131]. P. Wang, J. Wang, X. Wang, H. Yu, J. Yu, Cu_2O-rGO-CuO Composite: An Effective Z-scheme Visible-Light Photocatalyst, Curr. Nanosci., 2015, 11, 462-469.

[132]. H. Ma, Y. Liu, Y. Fu, C. Yu, X. Dong, X. Zhang, W. Xue, Improved photocatalytic activity of copper heterostructure composites (Cu-Cu_2O-CuO/AC) prepared by simple carbothermal reduction, Aust. J. Chem., 2014, 67, 749-756.

[133]. H. Li, Z. Su, S. Hu, Y. Yan, Free-standing and flexible Cu/Cu_2O/CuO heterojunction net: A novel material as cost-effective and easily recycled visible-light photocatalyst, Appl. Catal. B., 2017, 207, 134-142.

[134]. A. Ajmal, I. Majeed, R. N. Malik, M. Iqbal, M. A. Nadeem, I. Hussain, M. A. Nadeem, Photocatalytic degradation of textile dyes on Cu_2O-CuO/TiO_2 anatase powders, J. Environ. Chem. Eng., 2016, 4, 2138-2146.

[135]. Yu-Fei Zhao, Zhi-Yu Yang, Yu-Xia Zhang, Lin Jing, Xin Guo, Zhengtai Ke, Panwei Hu, Guoxiu Wang, Yi-Ming Yan, Ke-Ning Sun, Cu_2O decorated with

cocatalyst MoS_2 for solar hydrogen production with enhanced efficiency under visible light, J. Phys. Chem. C, 2014, 118 , 14238-14245

[136]. S. K. Lakhera, A. Watts, H. Y. Hafeez, B. Neppolian, Interparticle double charge transfer mechanism of heterojunction α-Fe_2O_3/Cu_2O mixed oxide catalysts and its visible light photocatalytic activity, Cata. Today., 2018, 300: 58-70.

[137]. Q. Tian, W. Wu, L. Sun, S. Yang, M. Lei, J. Zhou, V. A. Roy, Tube-like ternary α-Fe_2O_3@SnO_2@Cu_2O sandwich heterostructures: synthesis and enhanced photocatalytic properties, ACS Appl. Mater. Inter., 2014, 6, 13088-13097.

[138]. F. Li, B. Dong Construction of novel Z-scheme Cu_2O/graphene/α-Fe_2O_3 nanotube arrays composite for enhanced photocatalytic activity, Ceram. Int., 2017, 43, 16007-16012.

[139]. H. Shen, G. Liu, X. Yan, J. Jiang, Y. Hong, M. Yan, W. Shi, All-solid-state Z-scheme system of RGO-Cu_2O/Fe_2O_3 for simultaneous hydrogen production and tetracycline degradation, Mater. Today. Energy., 2017, 5, 312-319.

[140]. Y. Luo, Q. Huang, B. Li, L. Dong, M. Fan, F. Zhang, Synthesis and characterization of Cu_2O-modified Bi_2O_3 nanospheres with enhanced visible light photocatalytic activity, App. Surf. Sci., 2015, 357, 1072-1079.

[141]. H. Shen, J. Wang, J. Jiang, B. Luo, B. Mao, W. Shi, All-solid-state Z-scheme system of RGO-Cu_2O/Bi_2O_3 for tetracycline degradation under visible-light irradiation, Chem. Eng. J., 2017, 313, 508-517.

[142]. S. Wei, Y. Ma, Y. Chen, L. Liu, Y. Liu, Z. Shao, Fabrication of WO_3/Cu_2O composite films and their photocatalytic activity, J. Hazard. Mater., 2011, 194, 243-249.

[143]. Z. P. Li, Y. Q. Wen, J. P. Shang, M. X. Wu, L. F. Wang, Y. Guo, Magnetically recoverable Cu_2O/Fe_3O_4 composite photocatalysts: Fabrication and photocatalytic activity. Chin. Chem. Lett., 2014, 25, 287-291.

[144]. Y. Bi, S. Ouyang, N. Umezawa, J. Cao, J. Ye, Facet effect of single-crystalline Ag_3PO_4 sub-microcrystals on photocatalytic properties, J. Am. Chem. Soc. 133 (2011) 6490-6492.

[145]. Z. Li, K. Dai, J. Zhang, C. Liang, G. Zhu, Facile synthesis of novel octahedral Cu_2O/Ag_3PO_4 composite with enhanced visible light photocatalysis, Mater. Lett., 2017, 206, 48-51.

[146]. G. Hou, X. Zeng, S. Gao Fabrication and photocatalytic activity of core@shell Ag_3PO_4@ Cu_2O heterojunction. Mater. Lett., 2019, 238, 116-120.

[147]. N. Kakuta, N. Goto, H. Ohkita, T. Mizushima, Silver bromide as a photocatalyst for hydrogen generation from CH_3OH/H_2O solution, J. Phys. Chem. B, 1999, 103, 5917-5919.

[148]. L. Liu, S. Lin, J. Hu, Y. Liang, W. Cui, Plasmon-enhanced photocatalytic properties of nano Ag@AgBr on single-crystalline octahedral Cu_2O (111) microcrystals composite photocatalyst, App. Surf. Sci., 2015, 330, 94-103.

[149]. X. Hu, X. Zhou, R. Wang, C. Hu, J. Qu, Characterization and photostability of Cu_2O-Ag-AgBr/Al_2O_3 for the degradation of toxic pollutants with visible-light irradiation, Appl. Catal. B., 2014, 154, 44-50.

[150]. J. He, D. W. Shao, L. C. Zheng, L. J. Zheng, D. Q. Feng, J. P. Xu, H. Dong, Construction of Z-scheme Cu_2O/Cu/AgBr/Ag photocatalyst with enhanced photocatalytic activity and stability under visible light, Appl. Catal. B,, 2017, 203, 917-926.

[151]. Z. K. Xu, L. Han, P. Hu, S. J. Dong, Facile synthesis of small Ag@AgCl nanoparticles via a vapor diffusion strategy and their highly efficient visible-light driven photocatalytic performance, Catal. Sci. Technol., 2014, 4, 3615-3619.

[152]. T. G. Kim, D. H. Yeon, T. Kim, J. Lee, S. J. Im, Silver silicates with three dimensional d^{10}-d^{10} interactions as visible light active photocatalysts for water oxidation, Appl. Phys. Lett., 2013, 103, 043904.

[153]. M. C. Long, W. M. Cai, Advanced nanoarchitectures of silver/silver compound composites for photochemical reactions, Nanoscale. 2014, 6, 7730-7742.

[154]. C. H. An, S. N. Peng, Y. G. Sun, Facile synthesis of sunlight-driven AgCl:Ag plasmonic nanophotocatalyst, Adv. Mater., 2010, 22, 2570-2574.

[155]. P. Wang, B.B. Huang, X.Y. Qin, X.Y. Zhang, Y. Dai, J.Y. Wei, M.H. Whangbo, Ag@ AgCl: a highly efficient and stable photocatalyst active under visible light, Angew. Chem. Int. Ed., 2008, 47, 7931-7933.

[156]. H.Y. Li, Y. J. Sun, B. Cai, S.Y. Gan, D. X. Han, L. Niu, T. S. Wu, Hierarchically Zscheme photocatalyst of Ag@AgCl decorated on $BiVO_4$ (040) with enhancing photoelectrochemical and photocatalytic performance, Appl. Catal. B, 2015, 170, 206-214.

[157]. P. Wang, C. D. Yu, J. J. Ding, X. F. Wang, H. G. Yu, Facile synthesis and improved photocatalytic performance of Ag-AgCl photocatalyst by loading basic zinc carbonate, J. Alloys Compd., 2018, 752, 238-246.

[158]. S. Lou, W. Wang, L. Wang, S. Zhou, In-situ oxidation synthesis of Cu_2O/Ag/AgCl microcubes with enhanced visible-light photocatalytic activity, J. Alloys Compd.,2019, 781, 508-514.

[159]. R. He, S. W. Cao, P. Zhou, J. G. Yu, Recent advances in visible light Bi-based photocatalysts, Chin. J. Catal., 2014, 35, 989-1007.

[160]. U. M. García-Pérez, A. Martínez-de la Cruz, S. Sepúlveda-Guzmán, J. Peral, Lowtemperature synthesis of $BiVO_4$ powders by Pluronic-assisted hydrothermal method: effect of the surfactant and temperature on the morphology and structural control, Ceram. Int., 2014, 40, 4631-4638

[161]. W. Wang, X. Huang, S. Wu, Y. Zhou, L. Wang, H. Shi, Y. Liang, B. Zou, Preparation of p–n junction $Cu_2O/BiVO_4$ heterogeneous nanostructures with enhanced visible-light photocatalytic activity, Appl. Catal. B., 2013,134-135,293-301.

[162]. H. Li, W. Hong, Y. Cui, X. Hu, S. Fan, L. Zhu, Enhancement of the visible light photocatalytic activity of $Cu_2O/BiVO_4$ catalysts synthesized by ultrasonic dispersion method at room temperature, Mat. Sci. Eng. B: Solid., 2014, 181, 1-8.

[163]. Q. Yuan, L. Chen, M. Xiong, J. He, S.L. Luo, C.T. Au, S.F. Yin, $Cu_2O/BiVO_4$ heterostructures: synthesis and application in simultaneous photocatalytic oxidation of organic dyes and reduction of Cr(VI) under visible light, Chem. Eng. J., 2014, 255, 394-402

[164]. W. Wang, X. Huang, S. Wu, Y. Zhou, L. Wang, H. Shi, B. Zou, Preparation of p-n junction $Cu_2O/BiVO_4$ heterogeneous nanostructures with enhanced visible-light photocatalytic activity, Appl. Catal. B., 2013, 134, 293-301.

[165]. Y. Deng, L. Tang, G. Zeng, C. Feng, H. Dong, J. Wang, Y. Pang, Plasmonic resonance excited dual Z-scheme $BiVO_4/Ag/Cu_2O$nanocomposite: synthesis and mechanism for enhanced photocatalytic performance in recalcitrant antibiotic degradation, Environ. Sci. Nano, 2017, 4, 1494-1511.

[166]. W. Chen, T. Y. Liu, T. Huang, X. H. Liu, J. W. Zhu, G. R. Duan, X. J. Yang, In situ fabrication of novel Z-scheme Bi_2WO_6 quantum dots/g-C_3N_4 ultrathin nanosheets heterostructures with improved photocatalytic activity, Appl. Surf. Sci., 2015, 355, 379-387.

[167]. S. Girish Kumar, K. S. R. Koteswara Rao, Tungsten-based nanomaterials (WO_3 Bi_2WO_6): modifications related to charge carrier transfer mechanisms and photocatalytic applications, Appl. Surf. Sci., 2015, 355, 939-958.

[168]. Liu L, Ding L, Liu Y, et al. Enhanced visible light photocatalytic activity by Cu_2O-coupled flower-like Bi_2WO_6 structures, Appl. Surf. Sci., 2016, 364: 505-515.

[169]. J. Li, H. Yuan, Z. Zhu, Fabrication of $Cu_2O/Au/BiPO_4$ Z-scheme photocatalyst to improve the photocatalytic activity under solar light, J. Mol. Catal. A, 2015, 410, 133-139.

[170]. Y. Xia, Z. He, W. Yang, B. Tang, Y. Lu, K. Hu, X. Li, Effective charge separation in BiOI/Cu_2O composites with enhanced photocatalytic activity, Mater. Res. Express., 2018, 5, 025504.

[171]. W. Cui, W. An, L. Liu, J. Hu, Y. Liang, Novel Cu_2O quantum dots coupled flower-like BiOBr for enhanced photocatalytic degradation of organic contaminant, J. hazard. Mater., 2014, 280, 417-427.

[172]. Y. Tian, B. Chang, J. Fu, B. Zhou, J. Liu, F. Xi, X. Dong, Graphitic carbon nitride/Cu_2O heterojunctions: Preparation, characterization, and enhanced photocatalytic activity under visible light, J. Solid. State. Chem., 2014, 212, 1-6.

[173]. D. Li, J. Zan, L. Wu, S. Zuo, H. Xu, D. Xia, Heterojunction Tuning and Catalytic Efficiency of g-C_3N_4-Cu_2O with Glutamate, Ind. Eng. Chem. Res., 2019, 58, 4000-4009.

[174]. L. Liu, Y. Qi, J. Hu, W. An, S. Lin, Y. Liang, W. Cui, Stable Cu_2O@ g-C_3N_4 core@ shell nanostructures: Efficient visible-light photocatalytic hydrogen evolution, Mater. Lett., 2015, 158, 278-281.

[175]. X. Yan, R. Xu, J. J. Guo, X. Cai, D. Chen, L. Huang, S. Tan, Enhanced photocatalytic activity of Cu_2O/g-C_3N_4 heterojunction coupled with reduced graphene oxide three-dimensional aerogel photocatalysis, Mater. Res. Bull., 2017, 96, 18-27.

[176]. S. Liang, Y. Zhou, Z. Cai, C. She, Preparation of porous g-C_3N_4/Ag/Cu_2O: a new composite with enhanced visible-light photocatalytic activity, Appl. Organomet. Chem., 2016, 30, 932-938.

[177]. S. Zuo, Y. Chen, W. Liu, C. Yao, X. Li, Z. Li, X. Liu, A facile and novel construction of attapulgite/Cu_2O/Cu/g-C_3N_4 with enhanced photocatalytic activity for antibiotic degradation, Ceram. Int., 2017, 43, 3324-3329.

[178]. A. Kumar, A. Kumar, G. Sharma, H. Ala'a, M. Naushad, A. A. Ghfar, F. J. Stadler, Quaternary magnetic BiOCl/g-C_3N_4/Cu_2O/Fe_3O_4 nano-junction for visible

light and solar powered degradation of sulfamethoxazole from aqueous environment, Chem. Eng. J., 2018, 334, 462-478.

[179]. S. Zhang, Q. Chen, Y. Wang, L. Guo, Synthesis and photoactivity of CdS photocatalysts modified by polypyrrole, Int. J. Hydrogen Energy., 2012, 37, 13030-13036.

[180]. H. Choi, P.V. Kamat, CdS nanowire solar cells: dual role of squaraine dye as a sensitizer and a hole transporter, J. Phys. Chem. C, 2013, 4, 3983-3991.

[181]. S. Rengaraj, S. Venkataraj, S. H. Jee, Y. Kim, C. W. Tai, E. Repo, A. Koistinen, A. Ferancova, M. Sillanpaa, Cauliflower-like CdS microspheres composed of nanocrystals and their physicochemical properties, Langmuir: ACS J. Surf. Colloids, 2011, 27, 352-358.

[182]. J. Zhai, L. Wang, D. Wang, H. Li, Y. Zhang, D.Q. He, T. Xie, Enhancement of gas sensing properties of CdS nanowire/ZnO nanosphere composite materials at room temperature by visible-light activation, ACS Appl. Mater. Interfaces., 2011, 3, 2253–2258

[183]. Y. Liu, H. Dong, H. Jia, B. Xu, C. Yu, Z. Zhang, CdS nanowires decorated with Cu_2O nanospheres: Synthesis, formation process and enhanced photoactivity and stability. J. Alloys Compd., 2015, 644, 159-164.

[184]. J. Lin, J. Lin, Y. F. Zhu, Controlled Synthesis of the $ZnWO_4$ Nanostructure and Effects on the Photocatalytic Performance, Inorg. Chem., 2007, 46, 8372-8378.

[185]. L. Tian, Y. Rui, K. Sun, W. Cui, W. An, Surface decoration of $ZnWO_4$ nanorods with Cu_2O nanoparticles to build heterostructure with enhanced photocatalysis, Nanomaterials., 2018, 8, 33.

[186]. Y. Yue, P. Zhang, W. Wang, Y. Cai, F. Tan, X. Wang, P. K. Wong, Enhanced dark adsorption and visible-light-driven photocatalytic properties of narrower-band-gap Cu_2S decorated Cu_2O nanocomposites for efficient removal of organic pollutants, J. Hazard. Mater., 2020, 384, 121302.

[187]. S. Balaji, R. K. Selvan, L. J. Berchmans, S. Angappan, K. Subramanian, C. O. Augustin. Combustion synthesis and characterization of Sn^{4+}substituted nanocrystalline $NiFe_2O_4$, Mater. Sci Eng. B, 2005, 119, 119-124.

[188]. Sohrabnezhad S, Rezaeimanesh M. Synthesis and characterization of novel magnetically separable $NiFe_2O_4$@ AlMCM-41-Cu_2O core-shell and its performance in removal of dye, Adv. Powder. Technol., 2017, 28, 3039-3048.

[189]. Z. He, Y. Xia, B. Tang, J. Su, Fabrication and photocatalytic property of magnetic $NiFe_2O_4$/Cu_2O composites, Mater. Res. Express, 2017, 4, 095501.

[190]. S. F. Yang, C. G. Niu, D. W. Huang, H. Zhang, C. Liang, G. M. Zeng, $SrTiO_3$ nanocubes decorated with Ag/AgCl nanoparticles as photocatalysts with enhanced visible-light photocatalytic activity towards the degradation of dyes, phenol and bisphenol A, Environ. Sci. J. Integr. Environ. Res.: Nano, 2017, 4, 585-595.

[191]. J. J. Guo, S. X. Ouyang, P. Li, Y. J. Zhang, T. Kako, J. H. Ye, A new heterojunction Ag_3PO_4/Cr-$SrTiO_3$ photocatalyst towards efficient elimination of gaseous organic pollutants under visible light irradiation, Appl. Catal. B, 2013,134-135, 286-292.

[192]. Y. M. Xia, X. Q. Yu, Z. M. He, Y. L. Lu, Y. F. Zhang, S. P. Sun, S. Q. Zhu, X. P. Li, Synthesis of novel copper-based oxide nanostructured film on copper via solution-immersion, Ceram. Int. 2017,43, 14499e14503

[193]. Y. Xia, Z. He, K. Hu, B. Tang, J. Su, Y. Liu, X. Li, Fabrication of n-$SrTiO_3$/p-Cu_2O heterojunction composites with enhanced photocatalytic performance, J. Alloys Compds., 2018, 753, 356-363.

[194]. K. Zhou, Y. Shi, S. Jiang, Y. Hu, Z. Gui, Facile preparation of Cu_2O/carbon sphere heterostructure with high photocatalytic activity, Mater. Lett., 2013, 98, 213-216. Cu_2O/ Carbon Nanotubes (CNTs)

[195]. Z. Ai, H. Xiao, T. Mei, J. Liu, L. Zhang, K. Deng, J. Qiu, Electro-Fenton degradation of rhodamine B based on a composite cathode of Cu_2O nanocubes and carbon nanotubes, J. Phys. Chem. C, 2008, 112,1192-11935.

[196]. Y.S. Luo, Q.F. Ren, J.L. Li, Z.J. Jia, Q.R. Dai, Y. Zhang, B.H. Yu, Synthesis and optical properties of multiwalled carbon nanotubes beaded with Cu_2O nanospheres, Nanotechnology, 2006, 17, 5836.

[197]. L. Yang, D. Chu, L. Wang, X. Wu, J. Luo, Synthesis and photocatalytic activity of chrysanthemum-like Cu_2O/Carbon Nanotubes nanocomposites, Ceram. Int., 2016, 42, 2502-2509.

[198]. Q. Zhao, J. Wang, Z. Li, Y. Qiao, Y. Guo, Preparation of Cu_2O/exfoliated graphite composites with high visible light photocatalytic performance and stability, Ceram. Int., 2016, 42, 13273-13277.

[199]. P. Khare, A. Singh, S. Verma, A. Bhati, A. K. Sonker, K. M. Tripathi, S. K. Sonkar, Sunlight-induced selective photocatalytic degradation of methylene blue in bacterial culture by pollutant soot derived nontoxic graphene nanosheets, ACS Sustain. Chem. Eng., 2018, 6, 579–589.

[200]. W. Du, M. Wu, M. Zhang, G. Xu, T, Gao, L. Qian, G. Shi, High-quality grapheme films and nitrogen-doped organogels prepared from the organic dispersions of grapheme oxide, Carbon, 2018,129, 15–20.

[201]. H. Yan, H. Wu, K. Li, Y. Wang, X. Tao, H. Yang, R. Cheng, Influence of the surface structure of graphene oxide on the adsorption of aromatic organic compounds from water, ACS Appl. Mater. Inter., 2015, 7, 6690–6697.

[202]. K. Tu, Q. Wang, A. Lu, L. Zhang, Portable visible-light photocatalysts constructed from Cu_2O nanoparticles and graphene oxide in cellulose matrix, The J. Phys. Chem. C, 2014, 118, 7202-7210.

[203]. J. Nie, C. Li, Z. Jin, W. Hu, J. Wang, T. Huang, Y. Wang, Fabrication of MCC/Cu_2O/GO composite foam with high photocatalytic degradation ability toward methylene blue, Carbohyd. Polym., 2019, 223, 115101.

[204].] H.L. Wang, L.S. Zhang, Z.G. Chen, J.Q. Hu, J.S. Liu, X.C. Wang, Chem. Soc. Rev. 2014, 43, 5234–5244.

[205]. A. Abulizi, G. H. Yang, J. J. Zhu. One-step simple sonochemical fabrication and photocatalytic properties of Cu_2O-rGO composites, Ultrason. Sonochem., 2014, 21, 129-135.

[206]. Y. C. Pu, H. Y. Chou, W. S. Kuo, K. H. Wei, Y. J. Hsu, Interfacial charge carrier dynamics of cuprous oxide-reduced graphene oxide (Cu_2O-rGO) nanoheterostructures and their related visible-light-driven photocatalysis, Appl. Catal. B, 2017, 204, 21-32.

[207]. W. Zou, L. Zhang, L. Liu, X. Wang, J. Sun, S. Wu, L. Dong, Engineering the Cu_2O-reduced graphene oxide interface to enhance photocatalytic degradation of organic pollutants under visible light, Appl. Catal. B, 2016, 181, 495-503.

[208]. W. Zhang, X. Li, Z. Yang, X. Tang, Y. Ma, M. Li, Y. Zhang, In situ preparation of cubic Cu_2O-RGO nanocomposites for enhanced visible-light degradation of methyl orange, Nanotechnology, 2016, 27, 265703.

[209]. J. Cai, W. Liu, Z. Li. One-pot self-assembly of Cu_2O/RGO composite aerogel for aqueous photocatalysis, A. Surf. Sci., 2015, 358: 146-151.

[210]. W. Zhang, B. Wang, C. Hao, Y. Liang, H. Shi, L Ao, W. Wang, Au/Cu_2O Schottky contact heterostructures with enhanced photocatalytic activity in dye decomposition and photoelectrochemical water splitting under visible light irradiation. J. Alloys Compds., 2016, 684, 445-452.

CHAPTER 2

Cu_2O Nanoparticle Hypercrosslinked Polymer Composites for the Visible-Light Photocatalytic Degradation of Methyl Orange

2.1 Introduction

In recent years, photocatalytic degradation of organic pollutants under visible light is regarded a promising way to solve the global energy crisis by using the inexhaustible solar energy. Among the numerous visible-light-driven photocatalysts, Cu_2O is a p-type semiconductor with narrow band gap energy ranging from 2.0-2.2 eV,[1,2] which could effectively utilize the large amount of visible light in the sunlight. Thusly, the Cu_2O based photocatalysts have been widely applied for the organic-pollutant decontamination nowadays. [3-5] However, there are still many constraints on its application, such as the instability in oxidizing conditions, the rapid recombination of photo-generated holes and electrons and the transformation of crystalline structure during the reaction. Therefore, further improvement of the Cu_2O photocatalytic characteristics is still required. Generally, this can be realized by compositing of it either with other materials, which include semiconductors such as TiO_2,[6,7] ZnO,[8] Fe_3O_4,[9] C_3N_4,[10] CdS,[11] AgBr,[12] and $BiVO_4$,[13] or conductive materials like the graphene oxide (GO),[14] reduced graphene oxide (RGO),[15] exfoliated graphite (EG),[16] carbon quantum dots (CQDs),[17] multi-walled carbon nanotube (MWCNTs),[18] carbon sphere (CS),[19] and polypyrrole (PPy).[20] However, photocatalytic efficiency and stability are still necessary to be further improved.

Hyper-cross-linked polymers (HCPs), a series of permanent microporous polymer materials with high surface areas, have been intensively used as solid absorbents for the treatment of wastewater, adsorption of organic vapors and so on.[21] Especially, HCPs

have abundant narrow micropores, which can let the adsorbate molecules transferred from the surface to the inner micropores so that the adsorption capacity and adsorption rate are greatly enhanced. In addition, HCPs have strong affinity towards organic molecules due to their hydrophobic skeleton.[22] Recently, a series of reasonably priced HCPs-based catalysts were reported for the organic transformations.[23-25] However, no studies have been reported yet on combining them with photocatalysts for the organic pollutants degradation by using visible light.

In this work, KAPs-B (Knitting Aromatic compound Polymers-Benzene), which is a kind of HCPs, was loaded on Cu_2O with various amounts by a one-step precipitation method.[26] The photocatalytic ability of the as-obtained catalyst was tested by degradation of methyl orange (MO) as the pollutant under visible light. Since KAPs-B is a hydrophobic, chemically robust and porous polymer with a structure that benzene rings are connected with methylene linkers (Fig 2.1), it is expected that the excellent adsorption ability of KAPs-B could enhance the catalytic performance of Cu_2O and meanwhile stabilize the Cu_2O in oxidizing environments.

2.2 Experimental

2.2.1 Chemicals and Materials

All chemicals (A. R. grade) were used without further treatment. Copper(II) chloride ($CuCl_2$) was provided by Tianjin Hongyan Chemical Corp. Sodium hydroxide, Hydroxylamine hydrochloride ($NH_2OH{\cdot}HCl$) and ethanol (EtOH) were provided by Tianjin Chemical Reagent Supply and Marketing Company.

2.2.2 Catalysts Preparation

KAPs-B was prepared by the method as reported in the reference[27]. The schematic diagram for the synthesis of KAPs-B/Cu_2O catalyst is shown in Figure 1. $CuCl_2$ was applied as the Cu_2O precursor. In a typical synthesis of KAPs-B loaded Cu_2O (KAPs-

B/Cu_2O), KAPs-B (0.007 g), deionized water (83.4 mL), EtOH (20 mL) and $CuCl_2$ solution (0.5 M, 5 mL) were successively added to a beaker (500 mL) with stirring and then ultrasound treated at 25 ℃ for 30 min. Thereafter, 9 mL of sodium hydroxide solution (1.0 M) and 30 mL of ethanol were added into the obtained suspension, and then 9.8 mL of $NH_2OH{\cdot}HCl$ solution (0.1 M) was rapidly introduced into it in a short time (5 s). After stirring for 10 minutes, the mixture was maintained for 3 hours with a constant temperature of 40 ℃ to enhance the growth of Cu_2O crystal. After that, the mixture was centrifuged for 10 minutes with the speed of 5000 rpm and the obtained solid was washed with mixed solution ($V_{H_2O}:V_{CH_3CH_2OH} = 1:1$). The operations of centrifugation and washing were conducted alternatively several times until the remaining reagents were completely removed. Finally, the solid was purified with 5 mL ethanol and dried at 35 ℃ under vacuum state. As such, 7 wt% of KAPs-B loaded Cu_2O (7% KAPs-B/Cu_2O) composite was obtained. Similarly, 1% KAPs-B/Cu_2O, 3% KAPs-B/Cu_2O, 5% KAPs-B/Cu_2O, 10% KAPs-B/Cu_2O composites were also synthesized by the same procedure. In addition, the pure Cu_2O without the loading of KAPs-B was synthesized using the same procedure.

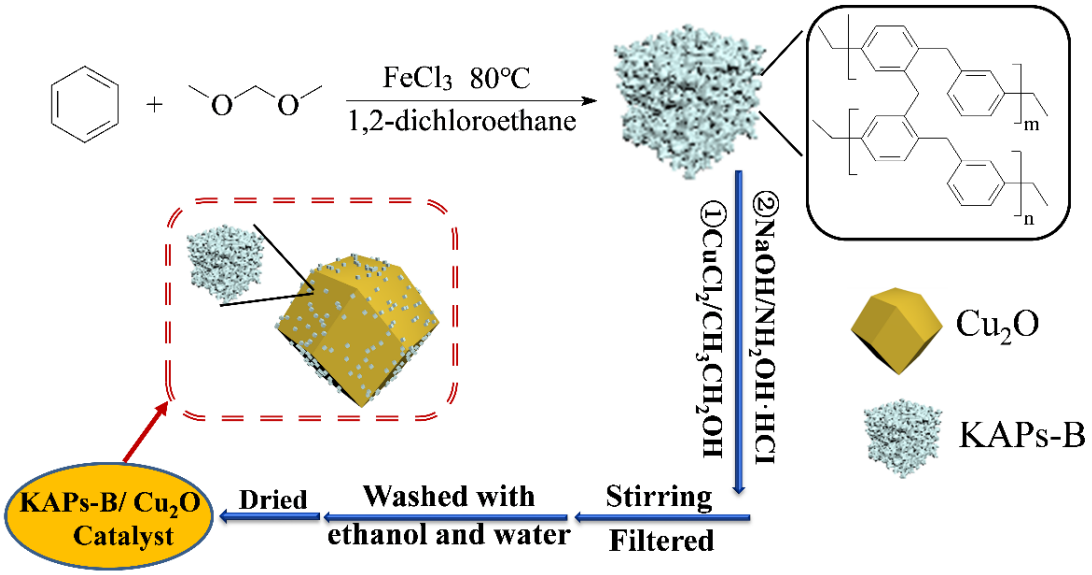

Figure 2.1 The schematic diagram for the synthesis process of KAPs-B/Cu_2O catalyst

2.2.3 Catalyst Characterizations

The crystal structure of the catalyst was measured by a Bruker D8 diffractometer in the 2θ range of 10-80° using Cu Kα radiation (λ = 1.5418 Å), the scanning rate is 4°/min during the test. Catalyst morphology and microstructure were characterized through a scanning electron microscope (SEM, TESCAN MAIA 3 LMH) and high-resolution transmission electron microstructure (HRTEM, JEOLJEM-2999FMII apparatus). Brunauer-Emmett-Teller (BET) surface area was measured on a Micrometrics ASAP-2020 PLUS HD88 adsorption apparatus using nitrogen adsorption at 77 K. UV-vis diffuse reflectance spectroscopy (UV-vis DRS) of catalyst powders was measured by an analytic Jena SPECORD® 210 PLUS spectrophotometer with $BaSO_4$ as the reference in the wavelength ranged from 200 to 800 nm. FT-IR spectrum was obtained by using a FTIR apparatus (CDS-2000 Bio-Rad FTS-165). X-ray photoelectron spectroscopy (XPS) spectrum was obtained by using a Thermo Fisher Scientific Escalab 250Xi system. Total organic carbon (TOC) analysis was conducted by a TOC/TNb Analyzer (Multi N/C 2100, Analytik Jena, Germany). The photocurrent response was measured in Na_2SO_4 solution (0.2 M) under the irradiation of visible-light, Ag/AgCl electrode was used as the reference and a Pt electrode was used as the counter. EIS measurements were conducted in a 2.5 mM $[Fe(CN)_6]^{3-/4-}$ solution with 0.1 M KCl at the open circuit potential.

2.2.4 Catalyst Activity Evaluation

The photocatalytic activity of the sample was tested by the degradation of MO in a double-jacket reactor, where a 500 W Xenon lamp with a cut off filter of 420 nm (CEL-S500, Beijing China Education Au light Co. Ltd) was used to provide the visible light. In a typical run, the photocatalyst (30 mg) was introduced into 90 mL of MO aqueous solution (30 mg/L) at first. Before the irradiation, the mixture was continuously stirred in dark for 50 minutes to achieve an adsorption equilibrium state. After that, the light

was turned on. Under continuous stirring at ambient temperature, 4 mL of suspension was extracted at the selected time interval, and the supernatant solution was obtained by centrifugal separation and then analyzed by a model 722E spectrophotometer at 464 nm. The photocatalytic efficiency (E) of the catalyst for MO degradation was calculated by using the following equation:

$$E = (1-C/C_0)\times 100\%$$

Herein, C_0 is the initial MO concentration and C the concentration at the time t for the sampling.

2.2.5 Photocatalytic Mechanism Investigation

The potential reactive species participating in the degradation process was studied by using different scavengers. In this study, isopropyl alcohol (IPA) was added as scavengers for hydroxyl radicals (OH•)[28] and ammonium oxalate (AO) for holes (h^+).[29] The proving experiment on the formation of $\bullet O_2^-$ was done under the atmosphere of nitrogen. 1 mM IPA or AO was added to the MO solution before adding the 7% KAPs-B/Cu_2O catalyst, and all other conditions of photocatalytic degradation experiment remained the same as before.

2.3 Results and discussion

2.3.1 Photocatalyst characterizations

XRD patterns of KAPs-B/Cu_2O catalysts with different loading amounts are presented in Fig 2.2. Herein, the peaks at 2θ of 29.3°, 36.2°, 42.1°, 61.3°, and 73.4° belong to the (110), (111), (200), (220), and (311) planes of Cu_2O, and no other peaks corresponding to other copper species (Cu and CuO) were found, implying that only pure Cu_2O existed in the composites. In addition, it should be noted that KAPs-B were amorphous materials and the formation of Cu_2O was not affected by the presence of KAPs-B during the synthesis process.

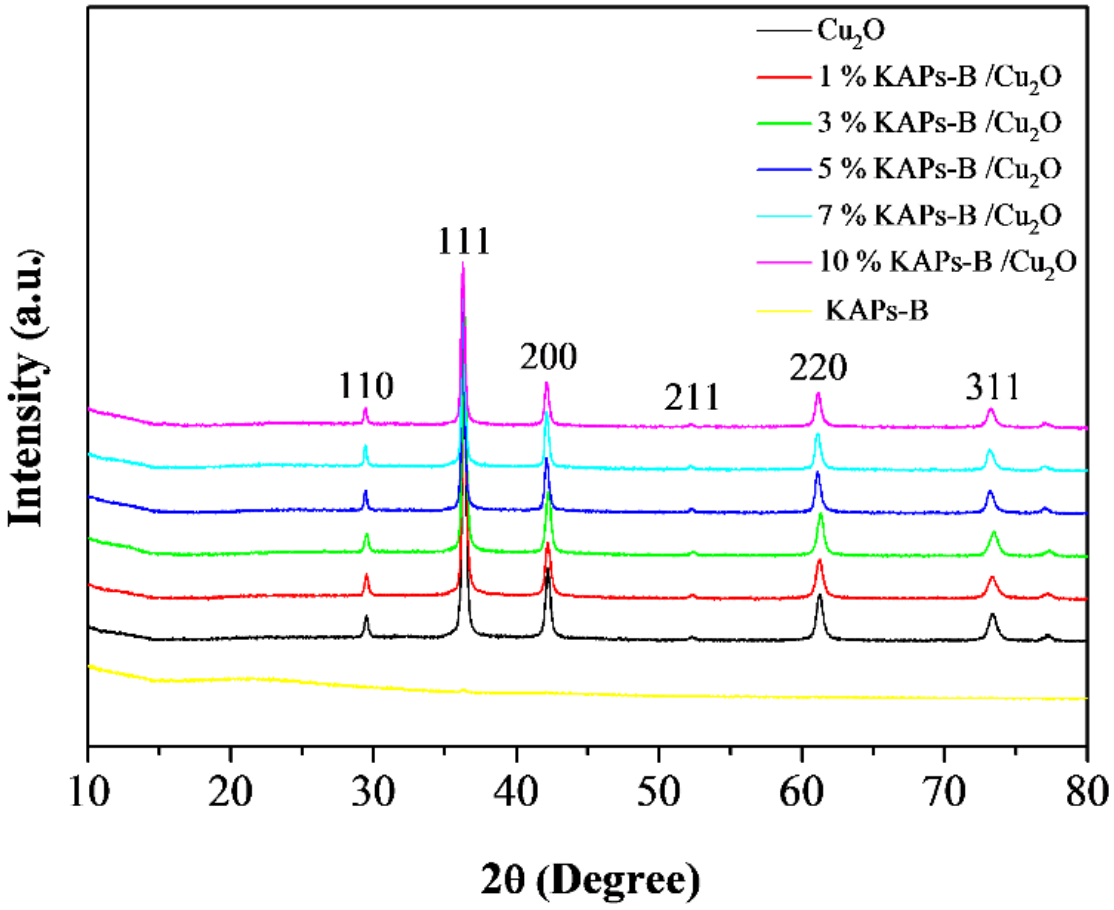

Figure 2.2 XRD patterns of KAPs-B/Cu_2O catalysts with different KAPs-B loading amounts.

The morphologies of as-prepared KAPs-B/Cu_2O catalysts and the typical TEM image are given in Fig 2.3 and Fig 2.4. One can see that the Cu_2O had rhombic dodecahedral structure in all samples with an average particle size of about 200-250 nm. In addition, with the increase in the amount of KAPs-B in the preparation process, the KAPs-B loading amount on the surface of Cu_2O increased. HRTEM images (the last one in Fig 2.3 and enlargement image in Fig 2.4) indicate that the KAPs-B combined with the Cu_2O surface very well.

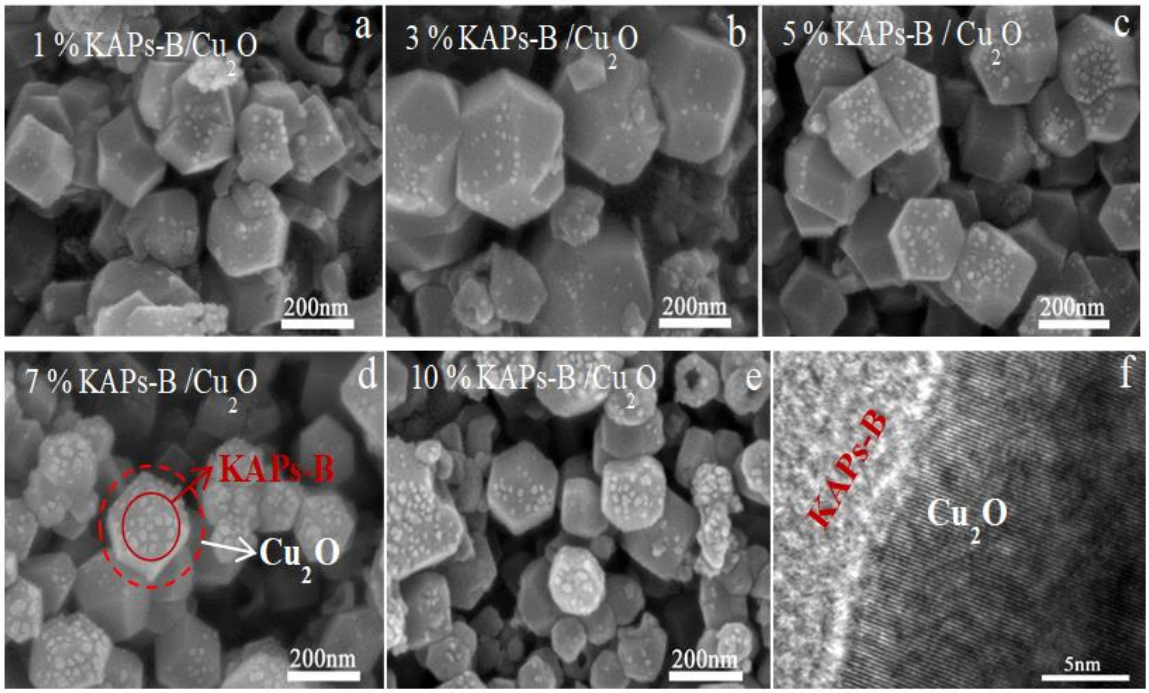

Figure 2.3 (a-e) SEM images of KAPs-B/Cu_2O catalysts with different KAPs-B loading amounts and (f) HRTEM image of 7%KAPs-B/Cu_2O catalyst.

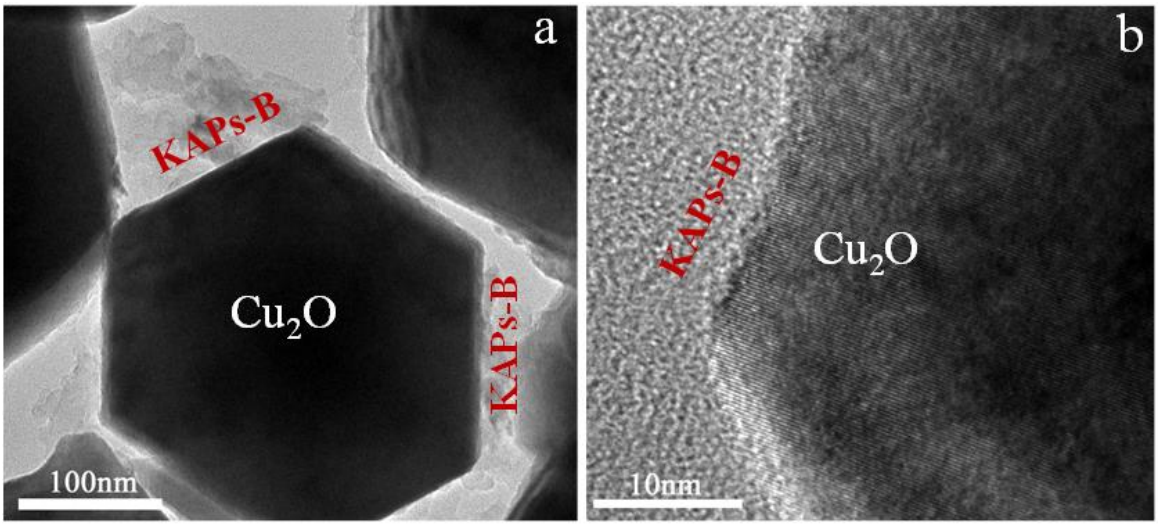

Figure 2.4 (a) TEM and (b) HRTEM image of 7% KAPs-B/Cu_2O catalyst.

The chemical structures of KAPs-B, Cu_2O and KAPs-B/Cu_2O catalysts were provided by FT-IR analysis. Fig 2.5 shows the characteristic vibration bands of the samples. One can see that the characteristic peaks of skeletal stretching of the aromatic ring in the 1450-1600 cm^{-1} region were obvious for KAPs-B.[24] For Cu_2O, the absorption peak observed at 623 cm^{-1} correspond to the Cu(I)-O bond vibrations [10]

while the sharp peak observed at 3420 cm^{-1} corresponds to the stretching vibration of OH. These results indicate that KAPs-B were successfully loaded on the Cu_2O particles.

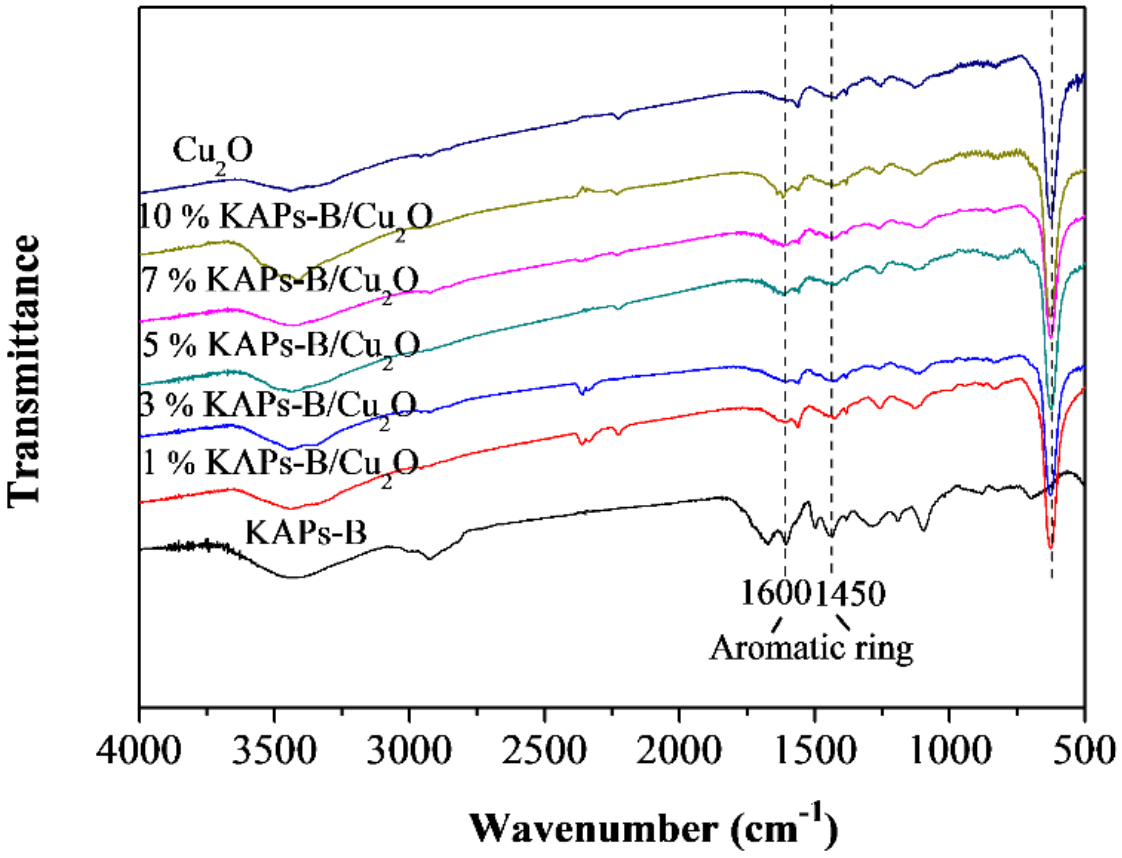

Figure 2.5 FT-IR spectra of KAPs-B/Cu_2O catalysts with different KAPs-B loading amounts.

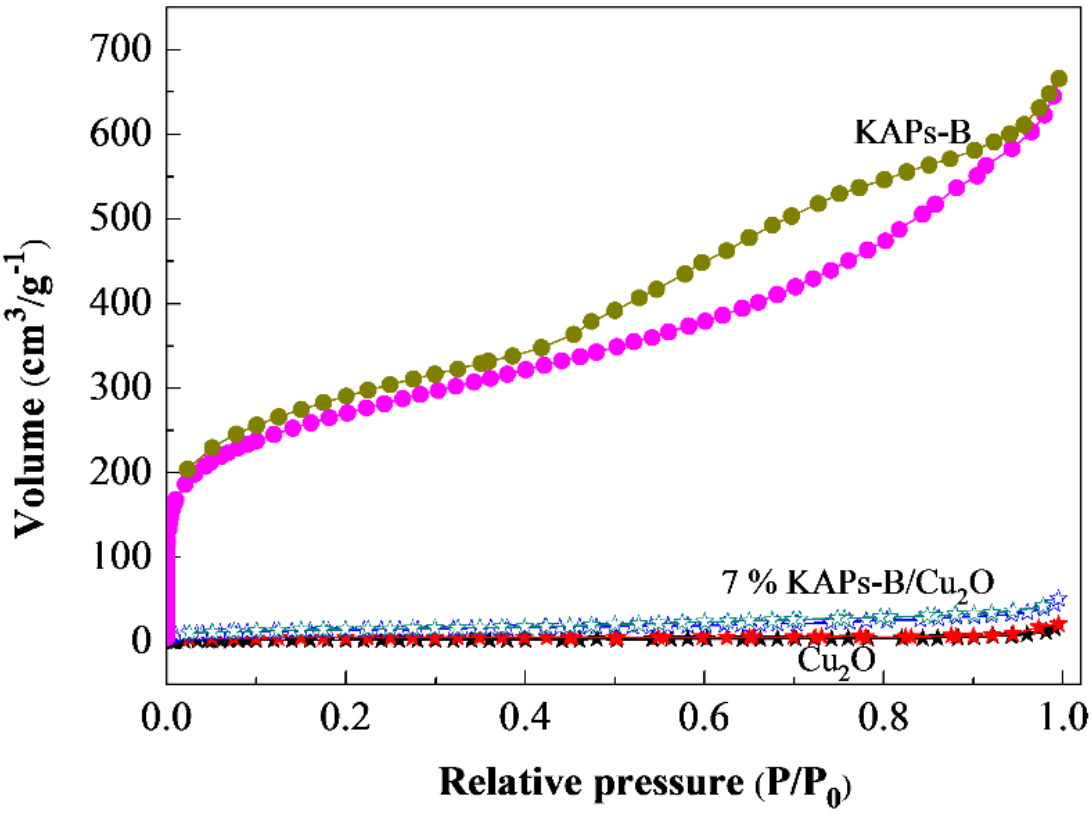

Figure 2.6 N_2 adsorption-desorption isotherms of KAPs-B, Cu_2O and 7% KAPs-B/Cu_2O.

Fig 2.6 shows the typical N_2 adsorption-desorption isotherms of KAPs-B, Cu_2O and 7% KAPs-B/Cu_2O, and the corresponding BET surface areas are summarized in Tab 2. 1. One can see that the surface areas of pure KAPs-B and Cu_2O were 983.00 m^2g^{-1} and 8.09 m^2g^{-1}, respectively. It is obvious that Cu_2O had very low specific surface area while KAPs-B had a high surface area microporous structure. By the loading of KAPs-B on Cu_2O, the obtained catalyst (7% KAPs-B/Cu_2O) exhibited a larger surface area (49.70 m^2g^{-1}) than the pure Cu_2O, which should be beneficial for the enhancement of organic pollutants adsorption on the photocatalyst.

Table 2. 1 BET surface areas of KAPs-B, Cu_2O and 7% KAPs-B/Cu_2O

Sample	Surface area (m^2/g)
KAPs-B	983.00
7% KAPs-B/Cu_2O	49.70
Cu_2O	8.09

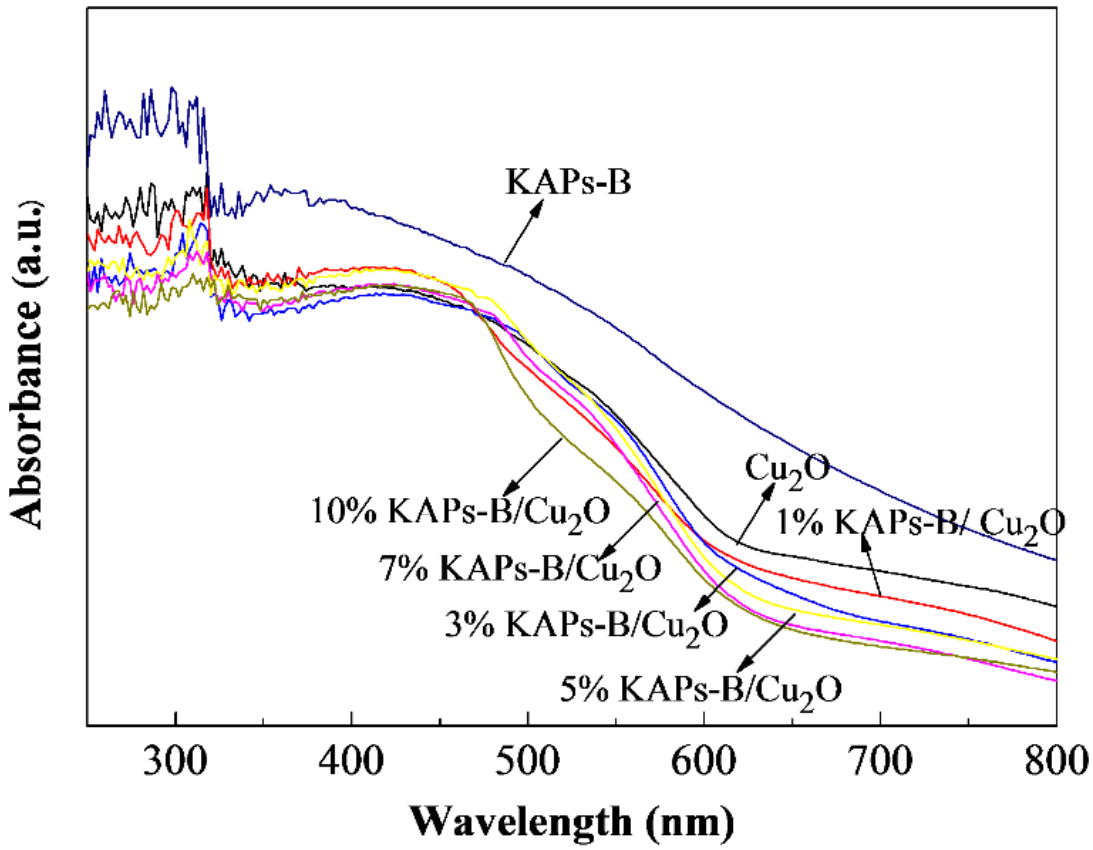

Figure 2.7 UV-vis DRS of KAPs-B/Cu_2O catalysts with different KAPs-B loading amounts.

Fig 2.7 shows the UV-vis DRS of KAPs-B, Cu_2O and KAPs-B/Cu_2O catalysts with different KAPs-B loading amounts. One can see that pure Cu_2O had a strong absorption with the absorption edge at about 630 nm, but KAPs-B displayed no noticeable adsorption peak for visible light. Moreover, with the increase in the loading amount of KAPs-B, the absorption edge of the KAPs-B/Cu_2O catalysts was almost no

red-shifting when comparing with that of the pure Cu_2O, but the absorbance was weakened slightly when compared with that of pure Cu_2O. Thusly, the KAPs-B/Cu_2O catalyst remained the main photo adsorption property of Cu_2O so that they could work under the visible light irradiation.

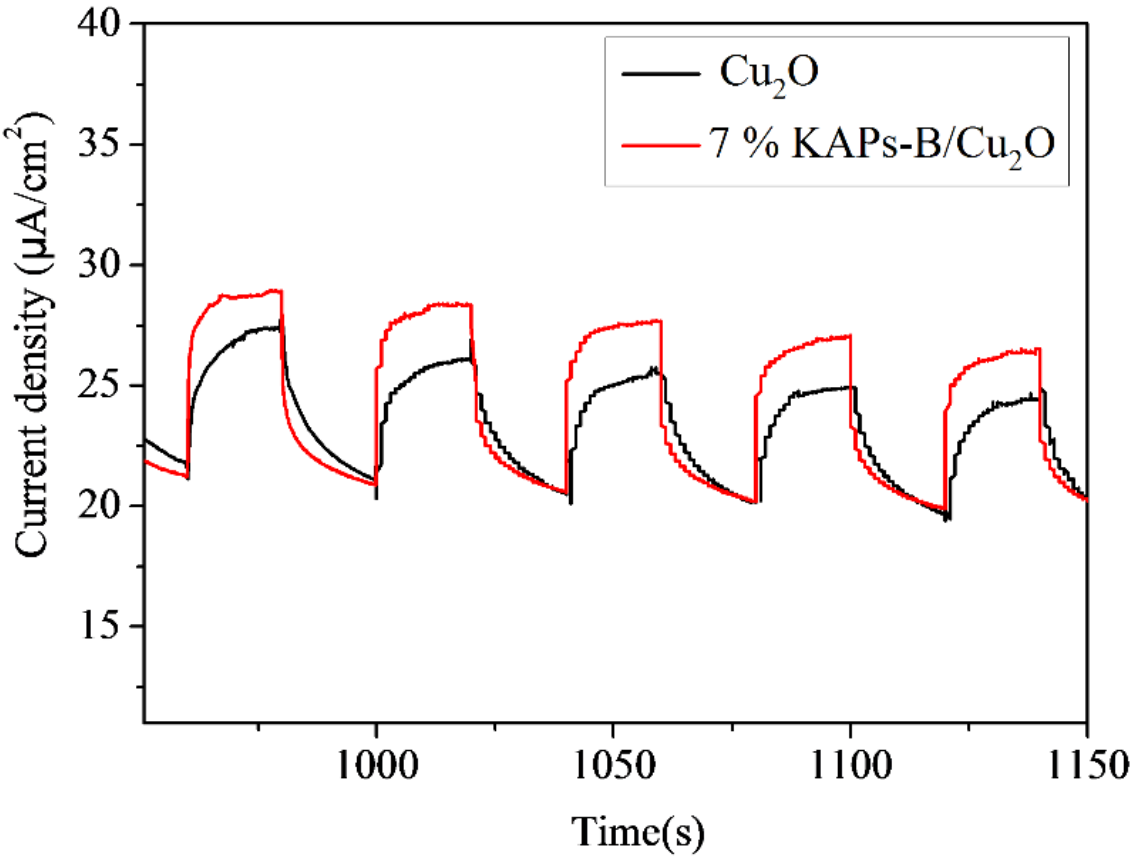

Figure 2.8 Photocurrent responses of Cu_2O and 7% KAPs-B/Cu_2O

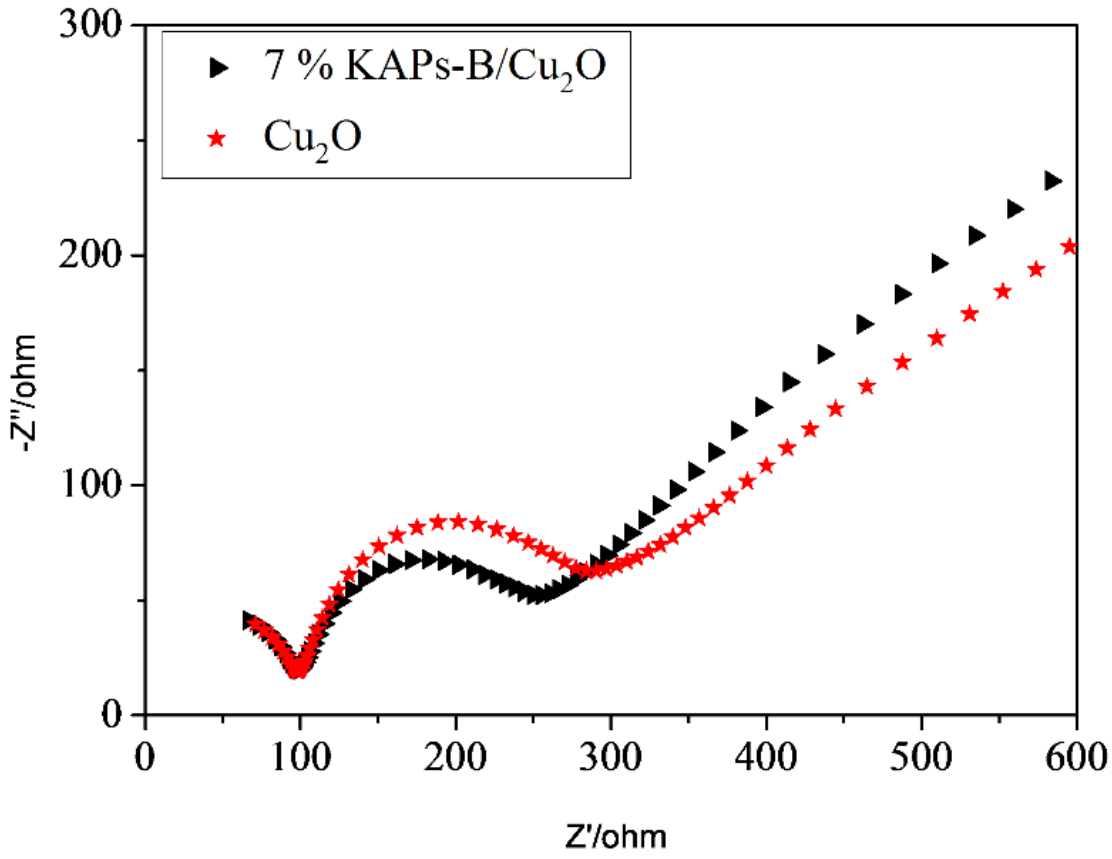

Figure 2.9 EIS Nyquist plots of the Cu_2O and 7% KAPs-B/Cu_2O.

To further investigate the efficiency of charge separation, the measurements of photocurrent and electrochemical impedance spectroscopy (EIS) were performed, and the results are presented in Fig 2.8 and Fig 2.9. From Fig 2.8, one can see that a higher current density was obtained in the case of 7% KAPs-B/Cu_2O catalyst, implying a larger photoinduced electron-hole pairs separation rate in it. [30,31] From Fig 2.9, one can see that the EIS Nyquist plot in the case of 7% KAPs-B/Cu_2O catalyst exhibited a smaller circular radius when comparing with the pure Cu_2O, indicating a fast charge carriers transportation and effective charge departure, further confirming that the loading of KAPs-B can effectively promote the photo-degradation process.[32]

2.3.2 Photocatalytic performance

Photocatalytic degradations of MO in aqueous solutions over various KAPs-B/Cu_2O composites under visible light were performed. As presented in Fig 2.10, after 50 min adsorption-desorption equilibrium test in the dark, the MO concentration dropped significantly, implying that a large amount of MO in the solution were adsorbed by the microporous KAPs-B on the surfaces of Cu_2O particles. Under the visible light irradiation, as the initial KAPs-B content on the Cu_2O particles was increased from 1 to 7 wt%, the photocatalytic activity was improved obviously. However, when the content of KAPs-B is greater than 7 wt %, the photocatalytic degradation efficiency did not increase significantly. For the 7% KAPs-B/Cu_2O catalyst, one can see that approximately 92% of MO was decomposed within 60 minutes. Comparing the reaction rates at the initial stage (0-10 min) of the photocatalytic reaction, C/C_0 was reduced from 0.74 to 0.41 in the presence of 7% KAPs-B/Cu_2O, while it was reduced from 0.92 to 0.70 in the presence of bare Cu_2O. Larger reduction of the MO concentration over 7% KAPs-B/Cu_2O than bare Cu_2O implies that the loading of KAPs-B can effectively promote the photo-degradation process.

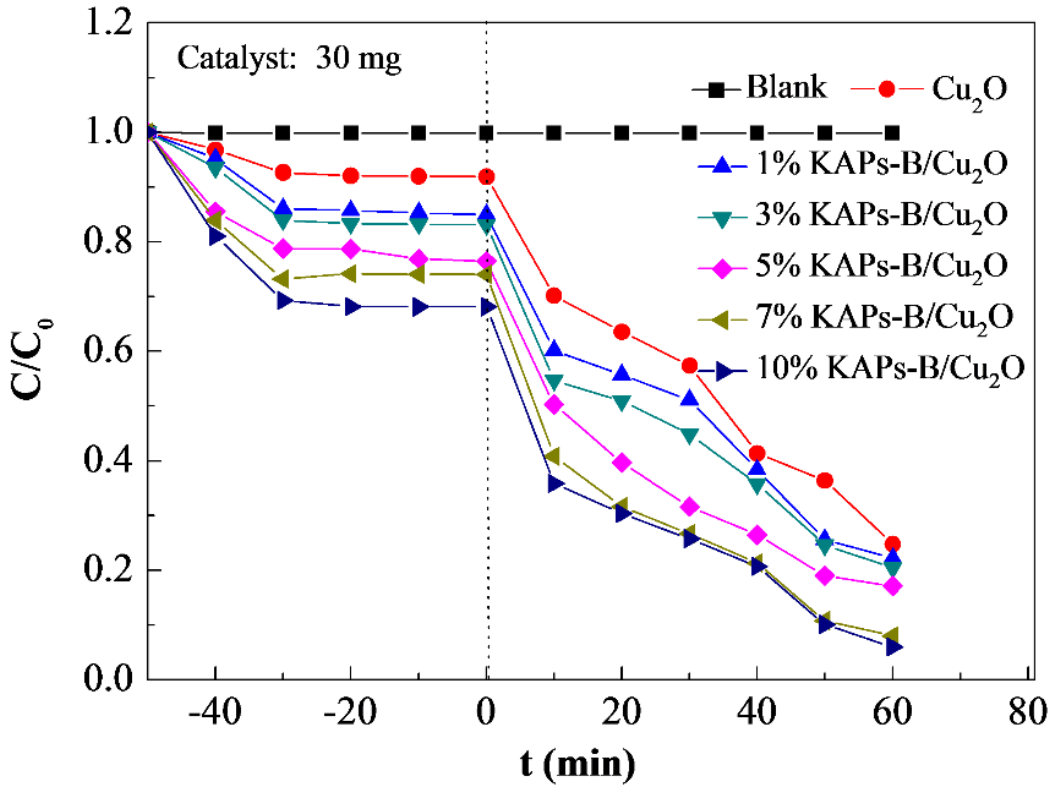

Figure 2.10 Photocatalytic degradation curves of MO degrading over Cu_2O and KAPs-B /Cu_2O composites with the degradation time.

Generally, the photocatalytic activity of Cu_2O-based catalyst is largely rely on the surface area, light-adsorption ability, the stability of Cu^+ species and the recombination rate of photo-generated electrons and holes.[33] As presented in Fig 2.3, with the increase in KAPs-B loading amount, more KAPs-B covered on the surface of Cu_2O particles, which should decrease the photo-adsorption area of Cu_2O. As shown in Fig 2.7, excessive loading of KAPs-B would weaken the absorbance to the visible light because KAPs-B was a material with weaker absorbance. Therefore, when the content of KAPs-B is greater than 7 wt %, the photocatalytic performance became weakened. As a result, in this work, the 7% KAPs-B/Cu_2O exhibited the highest photocatalytic activity among all samples.

Furthermore, the mineralization ratio of MO in water over 7% KAPs-B/Cu_2O under visible light was evaluated by the total organic carbon (TOC) analysis. As seen in Fig 2.11, the removal of TOC was about 35% after 30 min reaction and about 80.4%

after 60 min reaction. However, the TOC changed very little with the further increase of time under visible-light illumination. It indicated that about 80.4% organic carbon of MO was decomposed into inorganic carbon (CO_2) after a long-term photodegradation.

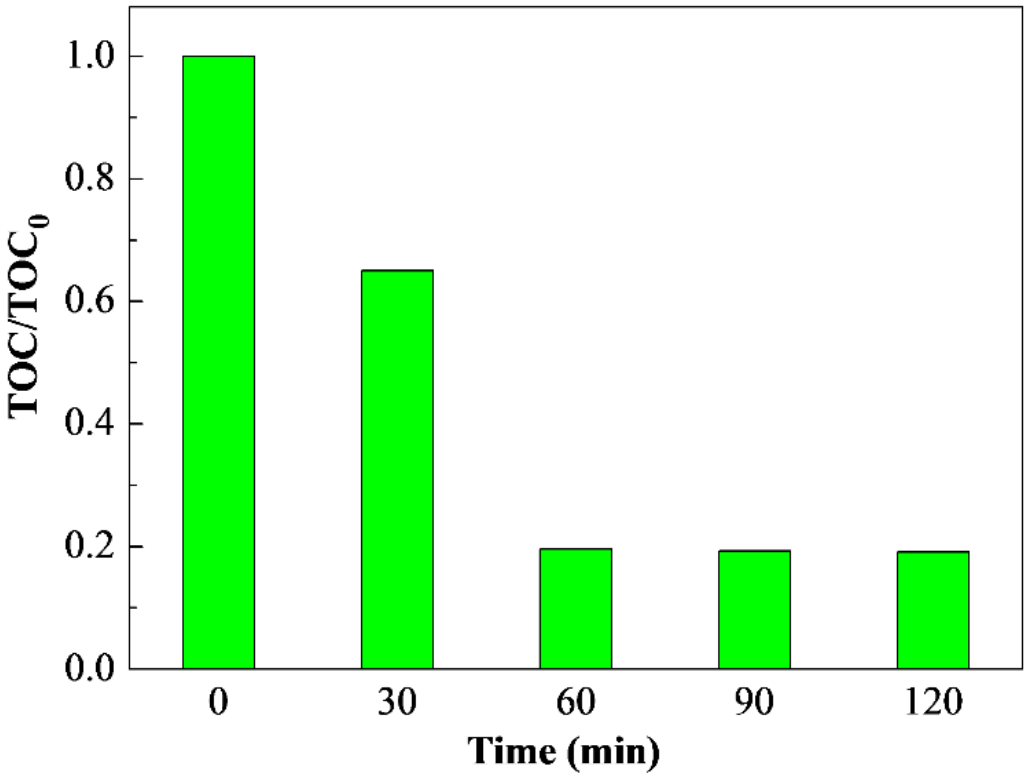

Figure 2.11 The removal of TOC over 7% KAPs-B/Cu_2O under visible light irradiation.

The stability of photocatalyst is an important factor in the course of application. Fig 2.12 shows the catalytic stability of 7% KAPs-B/Cu_2O for the MO degradation for 10 cycles. As presented in Fig 2.12, the photocatalytic conversion of MO maintained at approximately 88.6% after 10-cycle reusing of the spent catalyst. It indicated that this catalyst was stable and can be reused for several times. Fig 2.13 compares XRD patterns, UV-vis spectra, XPS spectra of 7% KAPs-B/Cu_2O catalyst before and after the 5-cycle testing. One can see that the XRD patterns (Fig 2.13 a) of the catalyst before and after the 5-cycle testing maintained almost unchanged while the UV-Vis DRS spectra (Fig 2.13 b) changed a little. The XPS survey spectra given in Fig 2.13 c indicate the

presences of Cu, O and C, and the catalyst spectrum mainmained almost unchanged before and after 5 cycles test. The chemical states of copper are shown in Fig 2.13 d. One can see that the Cu 2p XPS spectrum of the fresh catalyst exhibited two main peaks at 932.2eV and 951.9eV, corresponding to the Cu $2p_{1/2}$ and Cu $2p_{3/2}$ peaks of Cu^{+}, respectively.[28] However, distinguishing Cu^{0} and Cu^{+} from the Cu 2p XPS spectrum is difficult. According to previous report[29], the Cu LMM spectrum provides a clear means to differentiate the two states of oxidation. Fig 2.13 d shows the Cu LMM spectrum. One can see that no peak was observed at 918.6 eV for Cu^{0} species. The Cu LMM spectrum implied that Cu metal was not formed in catalyst. It can be concluded that Cu_2O was the only reduced species from Cu^{2+}, and there were no CuO and Cu species in fresh catalyst. However, after photocatalytic decolorization of MO solutions for 5 cycles, a small peak at 934.1 eV, which is attributed to Cu^{2+} in CuO, was detected, indicating that only a few amounts of Cu_2O on the KAPs-B/Cu_2O surface was changed to CuO after the photocatalytic degradation of MO for five cycles. However, it should be noted that the generated CuO amount was too low to be observed in XRD spectrum. The above results indicated that the Cu_2O stability was improved obviously by combining with KAPs-B.

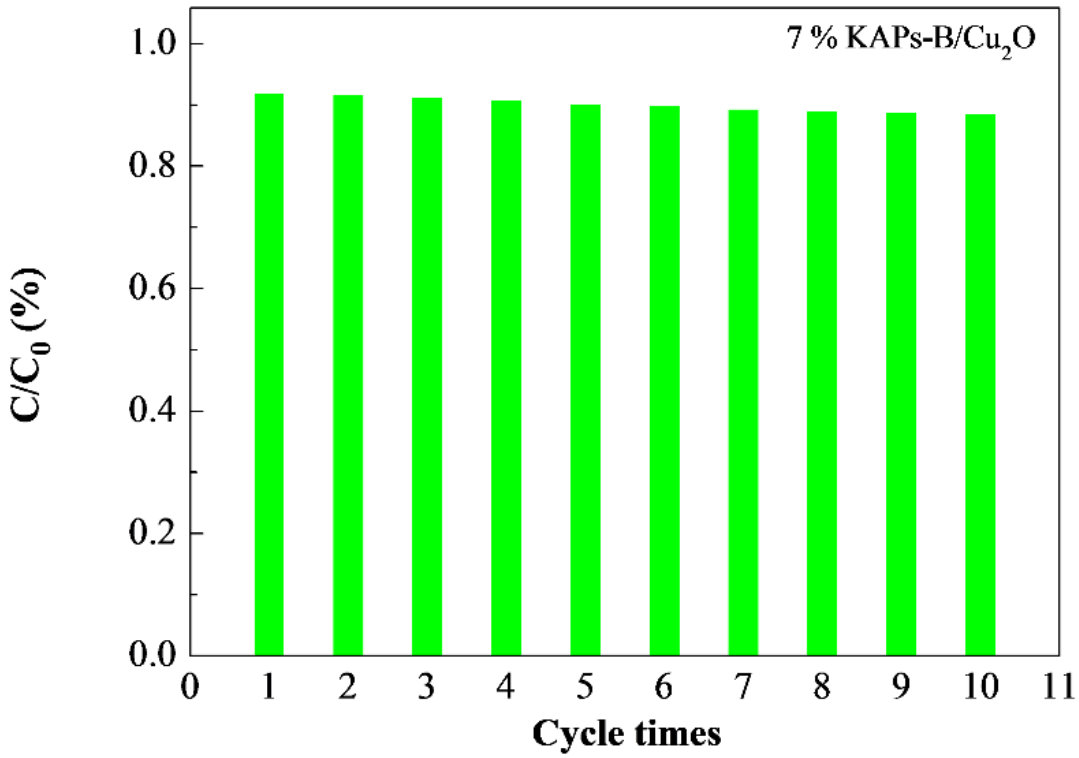

Figure 2.12 Stability test of MO photocatalytic degradation under visible light by reusing the spent 7% KAPs-B/Cu_2O catalyst.

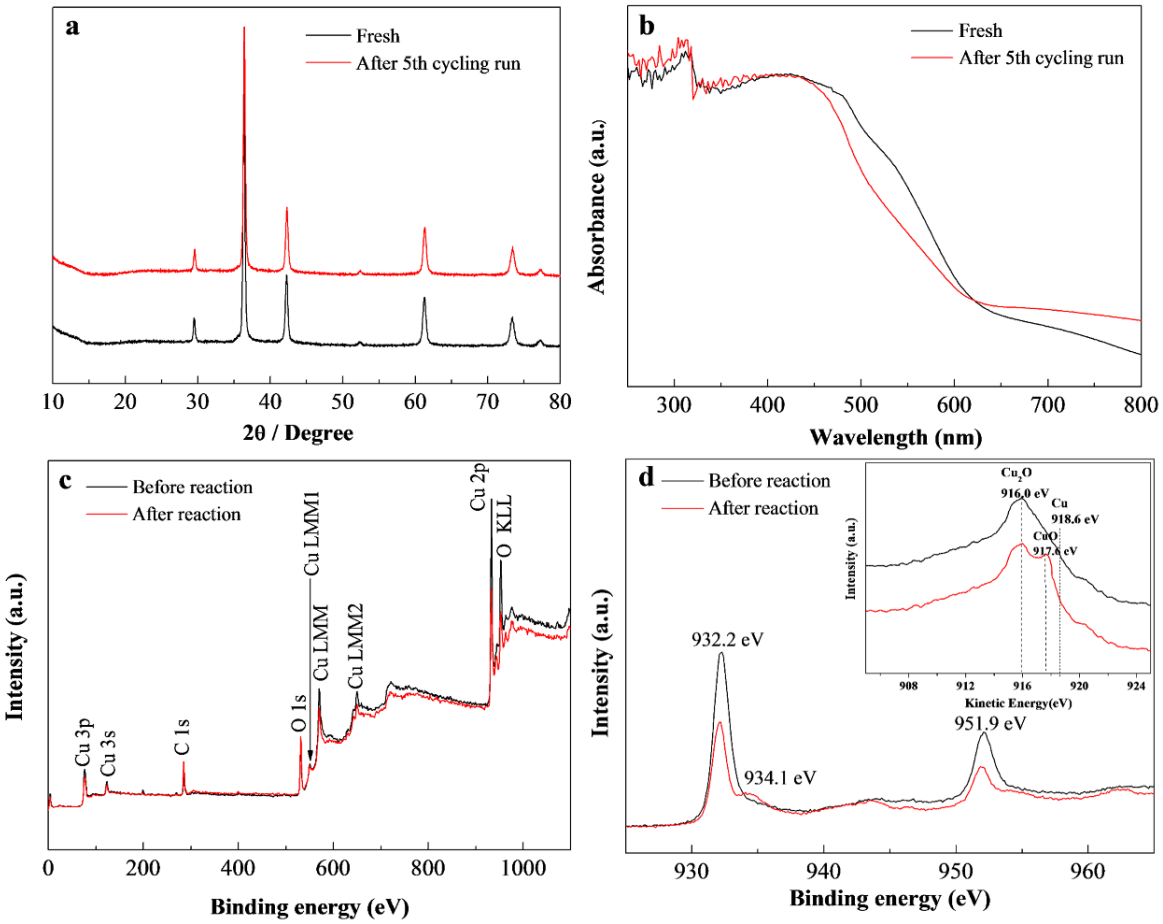

Figure 2.13 The characterizations of 7% KAPs-B/Cu_2O catalyst before and after photocatalytic decolorization of MO for 5-cycle testing. (a) XRD; (b) UV-Vis DRS; (c) Survey spectra; (d) The Cu 2p XPS spectra and the Cu LMM spectrum.

2.3.3 Photocatalytic mechanism

In order to reveal the photocatalysis mechanism of MO degradation over the KAPs-B/Cu_2O catalyst, the active species trapping experiments were carried out. Isopropyl alcohol (IPA) was introduced in reaction system as a HO• scavenger[28] and ammonium oxalate (AO) was introduced as a h^+ scavenger.[29] As presented in Fig 2.14, the addition of IPA did not bring obvious change during the MO degradation process, suggesting

that •OH should not play an important role as the active species involved in the reaction.[33] However, only a slight degradation of MO was observed when AO was added, which clearly suggested that the h^+ radicals were the major species participated in the MO degradation.[34] Besides, it also can be seen that the photocatalytic activity decreased under N_2 purging. During the photodegrading process, oxygen molecules were converted to O_2^-• by the photo-induced electrons on the KAPs-B/Cu_2O surface. Thusly, the O_2^-• and h^+ could be the major active species in the KAPs-B/Cu_2O photocatalyst system.

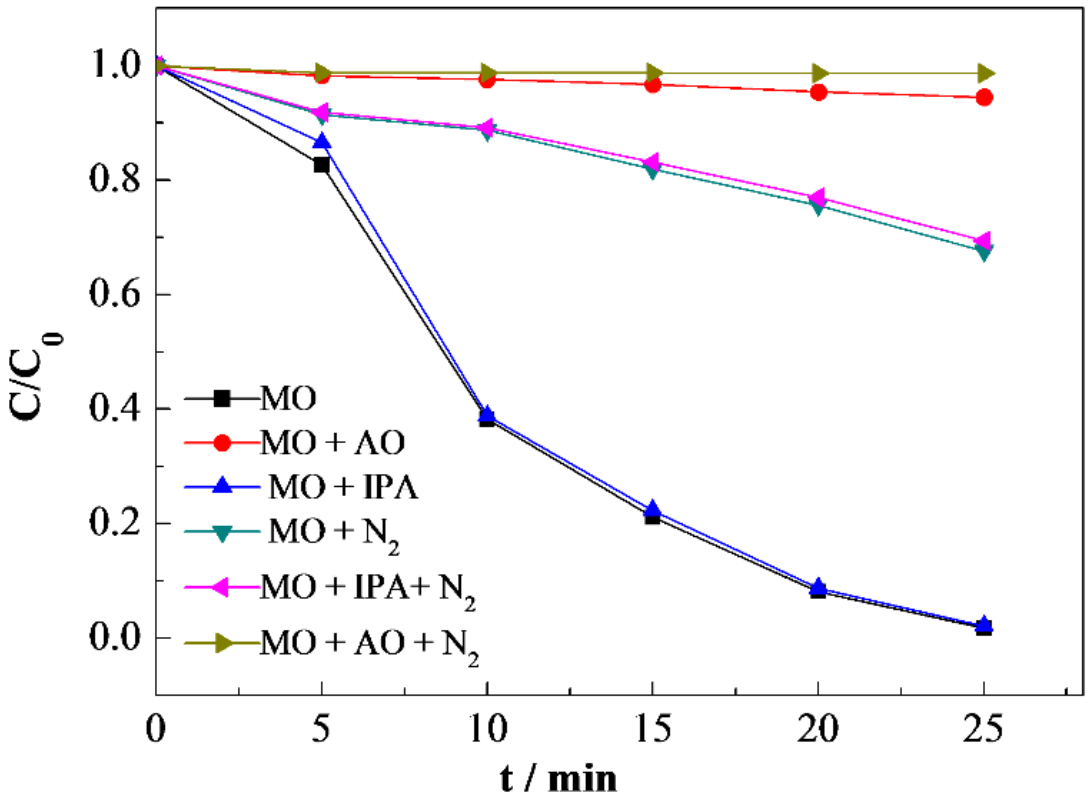

Figure 2.14 Active species trapping experiments with 7% KAPs-B/Cu_2O under visible light irradiation (AO: ammonium oxalate; IPA: isopropyl alcohol)

From these experimental results, the mechanism of MO photocatalytic degradation over KAPs-B/Cu_2O under visible-light irradiation can be illustrated as that illustrated in Fig 2.15.

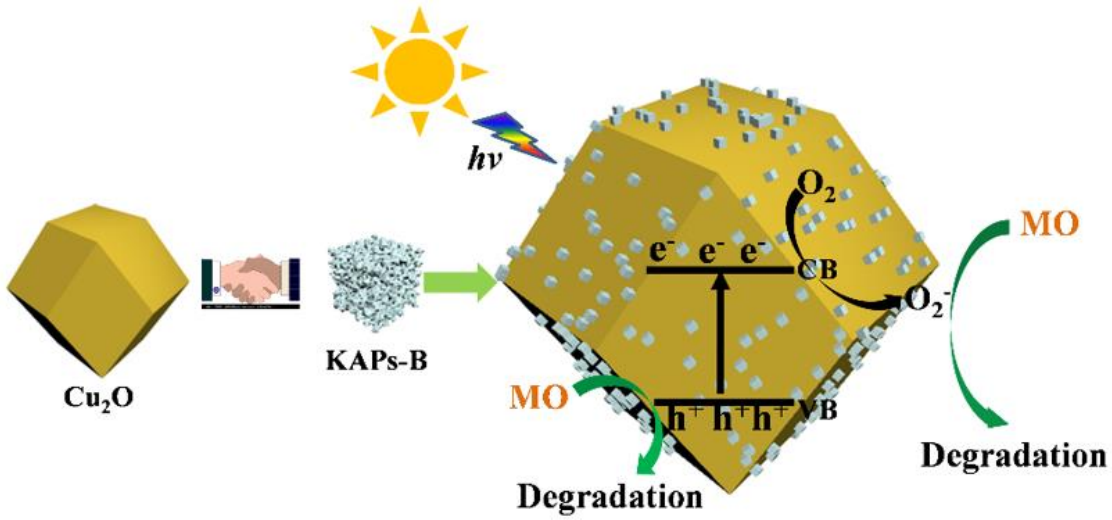

Figure 2.15 Photocatalytic mechanism of MO degradation over KAPs-B/Cu_2O under visible-light irradiation.

When the as-prepared catalyst is added in the MO solution, due to the strong absorption ability of KAPs-B, MO is quickly absorbed on the surface of KAPs-B and then moves from the surface to inner micropores through the microchannels and reaches the Cu_2O.[22] Under visible light illumination, the electrons of Cu_2O can be excited from the valence band (VB) to the conduction band (CB), resulting in the formation of holes in the conduction band. The generated h^+ with more positive potential (+1.91 V vs. NHE) has strong oxidization and could directly react with the adsorbed MO. It has been proven that h^+ on the Cu_2O is one of the major active species involving in the organic pollutants photo-degradation. Since the VB potential of Cu_2O is not positive compared with that of •OH/OH^-(H_2O) (+2.38 V vs. NHE),[13] the generated abundant holes h^+ on the VB of Cu_2O hardly oxidize the OH^-/H_2O absorbed on the catalyst surface to yield active species •OH. Thusly, the •OH should not be an important contributor to the photocatalytic process. In addition, the electrons on the CB potential of Cu_2O could be received by the KAPs-B molecule, electron distribution in the benzene rings could rearrange, leading to the overlapping of electronic structure [35]. The conductivity of the photocatalyst enhanced. The electrons could reduce the adsorbed O_2 to generate active

species $\bullet O_2^-$, because the CB potential of Cu_2O (-0.26 V) is more negative compared with $O_2/\bullet O_2^-$(-0.046 V vs. NHE). The active species $\bullet O_2^-$ have high oxidation activity and can result in the degradation of the MO. Based on the above analysis, it can be considered that the photo-generated h^+ radicals and $\bullet O_2^-$ are the major active species involved in the degradation of MO. It was also identified by the active species trapping experiments. Because the generated $\bullet O_2^-$ and h^+ could react with the adsorbed MO efficiently, the recombination rate of photo-generated electrons and holes in the catalyst would be reduced. As a result, the photocatalytic efficiency of this catalyst can be obviously enhanced.

2.4 Conclusions

In this work, the visible-light-induced KAPs-B/Cu_2O photocatalysts, in which KAPs-B with high specific surface area dispersed over the rhombic dodecahedral Cu_2O particles, were successfully synthesized. The average particle size of Cu_2O was about 200-250nm. The obtained KAPs-B/Cu_2O photocatalysts showed an obviously improved photocatalytic activity and stability under visible light for the MO degradation when compared with the bare Cu_2O. The KAPs-B/Cu_2O photocatalyst with 7.0% KAPs-B exhibited the highest photocatalytic performance, by which approximately 92% of MO was decomposed within 60 minutes. The active species trapping experiments indicated that $O_2^{-}\bullet$ and h^+ could be the major active species in the KAPs-B/Cu_2O photocatalyst system. This study can provide a new opportunity to develop KAPs-B loaded photocatalysts for organic pollutants removal.

References

[1]. Jiang, T.; Xie, T.; Yang,W.; Chen, L.; Fan, H.; Wang, D. Photoelectrochemical and Photovoltaic Properties of p-n Cu_2O Homojunction Films and Their Photocatalytic Performance. J. Phys. Chem. C 2013, 117, 4619-4624.

[2]. Yang, C.; Wang, J.; Mei, L.; Wang, X. Enhanced Photocatalytic Degradation of Rhodamine B by Cu_2O Coated Silicon Nanowire Arrays in Presence of H_2O_2. J. Mater. Sci. Technol. 2014, 30, 1124-1129.

[3]. Huang, W. C.; Lyu, L. M.; Yang, Y. C.; Huang, M. H. Synthesis of Cu_2O Nanocrystals from Cubic to Rhombic Dodecahedral Structures and Their Comparative Photocatalytic Activity. J. Am. Chem. Soc. 2011, 134, 1261-1267.

[4]. Zhang A. Y.; He, Y. Y.; Lin, T.; Huang, N. H.; Xu, Q.; Feng, J. W. A Simple Strategy to Refine Cu_2O Photocatalytic Capacity for Refractory Pollutants Removal: Roles of Oxygen Reduction and Fe(ii) Chemistry. J. Hazard. Mater. 2017, 330, 9-17.

[5]. Yoon, S.; Kim, M.; Kim, I. S.; Lim, J. H.; Yoo, B. Manipulation of Cuprous Oxide Surfaces for Improving Their Photocatalytic Activity. J. Mater. Chem. A. 2014, 2, 11621-11627.

[6]. Ye, F.; Su, Y.; Quan, X.; Chen, S.; Yu, H.; Li, H. Constructing Desired Interfacial Energy Band Alignment of Z-Scheme TiO_2-Pd-Cu_2O Hybrid by Controlling the Contact Facet for Improved Photocatalytic Performance. Appl. Catal. B-Environ. 2019, 244, 347-355.

[7]. Xu, X.; Gao, Z.; Cui, Z.; Liang, Y.; Li, Z.; Zhu, S.; Yang, X.; Ma, J. Synthesis of Cu_2O Octadecahedron/TiO_2 Quantum Dot Heterojunctions with High Visible Light Photocatalytic Activity and High Stability. ACS Appl. Mater. Inter. 2016, 8(1): 91-101.

[8]. Gao, S.; Zhang, J.; Li, W.; Jiao, S.; Nie, Y.; Fan, H.; Zhang, X. Near Room Temperature and Large-Area Synthesis of ZnO/Cu_2O Heterojunction for Photocatalytic Properties. Chem. Phys. Lett. 2018, 692, 14-18.

[9]. Li, Z. P.; Wen, Y. Q.; Shang, J. P.; Wu, M. X.; Wang, L. F.; Guo, Y. Magnetically Recoverable Cu_2O/Fe_3O_4 Composite Photocatalysts: Fabrication and Photocatalytic Activity. Chinese Chem. Lett. 2014, 25, 287-291.

[10]. Li, D.; Zan, J.; Wu, L.; Zuo, S.; Xu, H.; Xia, D. Heterojunction Tuning and Catalytic Efficiency of g-C_3N_4-Cu_2O with Glutamate. Ind. Eng. Chem. Res. 2019, 58: 4000-4009.

[11]. Huang, J. Y.; Hsieh, P. L.; Naresh, G.; Tsai, H. Y.; Huang, M. H. Photocatalytic Activity Suppression of CdS Nanoparticle-Decorated Cu_2O Octahedra and Rhombic Dodecahedra. J. Phys. Chem. C 2018, 122, 12944-12950.

[12]. He, J.; Shao, D. W.; Zheng, L. C.; Zheng, L. J.; Feng, D. Q.; Xu, J. P.; Dong, H. Construction of Z-scheme Cu_2O/Cu/AgBr/Ag Photocatalyst with Enhanced Photocatalytic Activity and Stability under Visible Light. Appl. Catal. B- Environ. 2017, 203, 917-926.

[13]. Wu, Z.; Cheung, G.; Wang, J.; Zhao, Z.; Osterloh, F. E. Wavelength Dependent Photochemical Charge Transfer at the Cu_2O-$BiVO_4$ Particle Interface-Evidence for Tandem Excitation. Chem. Commun. 2018, 54, 9023-9026.

[14]. Tu, K.; Wang, Q.; Lu, A.; Zhang, L. Portable Visible-Light Photocatalysts Constructed from Cu_2O Nanoparticles and Graphene Oxide in Cellulose Matrix. J. Phys. Chem. C 2014, 118, 7202-7210.

[15]. Wei, Q.; Wang, Y.; Qin, H.; Wu, J.; Lu, Y.; Chi, H.; Liu, J. Construction of rGO Wrapping Octahedral Ag-Cu_2O Heterostructure for Enhanced Visible Light Photocatalytic Activity. Appl. Catal. B-Environ. 2018, 227, 132-144.

[16]. Zhao, Q.; Wang, J.; Li, Z.; Qiao,Y.; Jin, C.; Guo, Y. Preparation of Cu_2O/Exfoliated Graphite Composites with High Visible Light Photocatalytic Performance and Stability. Ceram. Int. 2016, 42, 13273-13277.

[17]. Li, H.; Liu, R. Y.; Huang, H.; Yu, H.; Ming, H.; Kang, Z. Carbon Quantum Dots/ Cu_2O Composites with Protruding Nanostructures and Their Highly Efficient (Near) Infrared Photocatalytic Behavior. J. Mater. Chem. 2012, 22, 17470-17475.

[18]. Yang, L.; Chu, D.; Wang, L.; Wu, X.; Luo. J. Synthesis and Photocatalytic Activity of Chrysanthemum-Like Cu_2O/Carbon Nanotubes Nanocomposites. Ceram. Int. 2016, 42, 2502-2509.

[19]. Zhou, K.; Shi, Y.; Jiang, S.; Hu, Y.; Gui, Z. Facile Preparation of Cu_2O /Carbon Sphere Heterostructure with High Photocatalytic Activity. Mater. Lett. 2013, 98, 213-216.

[20]. Chen, J.; Gao, P.; Wang, H.; Han, L.; Zhang, Y.; Wang, P.; Jia, N. A PPy/Cu_2O Molecularly Imprinted Composite Film-Based Visible Light-Responsive Photoelectrochemical Sensor for Microcystin-LR. J. Phys. Chem. C. 2018, 6, 3937-3944.

[21]. Tsyurupa, M. P.; Blinnikova, Z. K.; Borisov, Y. A.; Ilyin, M. M.; Klimova, T. P.; Mitsen, K. V.; Davankov,V. A. Physicochemical and Adsorption Properties of Hypercross-Linked Polystyrene with Ultimate Cross-Linking Density. J. Sep. Sci. 2014, 37, 803-810.

[22]. Tan, L.; Tan, B. Hypercrosslinked Porous Polymer Materials: Design, Synthesis and Applications. Chem. Soc. Rev. 2017, 46, 3322-3356.

[23]. Jia, Z.; Wang, K.; Li, T.; Tan, B.; Gu, Y. Functionalized Hypercrosslinked Polymers with Knitted N-Heterocyclic Carbene-Copper Complexes as Efficient and Recyclable Catalysts for Organic Transformations. Catal. Sci. Technol. 2016, 6, 4345-4355.

[24]. Wang, K.; Jia, Z.; Yang, X.; Wang, L.; Gu, Y.; Tan, B. Acid and Base Coexisted Heterogeneous Catalysts Supported on Hypercrosslinked Polymers for One-Pot Cascade Reactions. J. Catal. 2017, 348, 168-176.

[25]. Jia, Z.; Wang, K.; Tan, B.; Gu, Y. Ruthenium Complexes Immobilized on Functionalized Knitted Hypercrosslinked Polymers as Efficient and Recyclable Catalysts for Organic Transformations. Adv. Synth. Catal. 2017, 359, 78-88.

[26]. Liu, S.; Hu, Q.; Zheng, J.; Xie, L.; Wei, S.; Jiang, R. Knitting Aromatic Polymers for Efficient Solid-Phase Microextraction of Trace Organic Pollutants. J. Chromatogr. A. 2016, 1450, 9-16.

[27]. Li, B.; Gong, R.; Wang, W.; Huang, X.; Zhang, W.; Li, H.; Tan, B. A New Strategy to Microporous Polymers: Knitting Rigid Aromatic Building Blocks by External Cross-Linker, Macromolecules. 2011, 44, 2410-2414.

[28]. Zou, W.; Zhang, L.; Liu, L.; Wang, X.; Sun, J.; Wu, S.; Dong, L. Engineering the Cu_2O–Reduced Graphene Oxide Interface to Enhance Photocatalytic Degradation of Organic Pollutants under Visible Light. Appl. Catal. B-Environ. 2016, 181, 495-503.

[29]. Toe,C. Y.; Zheng, Z.; Wu, H.; Scott, J.; Amal, R.; Ng, Y. H. Photocorrosion of Cuprous Oxide in Hydrogen Production: Rationalising Self-Oxidation or Self-Reduction. Angew. Chem Int. Edit. 2018, 130, 13801-13805.

[30]. Liu, H.; Tian, K.; Ning, J.; Zhong, Y.; Zhang, Z.; Hu, Y. One-step Solvothermal Formation of Pt Nanoparticles Decorated Pt^{2+}-doped α-Fe_2O_3 Nanoplates with Enhanced Photocatalytic O_2 evolution. ACS Catal. 2019, 9: 1211-1219.

[31]. Etogo, A.; Liu, R.; Ren, J.; Qi, L.; Zheng, C.; Ning, J.; Zhong, Y.; Hu, Y. Facile One-Pot Solvothermal Preparation of Mo-Doped Bi_2WO_6 Biscuit-Like Microstructures for Visible-Light-Driven Photocatalytic Water Oxidation. J. Mater. Chem. A 2016, 4(34): 13242-13250.

[32]. He, B.; Liu, R.; Ren, J.; Tang, C.; Zhong, Y.; Hu, Y. One-step Solvothermal Synthesis of Petalous Carbon-Coated Cu^{+}-Doped CdS Nanocomposites with Enhanced Photocatalytic Hydrogen Production. Langmuir 2017, 33(27): 6719-6726.

[33]. Meng, S.; Li, D.; Sun, M.; Li, W.; Wang, J.; Chen, J.; Xiao, G. Sonochemical Synthesis, Characterization and Photocatalytic Properties of A Novel Cube-Shaped $CaSn(OH)_6$. Catal. Commun. 2011, 12, 972-975.

[34]. Ye, L.; Liu, J.; Jiang, Z.; Peng, T.; Zan, L. Facets Coupling of Biobr-G-C_3N_4 Composite Photocatalyst for Enhanced Visible-Light-Driven Photocatalytic Activity. Appl. Catal. B-Environ. 2013, 142, 1-7.

[35]. Bandyopadhyay, A.; Pal, A. J. Large Conductance Switching and Memory Effects in Organic Molecules for Data-Storage Applications. Appl. Phys. Lett. 2003, 82, 1215-1217.

CHAPTER 3

UiO-66-NH_2/Cu_2O composite as an enhanced visible light photocatalyst for decomposition of organic pollutants

3.1 Introduction

Nowadays, water contamination is one of the main environmental issues. Degradation of the organic pollutants over semiconductor-based photocatalysts has been regarded as one of efficient and environmentally friendly methods [1, 2]. Among the photocatalysts, cuprous oxide (Cu_2O), as a p-type semiconductor has been widely studied because of its small bandgap energy of 2.0-2.2 eV [3]. But, the rapid recombination of the photo-induced e^--h^+ pairs and photocorrosion issues still exist and often result in lower photocatalytic efficiency [4]. The above problem could be solved by combining it with other noble metals or semiconductors. It is reported that visible-light photocatalytic performance can be improved by the heterojunction photocatalysts fabricated with two semiconductors having appropriate band edges [5-8]. Recently, Cu-based semiconductor heterojunction photocatalysts have been widely developed [9-14]. However, the activity and stability are still necessary to be improved for a practical application.

Microporous metal-organic frameworks (MOFs) are made up of metal clusters connected each other by organic ligands [15]. They always have high surface areas, adjustable pore sizes, and the possibility of being functionalized so that they have been attracted extensive attentions in many fields [16-18]. Especially, many MOFs could be excited under light irradiation, showing the semiconductor-like photocatalytic characteristics. In addition, the MOFs with high surface areas could serve as the ideal photocatalyst support to avoid the aggregation of the nanosized catalyst particles or combine with other photocatalyst to improve the activity as well as stability for the photocatalytic application in wastewater treatment [19-21]. Among them, a MOF

named as UiO-66-NH_2 has aroused extensive concern because of its high surface area, good chemical durability and the adsorption ability for visible light. To date, it has been combined with other visible light photocatalysts such as BiOBr [22], CdS [23] and g-C_3N_4 [24] to obtain a composite with excellent photocatalytic activity [22-26].

In this work, to further improve the photocatalytic activity and stability of Cu_2O, the UiO-66-NH_2/Cu_2O composites were prepared by using a facile impregnation method and applied for the MO degradation under visible light.

3.2 Experimental

3.2.1 Preparation of Cu_2O

Cu_2O was prepared by using $CuCl_2$ as the precursor. In a typical procedure, ethanol (20 mL) and $CuCl_2$ (0.5 mol/L, 5mL) were successively introduced into 83.4 mL of deionized water under stirring, followed by treatment with ultrasound at 25 ℃ for 30 min. Thereafter, ethanol (30 mL) and NaOH solution (1.0 mol/L, 9 mL) were introduced to the above solution. After that, under stirring, 9.8 mL of $NH_2OH{\cdot}HCl$ (0.1 mol/L) was rapidly introduced into it in 5 s. The solution was then maintained at 40 ℃ for 3 h in a water bath to promote Cu_2O crystal growth. Finally, the solution was centrifuged at 5000 rpm for 10 min to collect the product, which was further washed with water-ethanol mixed solution (V_{water}:$V_{ethanol}$=1:1). This step was repeatedly performed until all residual reagents was moved out. Finally, the obtained Cu_2O was washed with ethanol again and dried at 35 ℃ under vacuum.

3.2.2 Preparation of UiO-66-NH_2/Cu_2O

UiO-66-NH_2 was purchased from Shanghai Chemsoon Co, Ltd, which is a metal organic framework (MOF) with zirconium as metal and amino terephthalic acid as a linker [27]. The composites were obtained by using the impregnation method. In a specific process, 0.08 g of Cu_2O and 0.02 g of UiO-66-NH_2 were introduced into 20 mL of ethanol simultaneously, after 30 min ultrasonic processing, the mixture was dried

at 35 ℃ for 12 h. As such, 20% UiO-66-NH_2/Cu_2O composite was obtained. Similarly, other composites with different percentages of UiO-66-NH_2 were also prepared.

3.2.3 Catalyst characterizations

X-ray powder diffraction (XRD) analysis was conducted by a Bruker D8 diffractometer with Cu Kα as the radiation. The morphologies were observed by a TESCAN MAIA 3 LMH type scanning electron microscope (SEM, JEOLJEM-2999FMII apparatus), and a transmission electron microscope (TEM). The Brunauer-Emmet-Teller (BET) characterization was conducted by N_2 adsorption at 77 K on a Micrometrics ASAP-2020 PLUS HD88 adsorption apparatus. UV-vis diffuse reflectance spectroscopy (UV-vis DRS) was recorded by a Jena SPECORD® 210 PLUS spectrophotometer. X-ray photoelectron spectroscopy (XPS) analysis was carried out by a Thermo Fisher Scientific Escalab 250Xi system. TOC of the MO solution was analyzed by a TOC/TNb Analyzer (Multi N/C 2100, Analytik Jena, Germany). Electrochemical impedance spectroscopy (EIS) was measured in a solution containing KCl (0.1 M) and $[Fe(CN)_6]^{3-/4-}$ (2.5 mM). The photoelectrochemical properties were performed on a CHI 760E electrochemical system (Shanghai, China) using a standard three-electrode cell with a working electrode, a platinum wire counter electrode, and an Ag/AgCl reference electrode. The photocurrent response was measured in Na_2SO_4 solution (0.2 M) under the irradiation of visible-light. The working electrode was prepared as follows: 1 mg of as-prepared photocatalyst was suspended in 2 mL of acetone to produce slurry, which was then dip-coated on a 50 mm × 50 mm indium-tin oxide (ITO) glass electrode and dried.

3.2.4 Photocatalytic performance test

Photocatalytic degradation was carried out in a double-jacket reactor equipped with a 500 W Xe lamp with a cut off filter of 420 nm (CEL-S500). In a typical procedure, 30 mg of photocatalysts was dispersed into 90 mL of 30 mg/L MO solution with stirring. To reach the adsorption equilibrium between the MO and catalyst, the mixed solution

was firstly stirred for 40 min under dark. Thereafter, the mixture was exposed to the visible light with continuous stirring under ambient temperature. At the specific time, 4 mL of mixture was extracted and centrifuged. MO concentration was analyzed by a model 722E UV-*vis* spectrophotometer (Shanghai Lengguang Technology Co. Ltd) at 464 nm.

3.2.5 Active species trapping analysis

To understand the photocatalysis mechanism during the MO degradation, isopropyl alcohol (IPA) and ammonium oxalate (AO) were introduced as the scavenger for hydroxyl radical (•OH) and h^+ [28, 29], respectively, and all other experimental conditions were remained as the same as the above experiments. In addition, for further investigating the influence of $\bullet O_2^-$ during the process, the MO degradation experiment was also conducted under N_2 purging with an inert atmosphere.

3.3 Results and discussion

3.3.1 Photocatalytic characterization

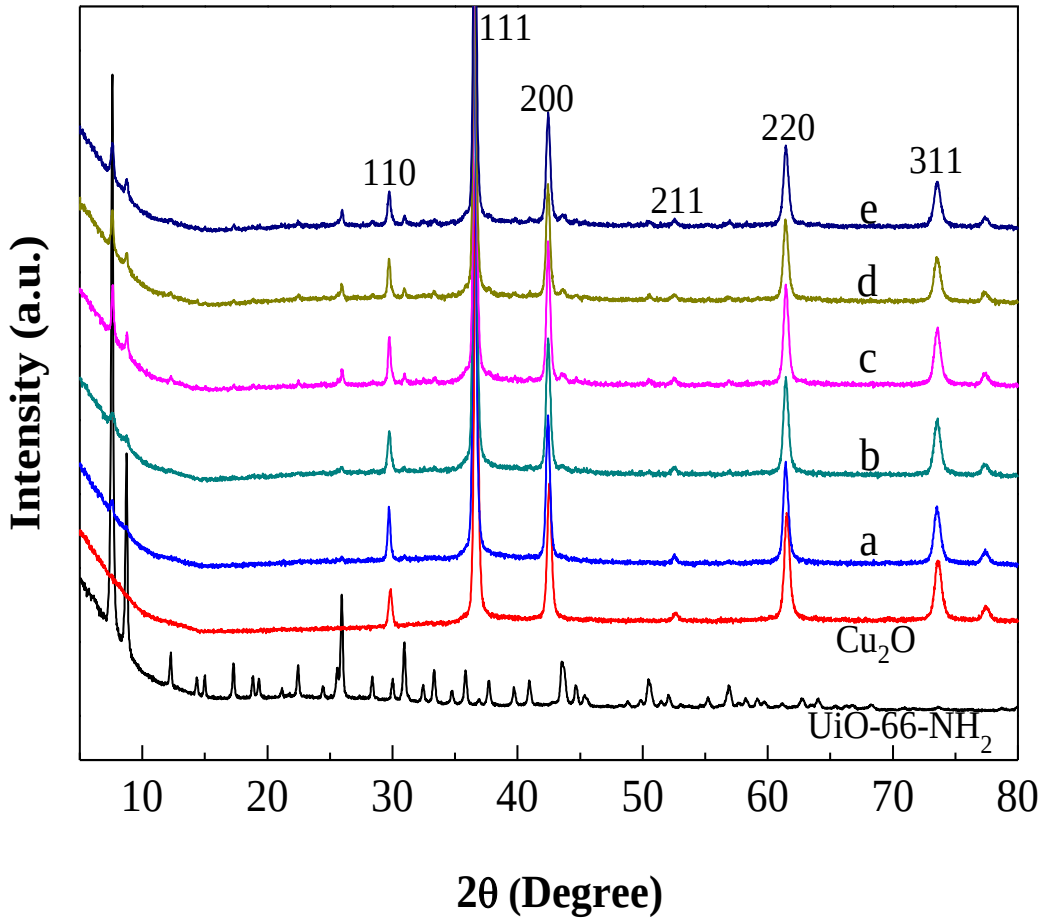

Figure 3.1 XRD patterns of UiO-66-NH_2, Cu_2O and UiO-66-NH_2/Cu_2O composites (a: 5% UiO-66-NH_2/Cu_2O; b: 10% UiO-66-NH_2/Cu_2O; c: 15% UiO-66-NH_2/Cu_2O; d: 20% UiO-66-NH_2/Cu_2O; e: 25% UiO-66-NH_2/Cu_2O).

XRD results of catalysts are given in Fig 3.1. The diffraction peaks for both Cu_2O and UiO-66-NH_2 [30] were observed whereas no obvious diffraction peaks of CuO and Cu can be seen, implying that the UiO-66-NH_2/Cu_2O composites were successfully obtained, in which the UiO-66-NH_2 kept its own structure during the synthesis process.

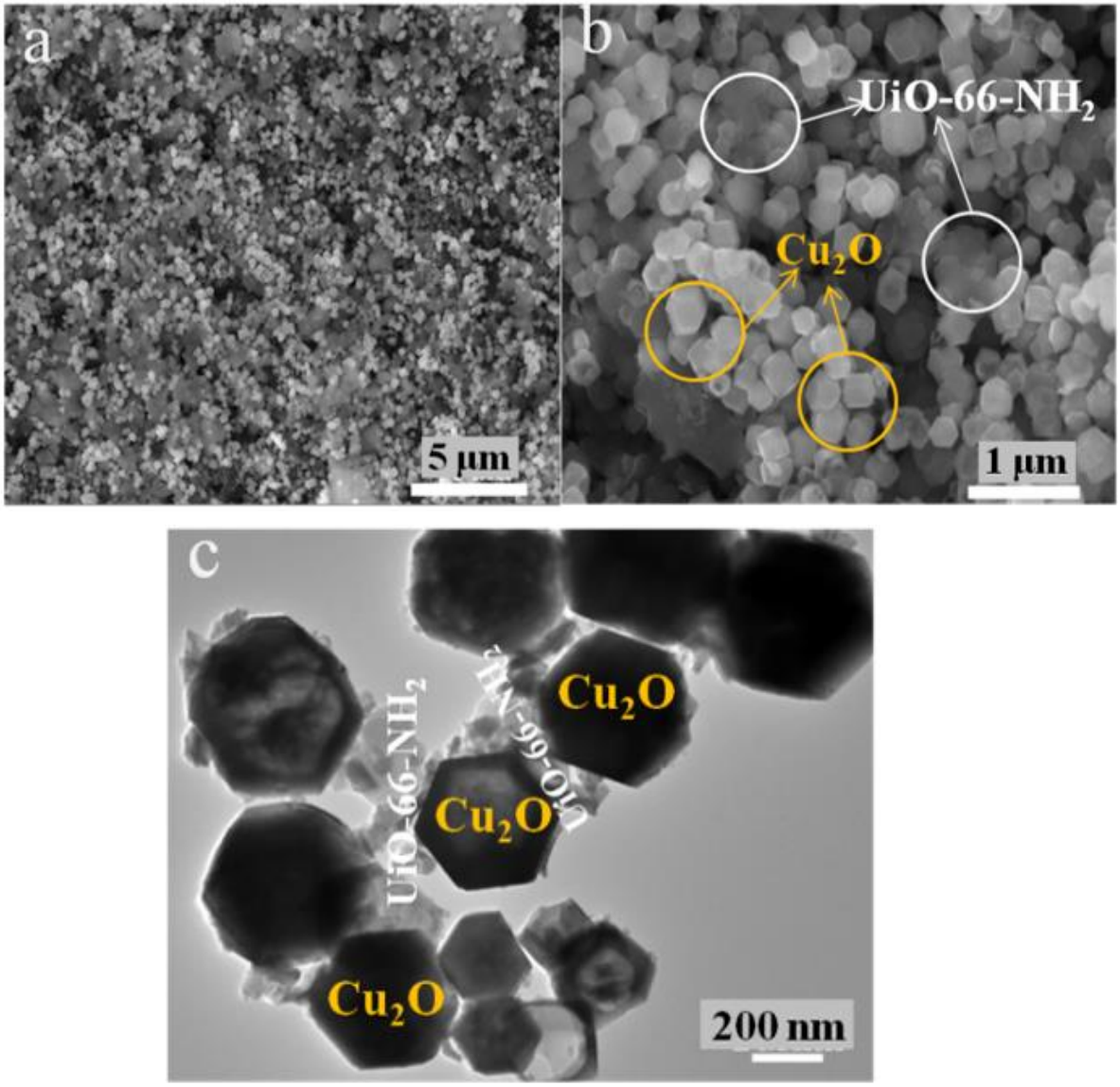

Figure 3.2 SEM (a, b) and TEM (c) images of 20% UiO-66-NH_2/Cu_2O composite photocatalyst.

The morphology of 20% UiO-66-NH_2/Cu_2O photocatalyst is given in Fig 3.2. From Figs 3.2(a) and (b), it is found that all Cu_2O had almost the same particle size with the rhombic dodecahedral structure. The particle size of Cu_2O in the 20% UiO-66-NH_2/Cu_2O composite was about 200-300 nm (Fig 3.2(c)). Moreover, it is observed that UiO-66-NH_2 homogeneously covered the Cu_2O particles (Fig 3.2(c)), indicating that the Cu_2O and UiO-66-NH_2 were well combined in the catalyst.

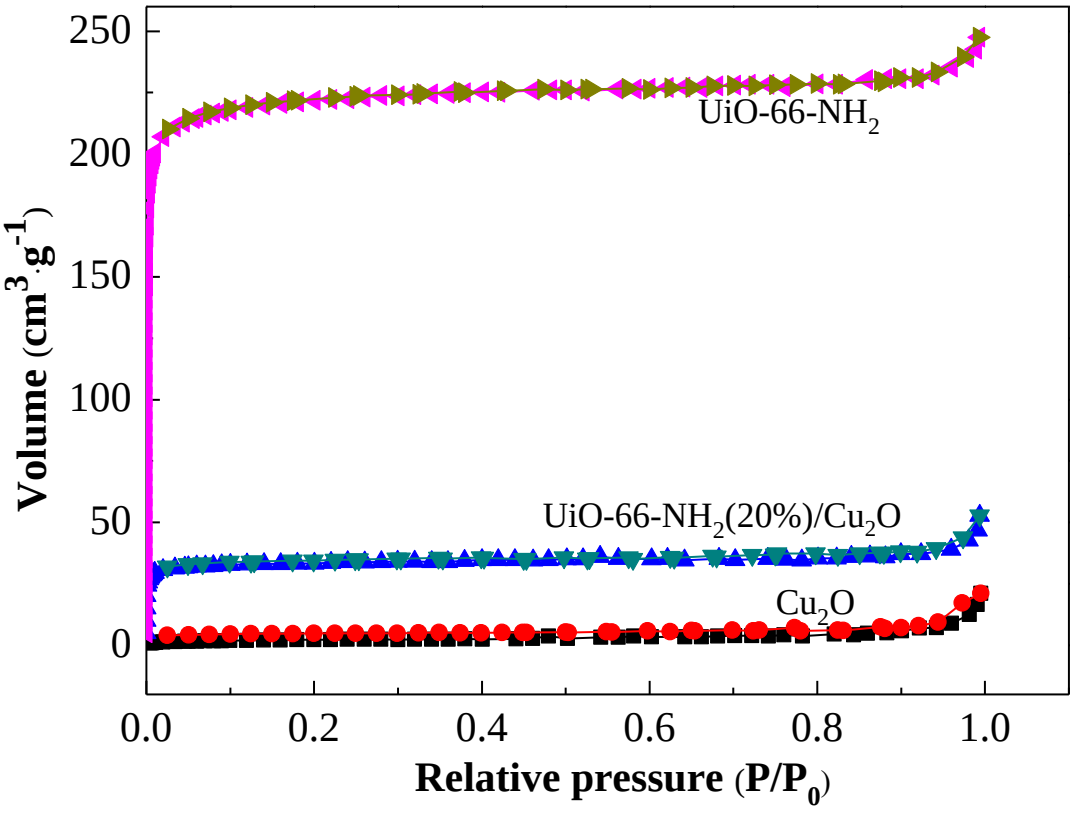

Figure 3.3 Typical N_2 adsorption-desorption isotherms of UiO-66-NH_2, Cu_2O and 20% UiO-66-NH_2/Cu_2O.

Table 3. 1 BET surface areas of samples

Sample	Surface area (m^2/g)
UiO-66-NH_2	831.9
20% UiO-66-NH_2/Cu_2O	125.9
Cu_2O	8.1

The BET results of the samples are given in Fig 3.3 and Tab 3. 1. One can see that the surface area of 20% UiO-66-NH_2/Cu_2O was 125.9 m^2g^{-1}, which was much larger than that of the pure Cu_2O (8.1 m^2g^{-1}). It is expected that such higher surface area will be favorable for the adsorption of MO to enhance the photocatalytic removal efficiency.

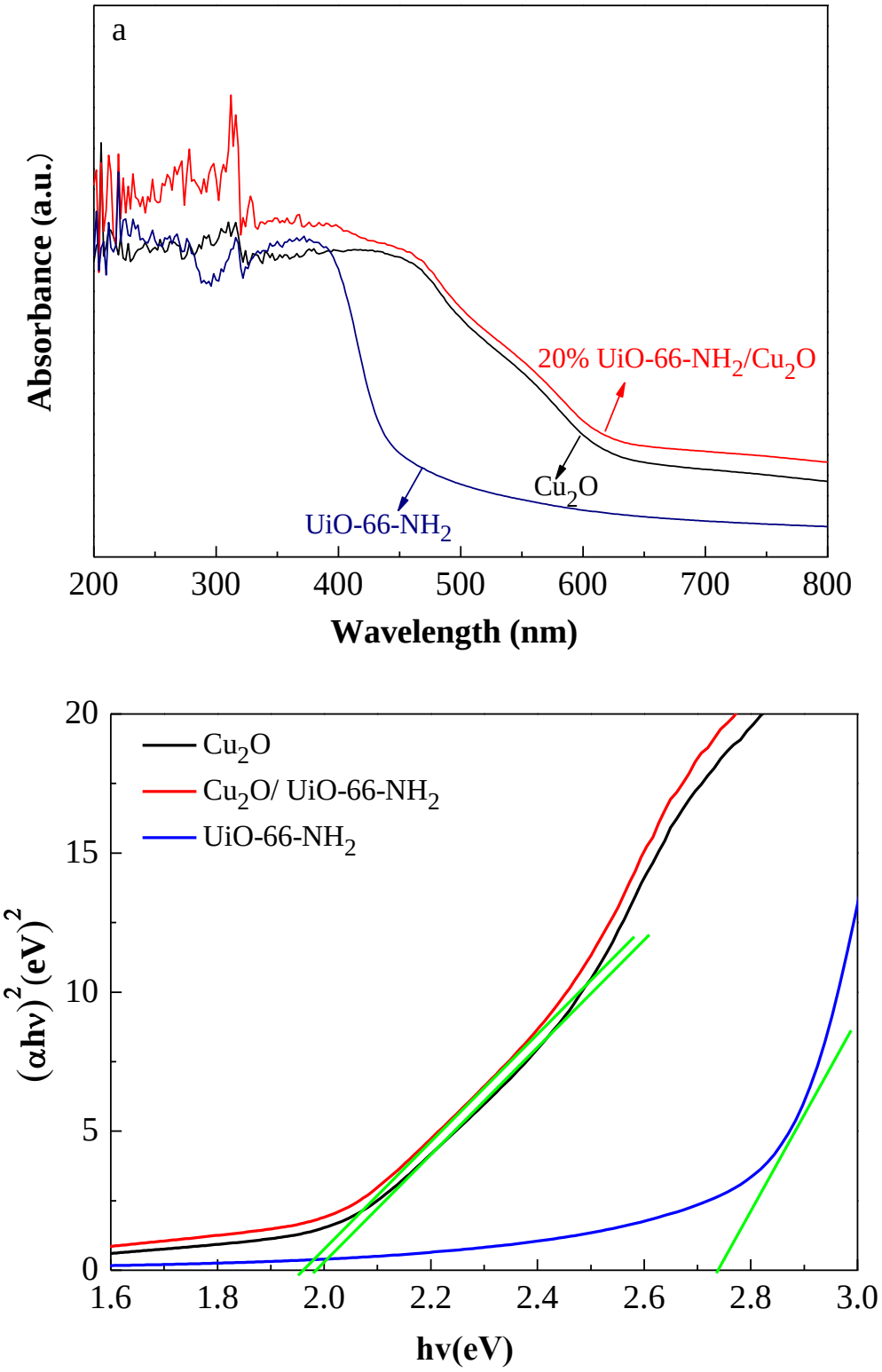

Figure 3.4 (a) UV-vis DRS spectra and (b) Optical absorption edges of UiO-66-NH_2, Cu_2O and 20% UiO-66-NH_2/Cu_2O composite.

The UV-vis DRS spectra and the corresponding optical absorption edges of

samples are given in Fig. 4. As seen in Fig 3.4(a), the Cu_2O had an absorption edge at about 630 nm and the UiO-66-NH_2 also had obvious response to the visible light. Moreover, although the adsorption property of the 20% UiO-66-NH_2/Cu_2O was similar as that of the Cu_2O, the absorbance was enhanced after combing with UiO-66-NH_2. Based on the results in Fig 3.4(b), the band gaps of Cu_2O, UiO-66-NH_2/Cu_2O, UiO-66-NH_2 were calculated to be 1.98eV, 1.96 eV, 2.73 eV, respectively. As such, the combination of UiO-66-NH_2 and Cu_2O decreased the apparent band gap, which could improve the absorption capability for visible light.

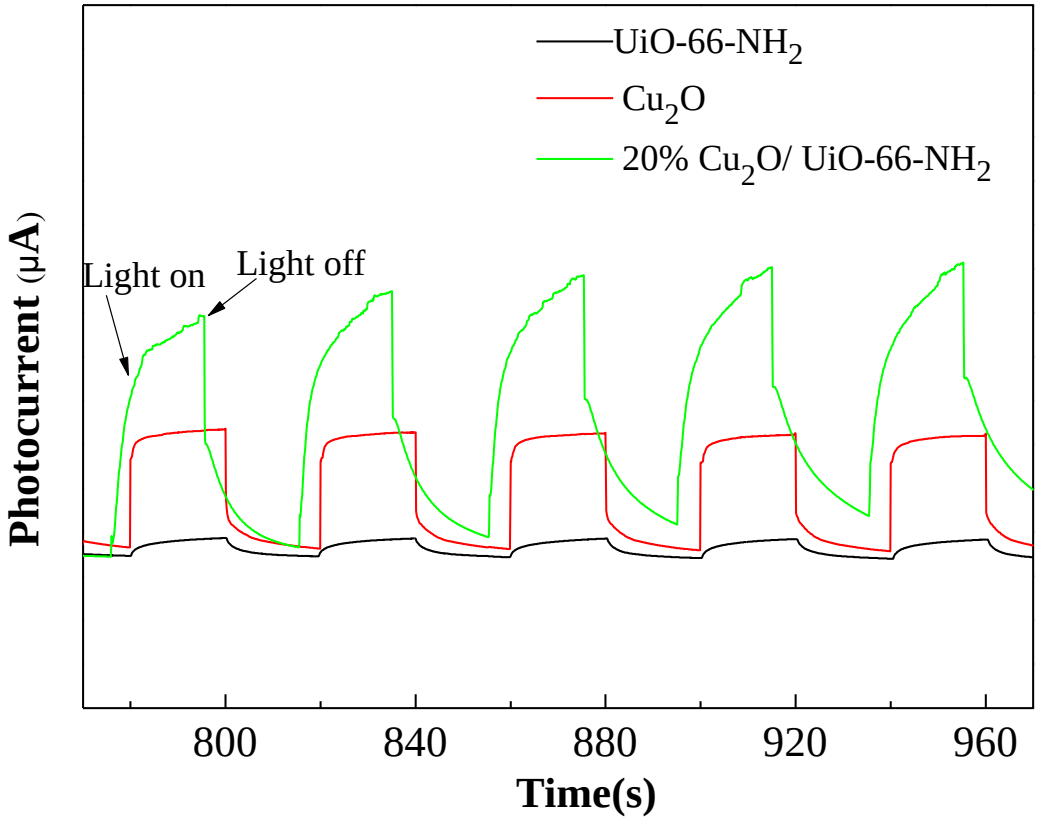

Figure 3.5 Photocurrent responses of UiO-66-NH_2, Cu_2O and 20% UiO-66-NH_2/Cu_2O composite.

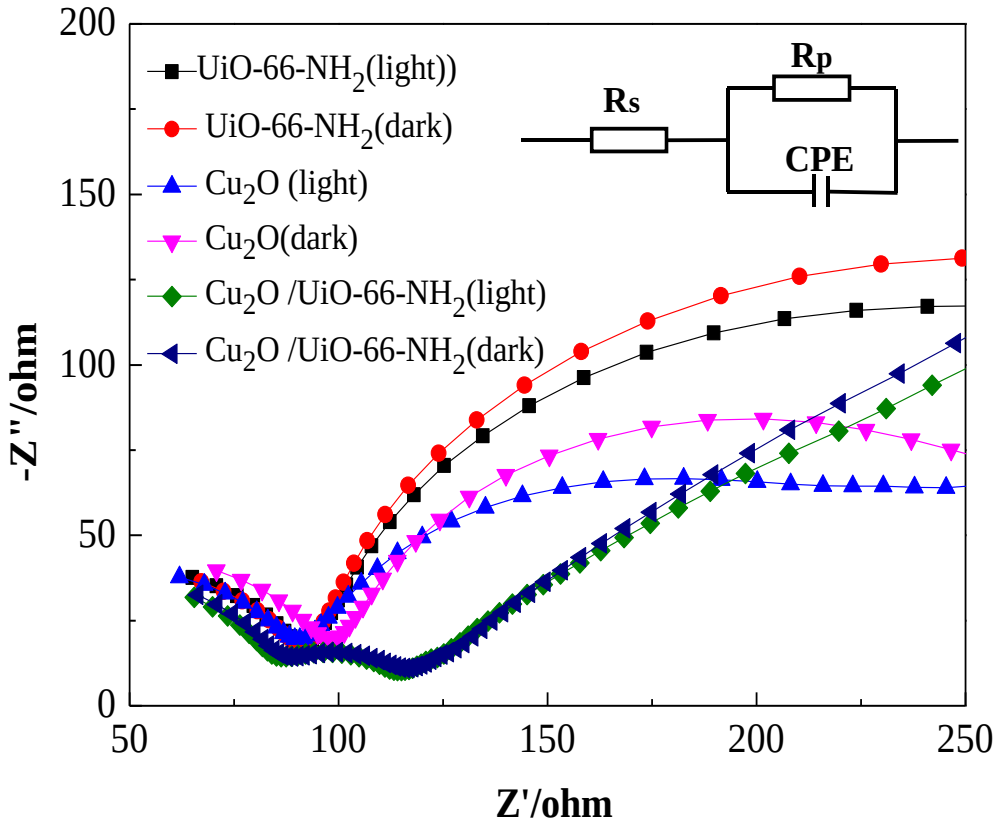

Figure 3.6 EIS Nyquist plots of the Cu_2O and 20% UiO-66-NH_2/Cu_2O composite in dark and under visible light irradiation.

The photocurrent and EIS were used to study the charge separation efficiency. As we known, the higher the separating efficiency of photogenerated e^--h^+ pairs in the catalyst, the larger the photocurrent could be measured. As such, from Fig 3.5, one can see that 20% UiO-66-NH_2/Cu_2O composite exhibited a higher current density under visible light, implying that the composite had a larger separation rate of photoinduced e^--h^+ pairs than the pure Cu_2O [31]. The inset in Fig 3.6 is the equivalent circuit plot for the fitting, where R_s is the resistance of the solution and R_p is the resistance to charge transfer at the interface between UiO-66-NH_2/Cu_2O and electrolyte, and CPE is the constant phase element [32]. From Fig 3.6, it also can be seen that the circular radius for 20% UiO-66-NH_2/Cu_2O composite was smaller than that for Cu_2O, indicating that the composite had a faster interfacial charge-electron transfer rate than Cu_2O [31]. Thus,

20% UiO-66-NH_2/Cu_2O composite should possess stronger ability to produce and deliver the photoindued charge carrier than the pure Cu_2O.

3.3.2 Photocatalytic performance

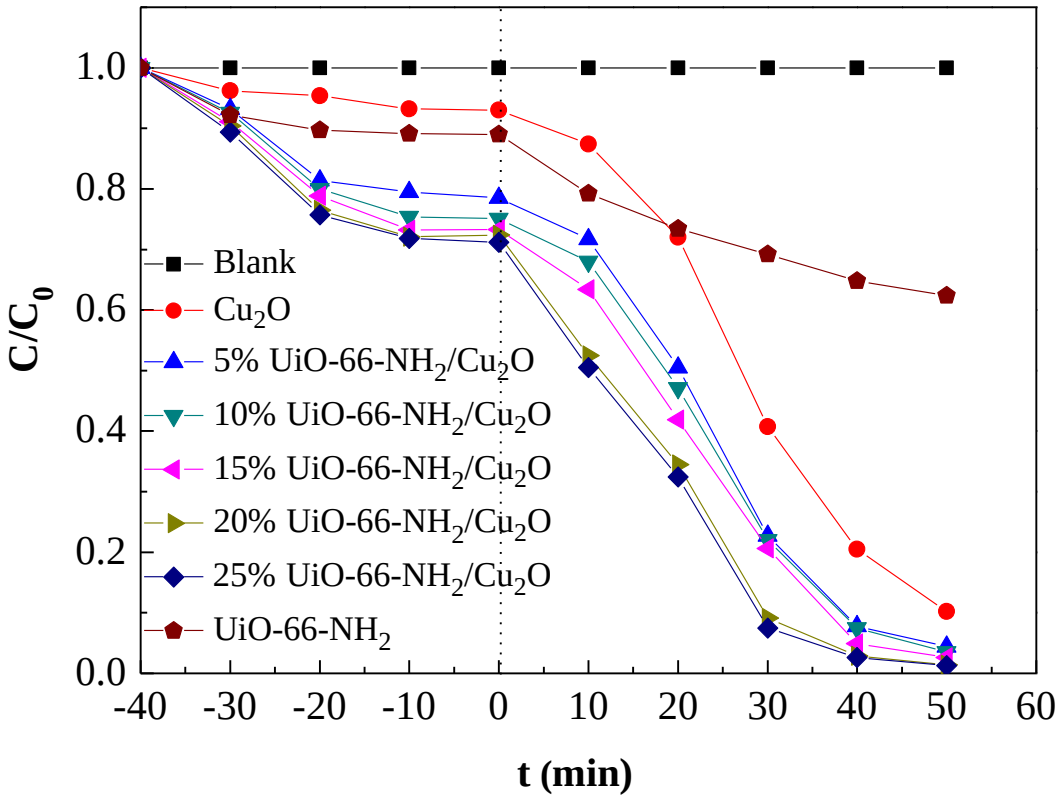

Figure 3.7 Photocatalytic degradation curves for decomposition of MO over the prepared UiO-66-NH_2/Cu_2O composites, pure Cu_2O and pure UiO-66-NH_2. (Herein, the amount of pure UiO-66-NH_2 was 5 mg and others were 30 mg)

The photocatalytic performances were investigated by MO degradation, and the obtained results are given in Fig 3.7. The blank test in Fig 3.7 showed that the self-photodegradation of MO can be ignored. Meanwhile, after 40 min stirring in the dark, the solution reached the adsorption equilibrium, the MO concentration dropped obviously for all UiO-66-NH_2/Cu_2O composites when compared with the Cu_2O, implying that UiO-66-NH_2 on the Cu_2O had high MO adsorption ability owing to the higher surface area (Tab 3.1). More importantly, all UiO-66-NH_2/Cu_2O composites

presented better photocatalytic degradation rate than the pure Cu_2O, and the composite with 20% of UiO-66-NH_2 showed the largest MO degradation rate, by which 98.6% of MO was decomposed within 50 minutes. In general, there are many influence factors on the photocatalytic activity of Cu_2O-based catalysts, which include the surface area, the stability of Cu^+ species, light-adsorption ability, and so on [33]. As stated above, the visible light absorbance of the Cu_2O was effectively improved by combining with UiO-66-NH_2. In addition, in the composite, Cu_2O belonged to the p-type semiconductor [11] while UiO-66-NH_2 was a n-type semiconductor-like material [20]. Thus, the UiO-66-NH_2/Cu_2O composite should be a photocatalyst with the p/n type heterostructure, which was a favorable structure for the charge collection and separation [6, 8]. That is why the UiO-66-NH_2/Cu_2O composite showed the better photocatalytic activity than the Cu_2O.

3.3.3 Removal of TOC over UiO-66-NH_2/Cu_2O

Along with irradiation of MO-containing solution, some MO could be decomposed to the intermediates, and then decomposed gradually to the smaller molecular fragments, and eventually transformed into inorganic carbon (CO_2). To evaluate the mineralization ratio of MO over Cu_2O / UiO-66-NH_2 composite under visible light, the total organic carbon (TOC) analysis was conducted. As shown in Fig 3.8, after 60 min reaction, about 81.8% of TOC was removed, suggesting that the mineralization occurred in the degradation of MO over the Cu_2O/UiO-66-NH_2 composite photocatalyst.

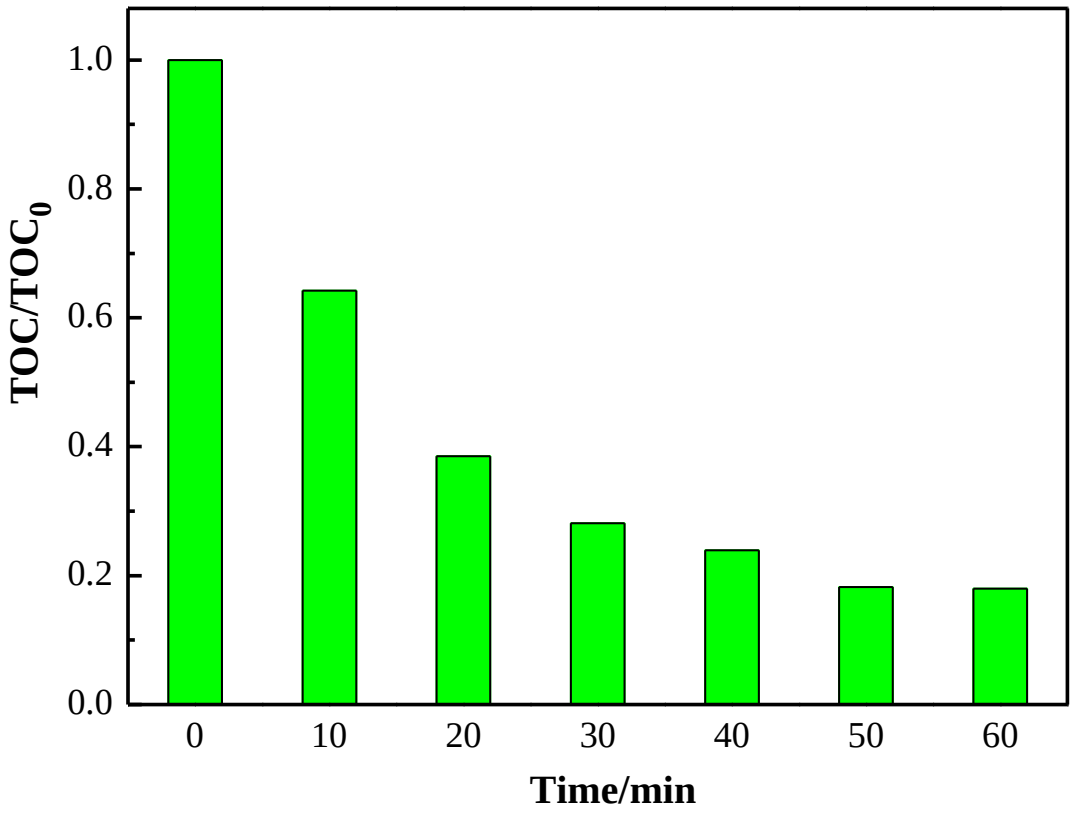

Figure 3.8 Removal of TOC over 20% UiO-66-NH_2/Cu_2O composite catalyst under visible light irradiation.

3.3.4 Stability of 20% UiO-66-NH_2/Cu_2O catalyst

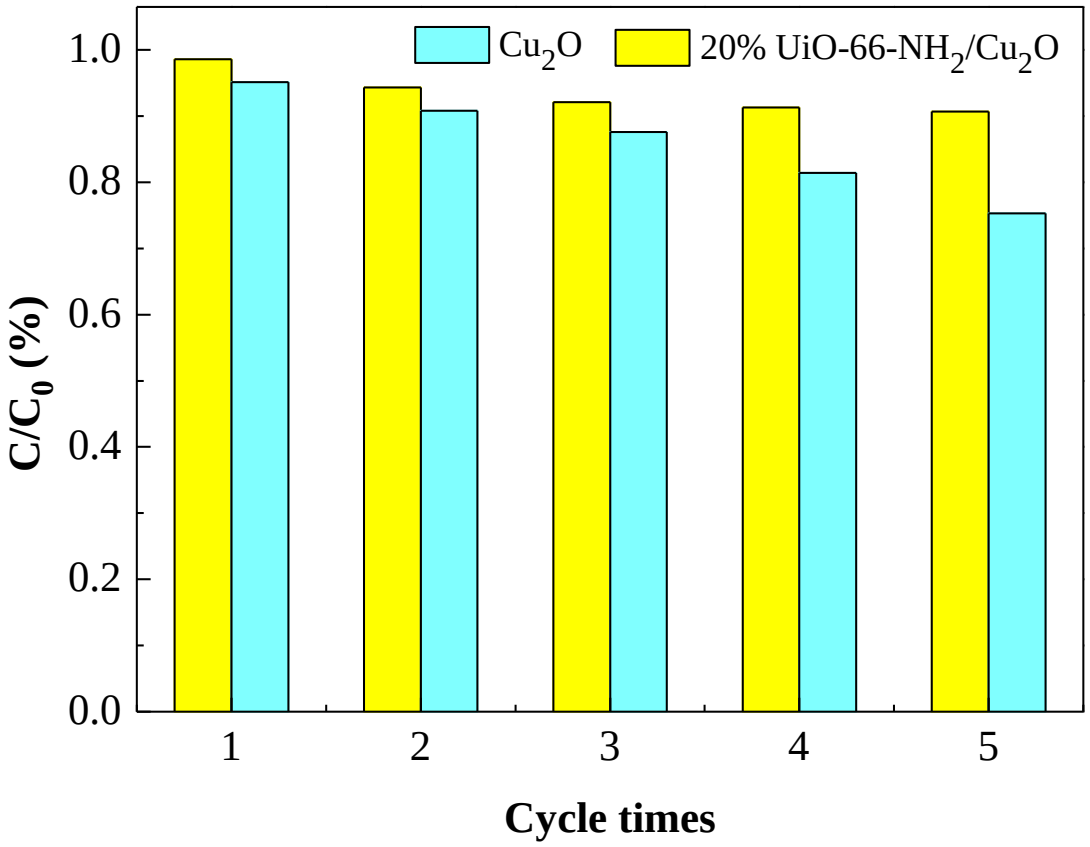

Figure 3.9 Repeated photocatalytic degradation of MO solution over Cu_2O and 20% UiO-66-NH_2/Cu_2O composite under visible light irradiation.

The degradation of MO by reusing the spent 20% UiO-66-NH_2/Cu_2O composite photocatalyst for 5 cycles were also conducted. As shown in Fig 3.9, one can see thathould be noted that approximately 1-2% spent catalysts cannot collected from the solution in each cycle due to the adhesion of fine particles on the walls of reactor. The the activity of this photocatalyst maintained at 90.7% even at the 5th cycle. Herein, its result implied that the stability of the Cu_2O photocatalyst can be significantly improved by combing with the UiO-66-NH_2.

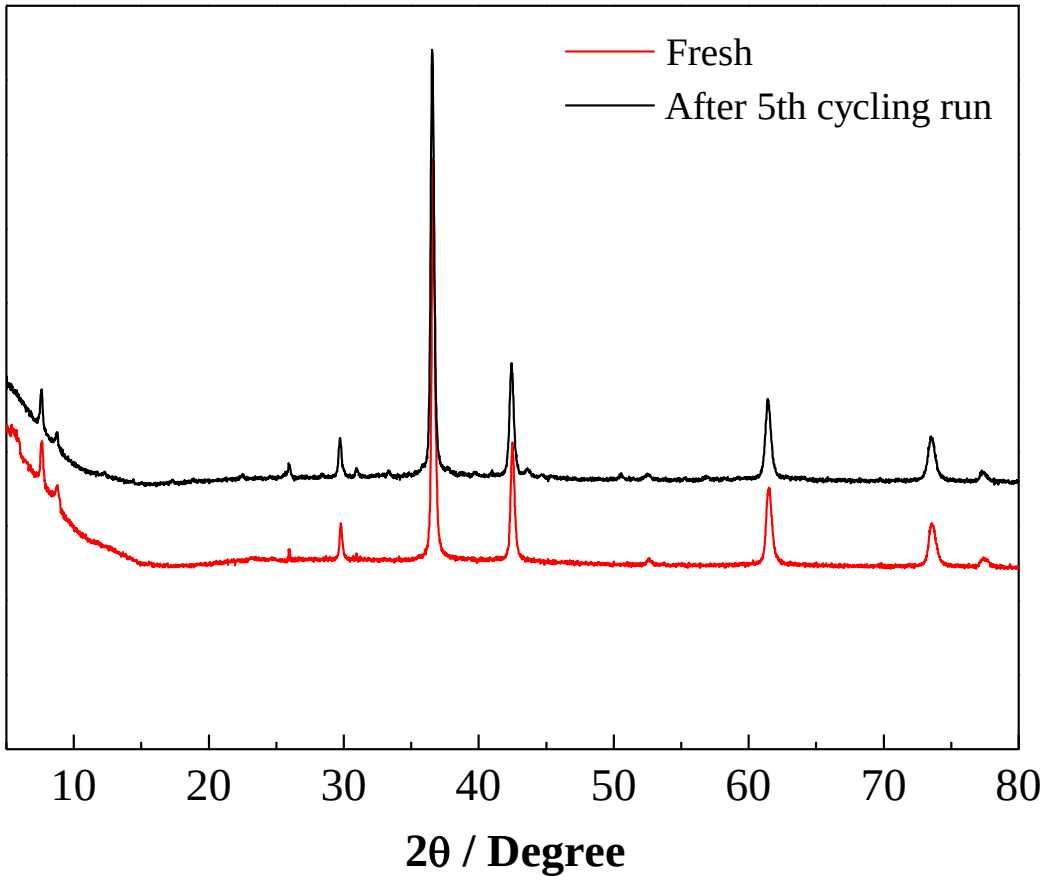

Figure 3.10 XRD patterns of 20%UiO-66-NH_2/Cu_2O composite catalyst before and after the photodegradation of MO for 5-cycle testing.

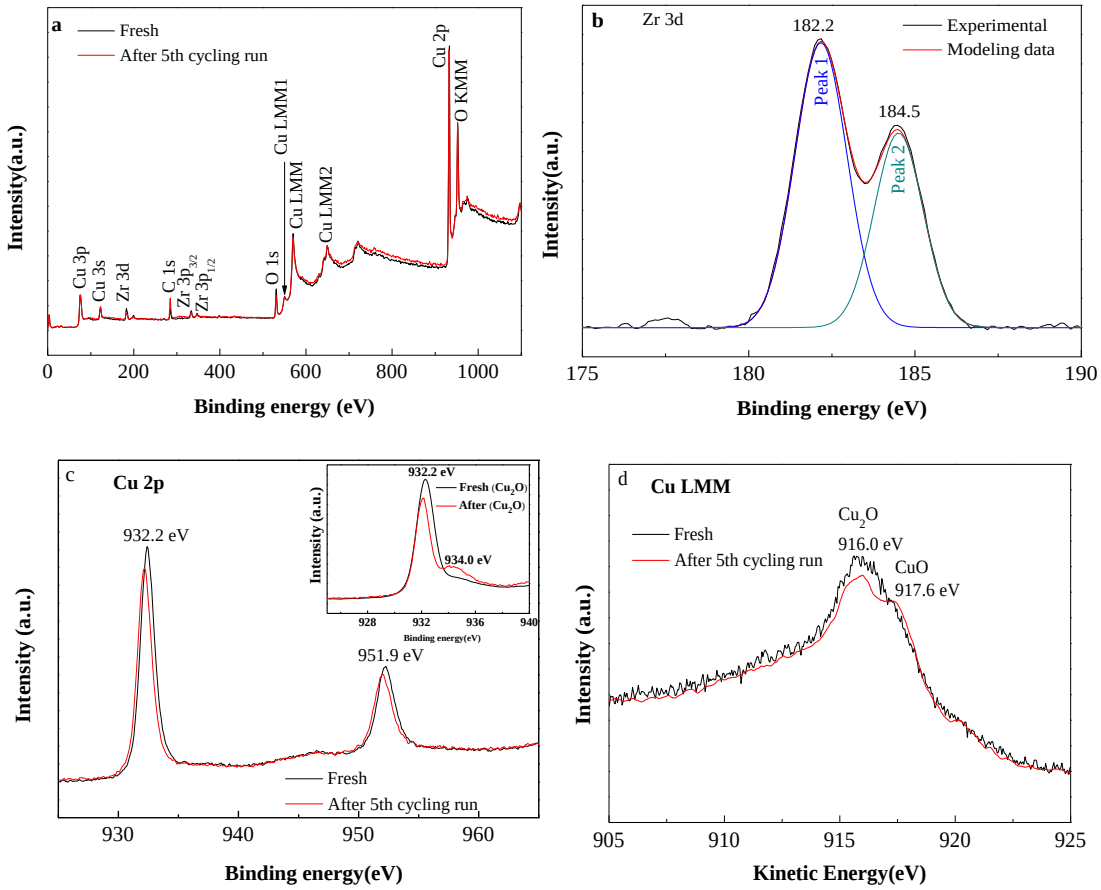

Figure 3.11 The XPS analyses of 20%UiO-66-NH_2/Cu_2O composite before and after photodegradation of MO for five cycling runs. (a) Survery spectrum; (b) The Zr 3d XPS spectra; (c) The Cu 2p XPS spectra of 20%UiO-66-NH_2/Cu_2O composite and Cu_2O (inset); (d) The Cu LMM spectra.

Furthermore, the XRD patterns and XPS spectra of this photocatalyst before and after the five cycles of photodegradation were also measured (Figs 3.10 and 3.11). From Fig 3.10, one can see that CuO and Cu species were not detected from the spent catalyst after five cycling runs, implying that the crystalline structure of Cu_2O maintained.

Meanwhile, the surface chemical states of the 20% UiO-66-NH_2/Cu_2O composite before and after the five cycling runs were further measured by XPS. Fig 3.11(a) presents the survey spectra, which indicates that the presences of Cu, Zr, C and O species in the UiO-66-NH_2/Cu_2O composite and the intensities remained almost unchanged before and after five cycling runs. Fig 3.11(b) shows the Zr 3d XPS spectra.

One can see that the signal of Zr 3d can be divided into two peaks which belong to the Zr $3d_{3/2}$ (184.5 eV) and Zr $3d_{5/2}$ (182.2 eV), respectively [22]. Comparing with the UiO-66-NH_2 peaks, the above two peaks shifted slightly due to the combining with the Cu_2O. In addition, the Zr 3d XPS spectrum after the five cycling runs also exhibited that the UiO-66-NH_2 basically remained unchanged. The Cu 2p XPS spectra given in Fig 3.11(c) showed that either fresh or the spent catalysts of 20%UiO-66-NH_2/Cu_2O composite had two main peaks: one is at 932.2eV belonged to the Cu $2p_{3/2}$ and the other is the Cu $2p_{1/2}$ peak of Cu^+ (951.9 eV) [33]. Moreover, compared with the Cu 2p XPS spectra of Cu_2O in the inset, the peak at 934.2 eV corresponding to Cu(II) in CuO was not detected in the spent catalyst of 20%UiO-66-NH_2/Cu_2O composite, implying that the Cu_2O in the UiO-66-NH_2/Cu_2O composite maintained stable during the photodegradation process. However, from the Cu LMM spectra in Fig 3.11(d), a trace CuO was detected from the spent catalyst even though its amount was too small to be observed from the Cu 2p XPS spectrum. In addition, the Cu^0 species (918.6 eV) was not observed in Fig 3.11 (d), implying that Cu was not produced in the used catalyst [4]. Therefore, the photocorrosion of Cu_2O can be significantly suppressed by the combining with the UiO-66-NH_2, and the stability of Cu^+ in Cu_2O was improved remarkably, resulting in the higher photocatalytic performance.

3.3.5 Photocatalytic mechanism

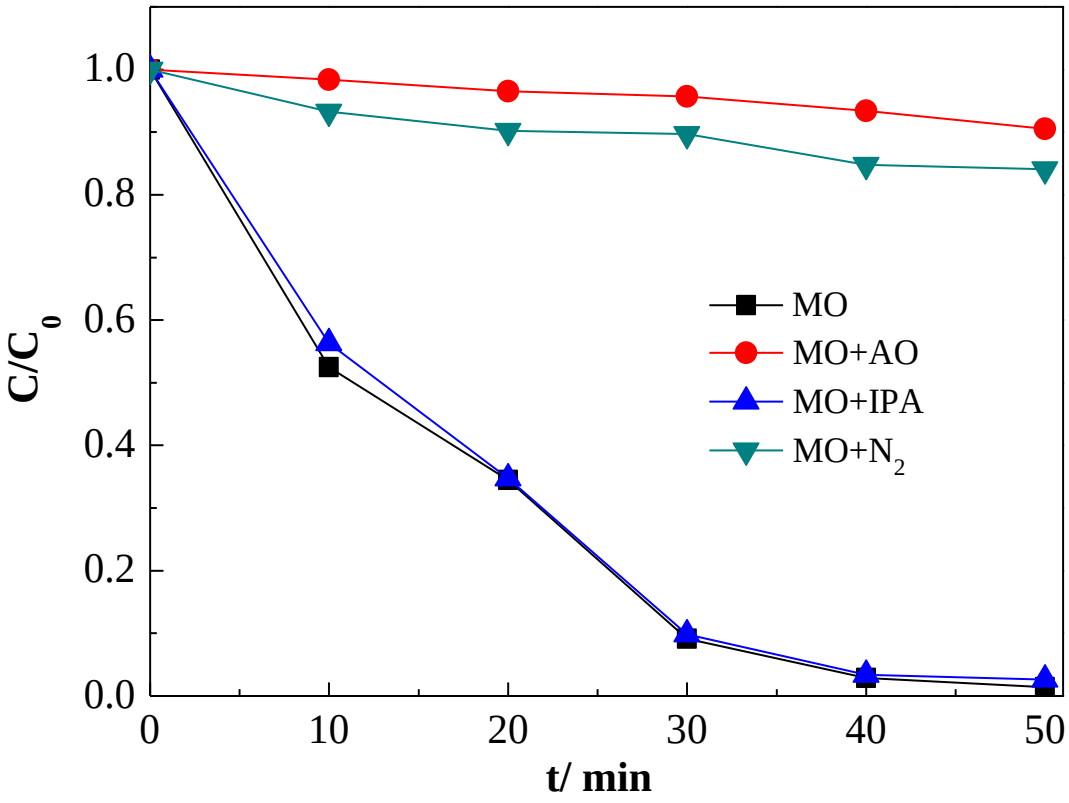

Figure 3.12 Active species trapping experiments with UiO-66-NH_2/Cu_2O composite under visible light irradiation (AO: ammonium oxalate; IPA: isopropyl alcohol).

For exploring the photocatalysis mechanism during MO degradation using the UiO-66-NH_2/Cu_2O composite as the catalyst, the active species trapping experiments were conducted. Herein, AO and IPA were introduced as the h^+ scavenger [28] and the •OH scavenger [29], respectively. From Fig 3.12, one can see that by adding the IPA (•OH scavenger), the MO degradation rate was not obviously changed, implying that •OH was not the important contributor in this process. However, after the introduction of AO, the photocatalytic activity decreased obviously and only a small amount of MO was degraded, implying that the hole was the major species during the degradation. In addition, oxygen molecules could be converted to $•O_2^-$ on the UiO-66-NH_2/Cu_2O composite by the photo-induced electrons. For evaluating the effect of $•O_2^-$ active

species, the catalyst activity evaluation experiment was also conducted under N_2 purging atmosphere. Seen in Fig 3.12, the degradation rate was greatly decreased, implying that $\bullet O_2^-$ was also the major active species in the photodegrading process over the UiO-66-NH_2/Cu_2O composite. Therefore, the h^+ and $\bullet O_2^-$ should be the major active species during the MO degradation over the UiO-66-NH_2/Cu_2O composite catalysts.

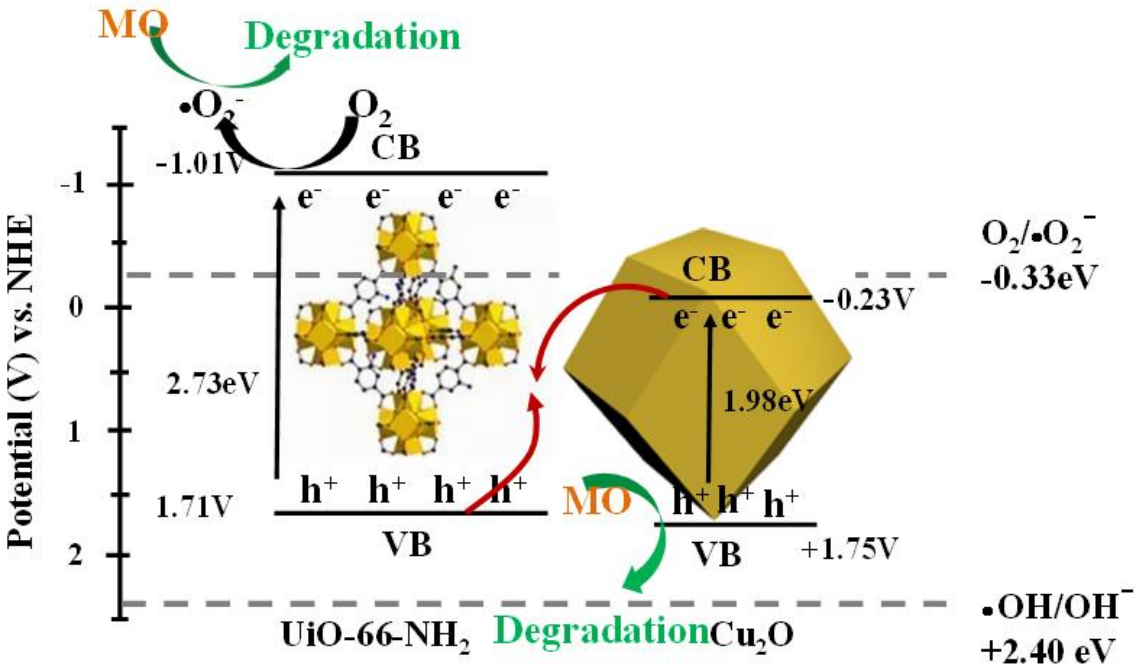

Figure 3.13 Proposed Z-scheme mechanism for the degradation of MO over UiO-66-NH_2/Cu_2O composite.

Based on the above experiments, the possible mechanism of MO degradation using UiO-66-NH_2/Cu_2O composite as catalyst was proposed and given in Fig 3.13. The UiO-66-NH_2/Cu_2O composite catalyst is composed of a p-type Cu_2O (E_{CB} = -0.23 eV and E_{VB} = +1.75 eV vs. NHE [34]) and an n-type UiO-66-NH_2 (E_{VB} = +1.71 eV and E_{CB} = -1.01 eV vs. NHE [35]). As such, both semiconductors can be excited to yield e^--h^+ pairs under visible light. Once the Cu_2O and UiO-66-NH_2 are combined together, the p/n type heterostructure could be formed. In this case, because the potential of the CB of Cu_2O is more positive, the photoinduced e^- at the CB of UiO-66-NH_2 will move to the CB of Cu_2O. However, since the CB of Cu_2O is located at -0.23eV vs. NHE, the

adsorbed O_2 cannot accept the electrons to produce $\bullet O_2^-$ ($E_{O_2/\bullet O_2^-}$=-0.33eV vs.NHE). It should be noted that this is inconsistent with the results obtained by the active species trapping experiment, in which $\bullet O_2^-$ was also considered as the major active species in the photodegrading process. As such, a Z-scheme structure was proposed as shown in Fig 3.13 to explain the photocatalytic process. Herein, under visible light, the photoinduced e^- at the CB of Cu_2O would be quickly quenched by the h^+ at the VB of UiO-66-NH_2 [36]. As a consequence, the e^- enriched in CB of UiO-66-NH_2 can reduce the O_2 to yield $\bullet O_2^-$, which exerts high oxidation activity for the MO degradation [37]. Meanwhile, the generated hole on the Cu_2O, the one of the active species, would also quickly react with the MO. As such, the obvious suppression of the photogenerated e^--h^+ pairs recombination could be realized by Z-scheme heterojunction. In addition, the combination of UiO-66-NH_2 and Cu_2O decreased the band gap (Fig 3.4) so that the visible light in the longer wavelength region can be utilized. Therefore, the photocatalytic efficiency and stability were obviously enhanced.

3.4 Conclusions

The UiO-66-NH_2/Cu_2O composite catalysts were successfully prepared using a facile impregnation way and used for the MO photocatalytic degradation process. The as-prepared composites presented higher photocatalytic performances than the Cu_2O. Specially, the UiO-66-NH_2/Cu_2O composite with 20% of UiO-66-NH_2 exhibited the excellent photocatalytic activity, 98.6% of MO was decomposed within 50 minutes. The improved photocatalytic performance could be ascribed to the efficient separation of photoinduced e^--h^+ pairs within the Z-scheme heterojunction and the synergistic effect between Cu_2O and UiO-66-NH_2. The photo-generated h^+ and $\bullet O_2^-$ were the crucial species during this process.

References

[1]. X. Meng, Z. Li, J. Chen, H. Xie, Z. Zhang, Enhanced visible light-induced photocatalytic activity of surface-modified BiOBr with Pd nanoparticles. Appl. Surf. Sci. 433(2018) 76-87.

[2]. Z. Yu, F. Li, Q. Yang, Nature-mimic method to fabricate polydopamine/graphitic carbon nitride for enhancing photocatalytic degradation performance. ACS Sustain. Chem. Eng. 5(2017) 7840-7850.

[3]. W. C. Huang, L. M. Lyu, Y. C. Yang, M. H. Huang, Synthesis of Cu_2O nanocrystals from cubic to rhombic dodecahedral structures and their comparative photocatalytic activity. J. Am. Chem. Soc. 134(2011)1261-1267.

[4]. C. Y. Toe, Z. Zheng, H. Wu, Photocorrosion of cuprous oxide in hydrogen production: rationalising self-oxidation or self-reduction. Angew. Chem. 130(2018) 13801-13805.

[5]. D.Y. Li. S. Y. Zuo, H. M. Xu, J. Zan, L. Sun, D. Han, D. S. Xia, Synthesis of a g-C_3N_4-Cu_2O heterojunction with enhanced visible light photocatalytic activity by PEG. J. Colloid. Interf. Sci. 531(2018) 28-36.

[6]. H. Wang, L. Zhang, Z. Chen, Semiconductor heterojunction photocatalysts: design, construction, and photocatalytic performances. Chem. Soc. Rev. 43(2014) 5234-5244.

[7]. S. Tao, M. Yang, H. Chen, M. Ren, G. Chen. Microfluidic synthesis of Ag@ Cu_2O core-shell nanoparticles with enhanced photocatalytic activity. J.Colloid.Interf. Sci. 486(2017) 16-26.

[8]. H. Li, Y. Zhou, W. Tu, State-of-the-art progress in diverse heterostructured photocatalysts toward promoting photocatalytic performance. Adv. Funct. Mater. 25(2015) 998-1013.

[9]. B. Liu, Y. Wu, J. Zhang, X. Han, H. Shi, Visible-light-driven g-C_3N_4/Cu_2O heterostructures with efficient photocatalytic activities for tetracycline degradation and microbial inactivation. J. Photochem. Photobiol. A: Chem, 378(2019) 1-8.

[10]. S. Gao, J. Zhang, W. Li, S. Jiao, Y. Nie, H. Fan, X. Zhang, Near room temperature and large-area synthesis of ZnO/Cu_2O heterojunction for photocatalytic properties. Chem. Phys. Lett. 692(2018)14-18.

[11]. J. Y. Huang, P. L. Hsieh, G. Naresh, H. Y. Tsai, M. H. Huang, Photocatalytic activity suppression of CdS nanoparticle-decorated Cu_2O octahedra and rhombic dodecahedra. J. Phys. Chem. C. 122(2018) 12944-12950.

[12]. J. He, D. W. Shao, L. Zheng, L. Zheng, D. Feng, J. Xu, H. Dong, Construction of Z-scheme Cu_2O/Cu/AgBr/Ag photocatalyst with enhanced photocatalytic activity and stability under visible light. Appl. Catal. B. 203(2017)917-926.

[13]. N. Omrani, A. Nezamzadeh-Ejhieh, A comprehensive study on the enhanced photocatalytic activity of Cu_2O/$BiVO_4$/WO_3 nanoparticles. J. Photochem. Photobiol. A: Chem, 389(2020)112223.

[14]. M. Li, Y. Li, Q. Zhang, C. Qin, W. Zhao, Z. Wang, A. Inoue, Ultrafine Cu_2O/CuO nanosheet arrays integrated with NPC/BMG composite rod for photocatalytic degradation. Appl. Surf. Sci. 483(2019)285-293.

[15]. O. M. Yaghi, M. O. Keeffe, N.W. Ockwig, H.K. Chae, M. Eddaoudi, J. Kim, Reticular synthesis and the design of new materials, Nature. 423(2003)705–714.

[16]. S. Hasegawa, S. Horike, R. Matsuda, S. Furukawa, K. Mochizuki, Y. Kinoshita, S. Kitagawa, Three-dimensional porous coordination polymer functionalized with amide groups based on tridentate ligand: selective sorption and catalysis, J. Am. Chem. Soc. 129(2007) 2607–2614.

[17]. M. Eddaoudi, J. Kim, N. Rosi, D. Vodak, J. Wachter, M.O.Õ. Keeffe, O.M. Yaghi, Systematic design of pore size and functionality in isoreticular MOFs and their application in methane storage, Science. 295(2002) 469–472.

[18]. P. Horcajada, C. Serre, M. Vallet-Regí, M. Sebban, F. Taulelle, G. Férey, Metal-organic frameworks as efficient materials for drug delivery, Angew. Chem.45(2006) 5974–5978.

[19]. H. Ramezanalizadeh, F. Manteghi, Synthesis of a novel MOF/$CuWO_4$ heterostructure for efficient photocatalytic degradation and removal of water pollutants. J. Clean. Prod. 172(2018) 2655-2666.

[20]. E. H. Zhou, B. H. Li, W. X. Chen, Z. Luo, J. Liu, A. Singh, J. C. Jin, Photocatalytic degradation of organic dyes by a stable and biocompatible Zn (II) MOF having ferulic acid: experimental findings and theoretical correlation. J. Mol. Struct. 1149(2017) 352-356.

[21]. C. Yang, X. You, J. Cheng, H. Zheng, Y. Chen, A novel visible-light-driven In-based MOF/graphene oxide composite photocatalyst with enhanced photocatalytic activity toward the degradation of amoxicillin. Appl. Catal. B. 200(2017) 673-680.

[22]. R. Bibi, Q. Shen, L. Wei, Hybrid BiOBr/UiO-66-NH_2 composite with enhanced visible-light driven photocatalytic activity toward RhB dye degradation. RSC Adv. 8(2018) 2048-2058.

[23]. Q. Liang, S. Cui, C. Liu, Construction of CdS@ UIO-66-NH_2 core-shell nanorods for enhanced photocatalytic activity with excellent photostability. J. Colloid. Interf. Sci. 524(2018) 379-387.

[24]. Q. Liang, S. Cui, J. Jin, C. Liu, S. Xu, C. Yao, Z. Li, Fabrication of BiOI@ UIO-66 (NH_2)@g-C_3N_4 ternary Z-scheme heterojunction with enhanced visible-light photocatalytic activity. Appl. Surf. Sci. 456(2018) 899-907.

[25]. X. Y. Xu, C. Chu, H. Fu, X. D. Du, P. Wang, W. Zheng, C. C. Wang, Light-responsive UiO-66-NH_2/Ag_3PO_4 MOF-nanoparticle composites for the capture and release of sulfamethoxazole. Chem. Eng. J. 350(2018) 436-444.

[26]. S. Li, X. Wang, Y. Xu, H. Yang, F. Wei, X. Liu, The excellent photocatalytic synergism of $PbBiO_2Br$/UiO-66-NH_2composites via multiple coupling effects. RSC Adv. 6(2016), 89907-89915.

[27]. C. Gomes Silva, I. Luz, F. X. Llabres i Xamena, A. Corma, H. García, Water stable Zr-benzenedicarboxylate metal-organic frameworks as photocatalysts for hydrogen generation. Chem.- Eur. J. 16 (2010) 11133-11138.

[28]. S. Meng, D. Li, M. Sun, Sonochemical synthesis, characterization and photocatalytic properties of a novel cube-shaped $CaSn(OH)_6$. Catal. Commun. 12(2011) 972-975.

[29]. L. Ye, J. Liu, Z. Jiang, Facets coupling of BiOBr-g-C_3N_4 composite photocatalyst for enhanced visible-light-driven photocatalytic activity. Appl. Catal. B. 142(2013) 1-7.

[30]. X. Hao, Z. Jin, H. Yang, Peculiar synergetic effect of MoS_2 quantum dots and graphene on Metal-Organic Frameworks for photocatalytic hydrogen evolution. Appl. Catal. B. 210 (2017) 45-56.

[31]. Y. Su, D. Ao, H. Liu, MOF-derived yolk-shell CdS microcubes with enhanced visible-light photocatalytic activity and stability for hydrogen evolution. J. Mater. Chem. A. 5(2017) 8680-8689.

[32]. Q. Sun, Y. P. Peng, H. Chen, K. L. Chang, Y. N. Qiu, S. W. Lai, Photoelectrochemical oxidation of ibuprofen via Cu_2O-doped TiO_2 nanotube arrays. J. Hazard. Mater. 319 (2016)121-129.

[33]. W. Zou, L. Zhang, L. Liu, Engineering the Cu_2O-reduced graphene oxide interface to enhance photocatalytic degradation of organic pollutants under visible light. Appl. Catal. B. 181(2016) 495-503.

[34]. E. Aguilera-Ruiz, U. M. García-Pérez, M. de la Garza-Galván, P. Zambrano-Robledo, B. Bermúdez-Reyes, J. Peral. Efficiency of $Cu_2O/BiVO_4$ particles prepared with a new soft procedure on the degradation of dyes under visible-light irradiation. Appl. Surf. Sci. 328 (2015) 361-367.

[35]. Y. C. Zhou, X. Y. Xu, P. Wang, H. Fu, C. Zhao, C. C. Wang, Facile fabrication and enhanced photocatalytic performance of visible light responsive UiO-66-NH_2/Ag_2CO_3 composite. Chin. J. Catal. 40 (2019) 1912-1923.

[36]. H. Zhou, Z. Wen, J. Liu, J. Ke, X. Duan, S. Wang. Z-scheme plasmonic Ag decorated WO_3/Bi_2WO_6 hybrids for enhanced photocatalytic abatement of chlorinated-VOCs under solar light irradiation. Appl. Catal. B. 242(2019) 76-84.

[37]. Q. Zhao, J. Wang, Z. Li, Preparation of Cu_2O/exfoliated graphite composites with high visible light photocatalytic performance and stability. Ceram. Int. 42(2016) 13273-13277.

CHAPTER 4

Heterostructured g-C_3N_4 nanosheets /Cu_2O composite as an enhanced visible light photocatalyst for decomposition of tetracycline antibiotics

4.1 Introduction

With the large and unreasonable use of antibiotics in human production and living, the wastewater with antibiotics produced from medical, agricultural, animal husbandry and industry have become a major pollutant to the environment. Among various antibiotics, the long-term pollution brought by tetracycline (TC) is very serious since the structure of TC is generally stable, and the natural degradation rate in water and soil is very low [1]. Photocatalytic degradation of pollutants from wastewater is considered as one of the prospective technologies with high efficiency and energy-saving advantage. Due to its excellent optoelectronic property, semiconductor material has received widespread attention as the photocatalyst in the treatment of environmental pollution [2-5]. Among various semiconductor materials, Cu_2O is an environmentally friendly p-type semiconductor and its narrow-band gap is 2.0 eV, which can be excited in the visible light. Moreover, it can be made from abundant resource of Cu on the earth with low price, and has advantages of non-toxicity and no secondary pollution. Thus, it has been widely used in the photocatalysis research [6-7]. Although the Cu_2O with cubic phase has good photocatalytic performance, low quantum efficiency and easy oxidation greatly limit its large-scale application. Therefore, the modification of Cu_2O is essential to improve its photocatalytic efficiency and stability. Generally, the photocatalytic efficiency and stability of the Cu_2O can be enhanced by doping with precious metals, loading it on the conductive carriers or coupling it with other

semiconductors to form heterostructured composites [8-13].

Graphitic carbon nitrides such as g-C_3N_4 are metal-free polymeric materials with the potential photocatalytic property [14]. Specially, the surface area of nanosheet-state g-C_3N_4 is relatively large and it can provide more abundant reactive sites for decomposition of organic pollutants and suppress the recombination probability of photogenerated e^--h^+ pairs [15-20]. Recently, many strategies to prepare g-C_3N_4 nanosheets have been proposed. It is found that combining g-C_3N_4 with other semiconductor to form heterojunction structure is an effective route to enhance its photocatalytic efficiency [21-24]. For instance, the fabricated g-C_3N_4-Cu_2O heterojunction exhibited high chemical stability, low toxicity and high oxidation capacity. Tian *et al.* [25] prepared the p-n type heterostructured g-C_3N_4–Cu_2O by the hydrothermal method. For the MO degradation, its photocatalytic activity is significantly higher than that of individual C_3N_4 or Cu_2O. Li *et al.* [26] also prepared the g-C_3N_4–Cu_2O in the presence of glutamate by a hydrothermal synthesis followed with the high-temperature calcination. The MO degradation rate was increased from 80 to 98% after modification with glutamate. So, by using the glutamate, the heterojunction effect was enhanced, resulting in better photocatalytic performance. Liu *et al.* [27] successfully coated g-C_3N_4 onto the Cu_2O nanosphere by combining the solvothermal and chemisorption methods. The obtained Cu_2O@g-C_3N_4 core@shell composite showed obviously enhanced photocatalytic performance for the hydrogen production. However, for practical applications, the photocatalytic efficiency of such C_3N_4-Cu_2O composites is still not enough and needed to be further improved. Especially, the specific surface area of g-C_3N_4 should be further increased to provide more abundant reactive sites and decrease the recombination rate of photo-generated e^--h^+ pairs for the decomposition of organic pollutants [28].

In this study, the g-C_3N_4 nanosheets with a larger surface area were obtained by using an expansion method and the g-C_3N_4 nanosheets/Cu_2O composite was then prepared by a simple co-precipitation method, which was applied for the photocatalytic

degradation of TC under visible light. Based on the experimental results, the possible photocatalytic mechanism was also proposed.

4.2 Experimental

4.2.1 Preparation of g-C_3N_4 nanosheets

The schematic diagram for preparing g-C_3N_4 nanosheets is shown in **Scheme 1**[19]. In a 250 mL beaker, g-C_3N_4 (1 g) was added in 20 mL of H_2SO_4 (98 wt %) and cooled down to 0 °C. Then, $NaNO_3$ (1 g) was slowly added with stirring. After reaction for 10 min, 3 g of $KMnO_4$ powder was added in it slowly. After stirring for 1 h, the ice-salt bath was removed. Then, 125 mL of deionized water was added dropwise with a rate of 1 drop/s. Sequentially, 10 mL of H_2O_2 (30 wt %) was then added with the same rate. Finally, the mixed solution was adjusted to neutral value with water and then the g-C_3N_4 nanosheets was separated by a high-speed centrifuge and dried at 35 ℃ for 12 h.

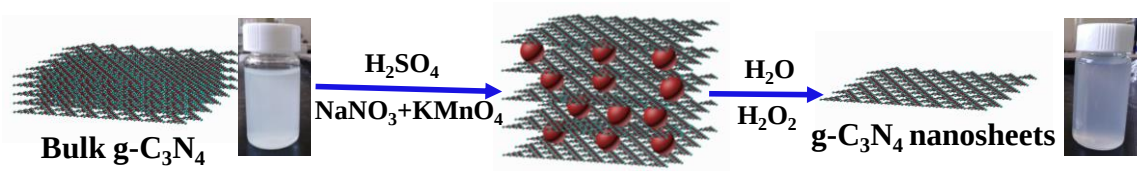

Scheme1. Illustration of the formation process of g-C_3N_4 nanosheets

4.2.2 Preparation of g-C_3N_4 nanosheets/Cu_2O

135.75 mL of distilled water, 0.003 g of g-C_3N_4 nanosheets and 1.5 mL of 0.1M $CuSO_4$ were introduced in a 500 mL beaker, after ultrasound-treating for 30 min, NaOH (5.25 mL, 1 mol / L) was added dropwise. Then, 7.5 mL of ascorbic acid (0.2 mol / L) was introduced and stand for 3 h. After high-speed centrifugation, the solids were washed with a water-ethanol mixed solution (V_{water}:$V_{Ethanol}$ =1:1) for two times, and then washed with CH_3CH_2OH and dried at 35 ° C for 12 h. As such, the photocatalyst 30 wt% g-C_3N_4 nanosheets/Cu_2O composite was obtained.

4.2.3 Catalyst characterization

X-ray powder diffraction (XRD) characterization was conducted through the Bruker D8 diffractometer using Cu Kα as the radiation. The morphology was obtained by transmission electron microscope (JEOLJEM, 200kV) and scanning electron microscope (TESCAN, 15kV). X-ray photoelectron spectroscopy (XPS) characterization was obtained by the Thermo Fisher Scientific Escalab 250Xi system. The Brunauer-Emmet-Teller (BET) characterization was conducted by N_2 adsorption on the Micrometrics ASAP-2020 PLUS HD88 adsorption equipment. FT-IR spectrum was recorded by the CDS-2000 Bio-Rad FTS-165 detector. UV-vis spectra were collected by Jena spectrophotometer (SPECORD® 210 PLUS). Electrochemical impedance spectroscopy (EIS) was conducted in a solution containing KCl (0.1 M) and $[Fe(CN)_6]^{3-/4-}$ (2.5 mM). The photocurrent response was conducted under visible light in 0.2 M Na_2SO_4 solution using Pt and Ag/AgCl as the counter electrode and reference electrode, respectively.

4.2.4 Photocatalytic performance test

The photocatalytic experiment was conducted in a reactor with an Xe lamp with a cut off filter of 420 nm (500 W，CEL-S500) and tetracycline (TC) was used as the degradation target. In a typical procedure, under magnetic stirring, 100 mg of catalyst was added into 90 mL TC solution (30 mg/L). The adsorbent equilibrium between the TC and catalyst was reached by stirring the mixed solution for 30 min under dark. Thereafter, the mixture was exposed to the visible light with continuous stirring under ambient temperature. At the selected time interval, 4 mL of solution was centrifuged to get rid of the solid for measurements. The concentration of TC was determined by a model 722E UV-vis spectrophotometer at 357nm.

4.2.5 Active species trapping analysis

For further investigating the influence of $\bullet O_2^-$ during the photocatalytic degradation

process, the TC degradation experiment was also conducted under N_2 atmosphere. In addition, to understand the photocatalysis mechanism, ammonium oxalate (AO) and isopropyl alcohol (IPA) were introduced as the scavenger for h^+ and •OH, respectively [29, 30], and all other experimental conditions were remained as the same as the above experiments.

4.3 Results and discussion

4.3.1 Characterizations

Table 4. 1 Surface areas of samples

Sample	Surface area (m^2/g)
Bulk g-C_3N_4	12.26
g-C_3N_4 nanosheets	150.16
Cu_2O	16.24
30 wt% g-C_3N_4 nanosheets/Cu_2O	36.36

Fig. 4.1 and Tab. 4. 1 shows the BET results of the samples. One can see that the BET surface area of g-C_3N_4 nanosheets prepared by the expansion method was about 12 times higher than that of bulk g-C_3N_4 (Tab. 4.1). In addition, the surface area of 30% g-C_3N_4 nanosheets/Cu_2O was 36.36 m^2g^{-1}, which was much larger than that of the pure Cu_2O (16.24 m^2g^{-1}), indicating that the combining of Cu_2O with g-C_3N_4 nanosheets obtained a relatively high surface area, which should be favorable for the adsorption of TC, and thereby enhancing the photocatalytic removal efficiency.

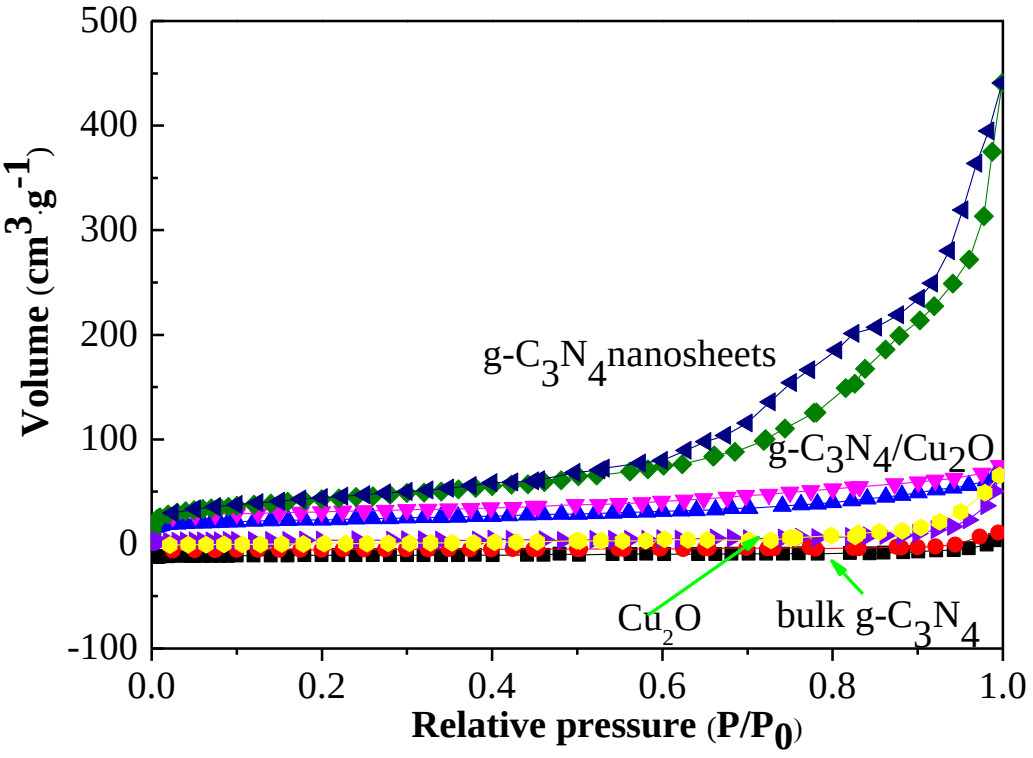

Figure 4.1 N_2 adsorption-desorption isotherms of bulk g-C_3N_4, g-C_3N_4 nanosheets, Cu_2O and 30 % g-C_3N_4 nanosheets/Cu_2O.

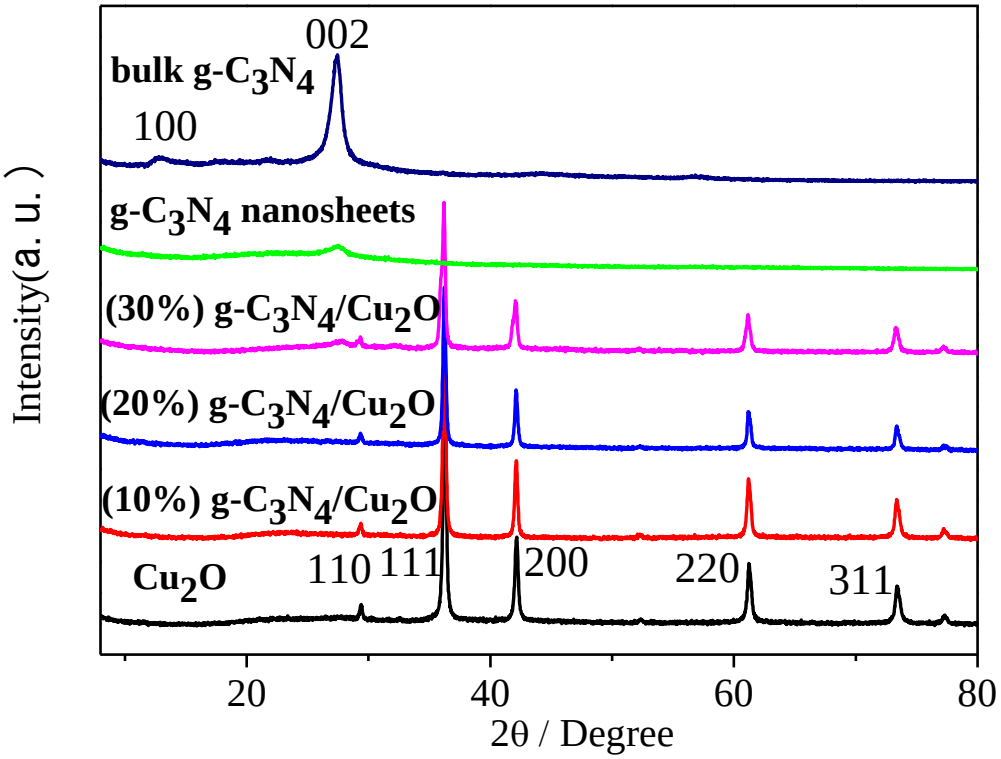

Figure 4.2 XRD patterns of Cu_2O, bulk g-C_3N_4, g-C_3N_4 nanosheets and g-C_3N_4 nanosheets/Cu_2O composites with different amounts of g-C_3N_4 nanosheets

In Fig. 4. 2**,** the (002) diffraction at about 27.4° related to the interlayer stacking structure whereas the (100) diffraction at 13.0° indicated the interplanar structural packing. Obviously, the intensity of (002) diffraction corresponding to the interlayer stacking was significantly decreased after the exfoliation. The peaks of (110), (111), (200), (220) and (311) showed the present of Cu_2O, and a weak peak of g-C_3N_4 nanosheets at 27.4° was also found in the g-C_3N_4 nanosheets/Cu_2O composite, indicating that g-C_3N_4 nanosheets were successfully combined with Cu_2O in the composite.

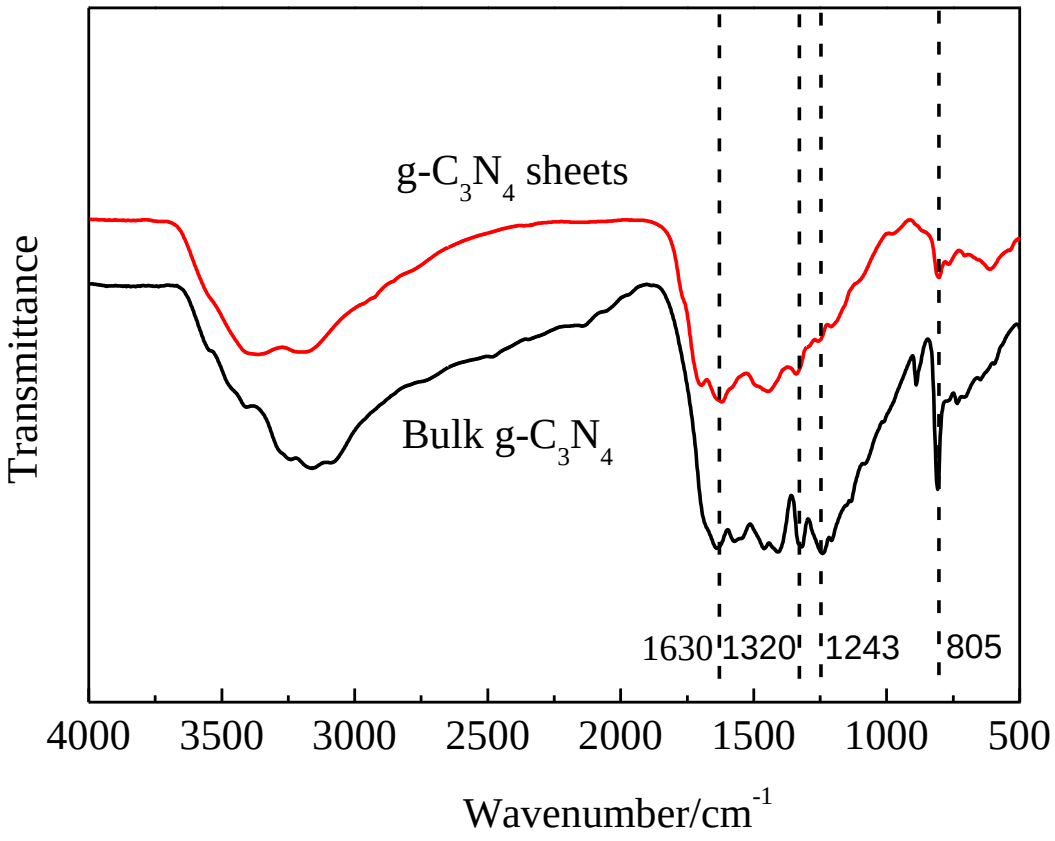

Figure 4.3 FTIR spectra of bulk g-C_3N_4 and g-C_3N_4 nanosheets

Fig. 4. 3 shows FTIR spectra of the samples, in which the peak near 1630 cm^{-1} was assigned to C=N stretching, the peaks at 1243 and 1320 cm^{-1} corresponded to aromatic C-N stretching, the absorption band at 805 cm^{-1} belonged to triazine ring mode, which corresponded to condensed C-N heterocycles, and the broad band in the range of 3000-3500 cm^{-1} corresponded to uncondensed terminal amino and hydroxyl groups [31].

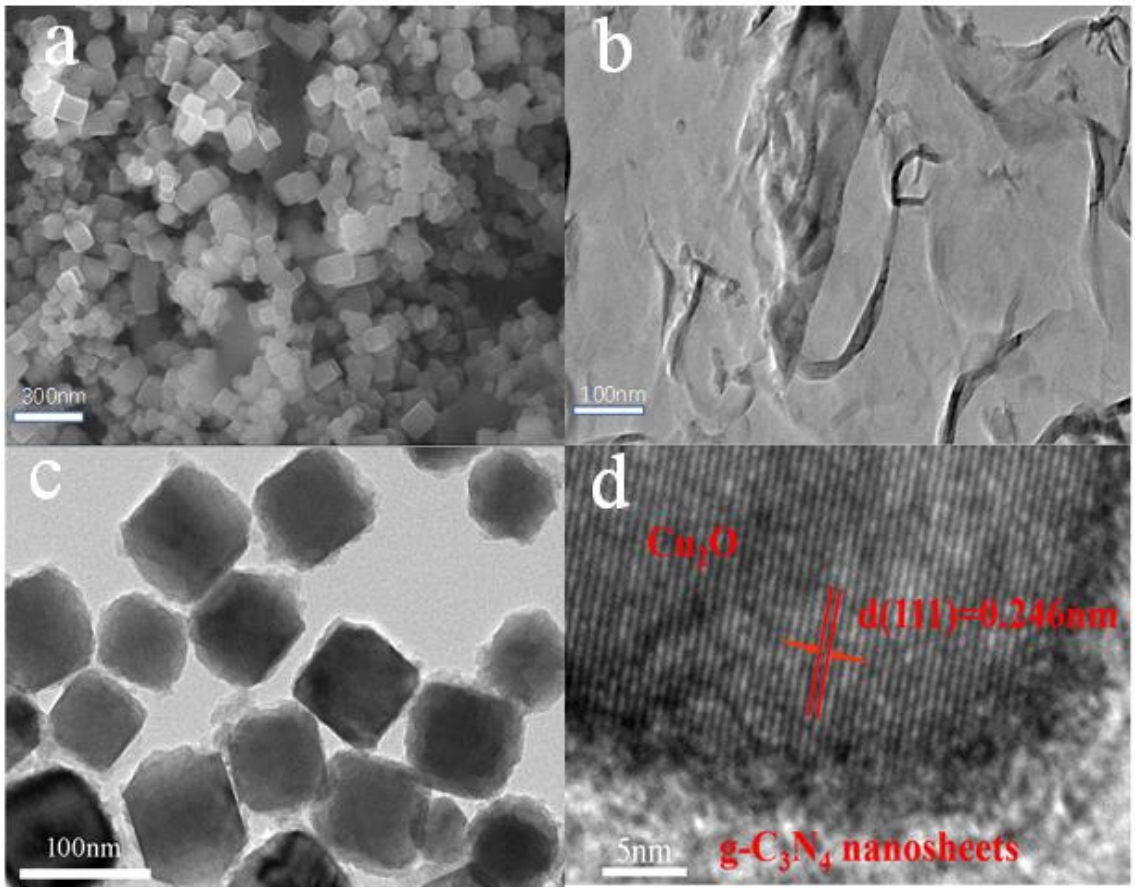

Figure 4.4 SEM (a) images of Cu_2O, TEM (b) images of g-C_3N_4 nanosheets and TEM (c) and HRTEM(d) images of 30 % g-C_3N_4 nanosheets /Cu_2O composite photocatalyst.

As shown in Fig. 4. 4, the obtained Cu_2O particle had cubic structure and the particle size is about 60-120 nm (Fig. 4.4 a). In Fig. 4.4 b, the pristine g-C_3N_4 nanosheets showed a representative sheet-like shape with smooth surface. The TEM image of g-C_3N_4 nanosheets/Cu_2O composite revealed that the g-C_3N_4 nanosheets covered Cu_2O (Fig. 4.4 c). Furthermore, HRTEM image in Fig. 4.4 d confirmed that the combination of Cu_2O and g-C_3N_4 nanosheets was successfully achieved. Herein, the crystal face spacing of 0.246 nm corresponded to the (111) crystal plane of Cu_2O, implying that the lattice structure of Cu_2O maintained unchanged after combining with the g-C_3N_4 nanosheets.

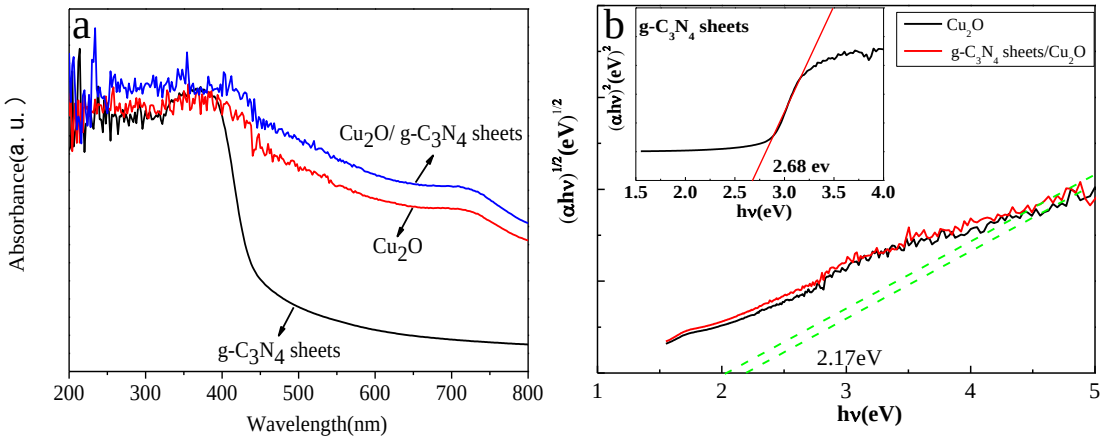

Figure 4.5 UV-vis DRS spectra of g-C_3N_4 nanosheets, Cu_2O and 30 % g-C_3N_4 nanosheets /Cu_2O composite.

The UV-vis DRS spectra and the optical absorption edges of g-C_3N_4 nanosheets, Cu_2O and g-C_3N_4 nanosheets /Cu_2O composite were given in Fig. 4.5. Herein, the fundamental absorption edge of g-C_3N_4 nanosheets was at 460 nm and the band gap is 2.68 eV[32]. Meanwhile, the absorption edge of Cu_2O appeared at 600 nm and its band gap is 2.17 eV[33]. From Fig. 4.5, one can see that the g-C_3N_4 nanosheets/Cu_2O composite had response to the visible light and the absorptive intensity of Cu_2O was enhanced by combining it with g-C_3N_4 nanosheets. Thus, the absorption capacity of g-C_3N_4 nanosheets/Cu_2O composite for visible light was enhanced, resulting in higher photocatalytic performance.

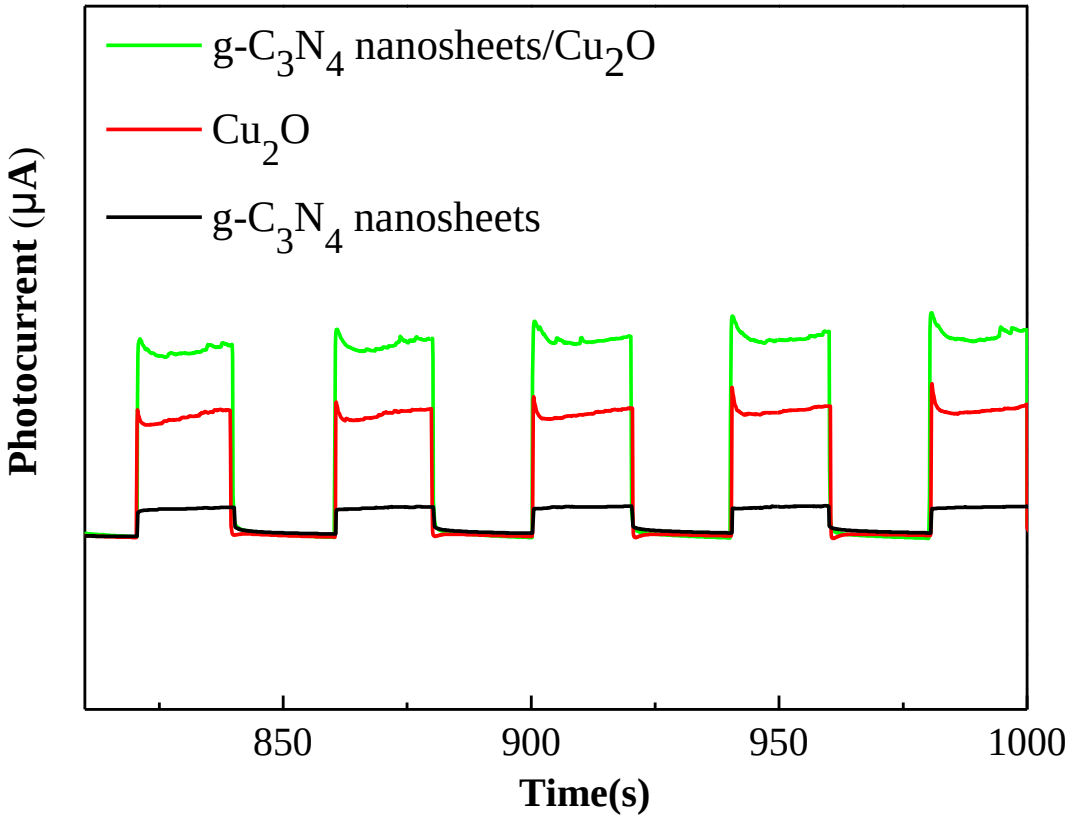

Figure 4.6 Photocurrent responses of g-C_3N_4 nanosheets, Cu_2O and 30 % g-C_3N_4 nanosheets /Cu_2O composite.

The photocurrent and EIS were used to evaluate the separation efficiency of e^--h^+ pairs. From Fig. 6, one can see that the photocurrent value of g-C_3N_4 nanosheets/Cu_2O composite was obviously increased, indicating that the photoinduced e^--h^+ pairs could be more effectively separated on the g-C_3N_4 nanosheets/Cu_2O composite.

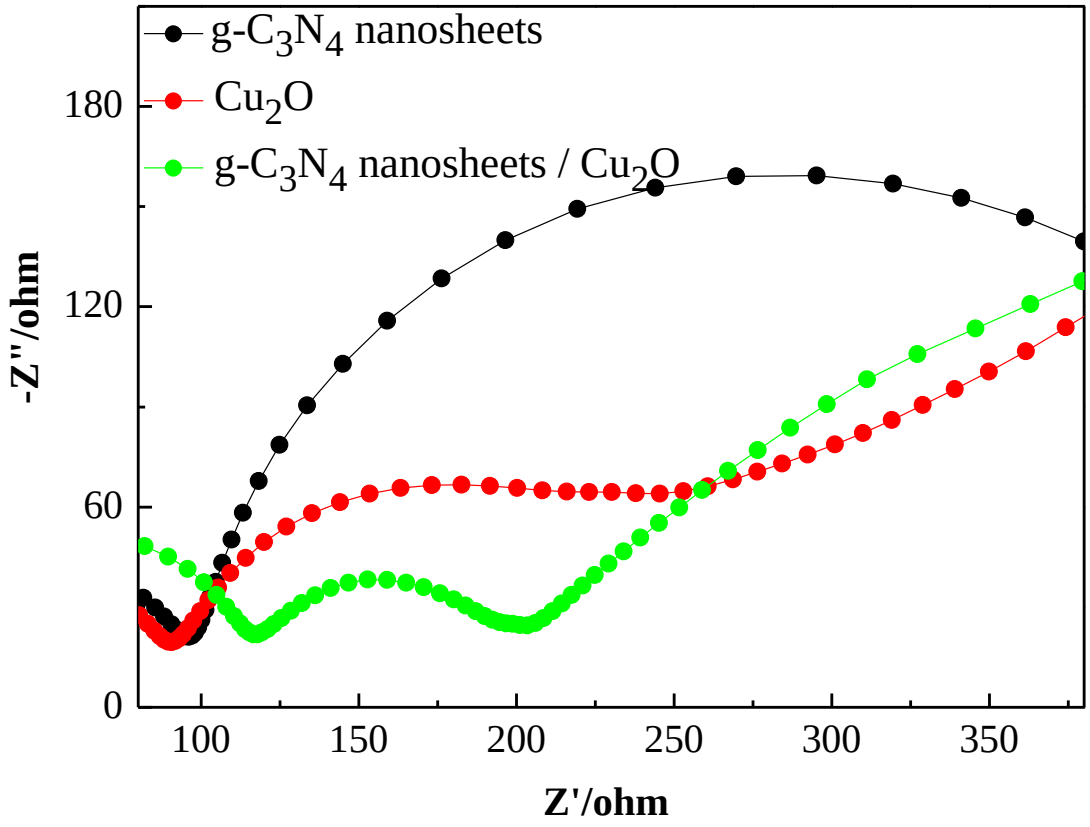

Figure 4.7 EIS Nyquist plots of g-C_3N_4 nanosheets, Cu_2O and 30 % g-C_3N_4 nanosheets /Cu_2O composite

Fig. 4.7 shows EIS Nyquist plots of the samples. One can see that the circular radius for the g-C_3N_4 nanosheets/Cu_2O composite was smaller than that for Cu_2O, indicating that the composite had a faster interfacial charge-electron transfer rate than Cu_2O [34]. Thus, the g-C_3N_4 nanosheets /Cu_2O composite should possess stronger ability to produce and deliver the photoinduced charge carrier than the pure Cu_2O.

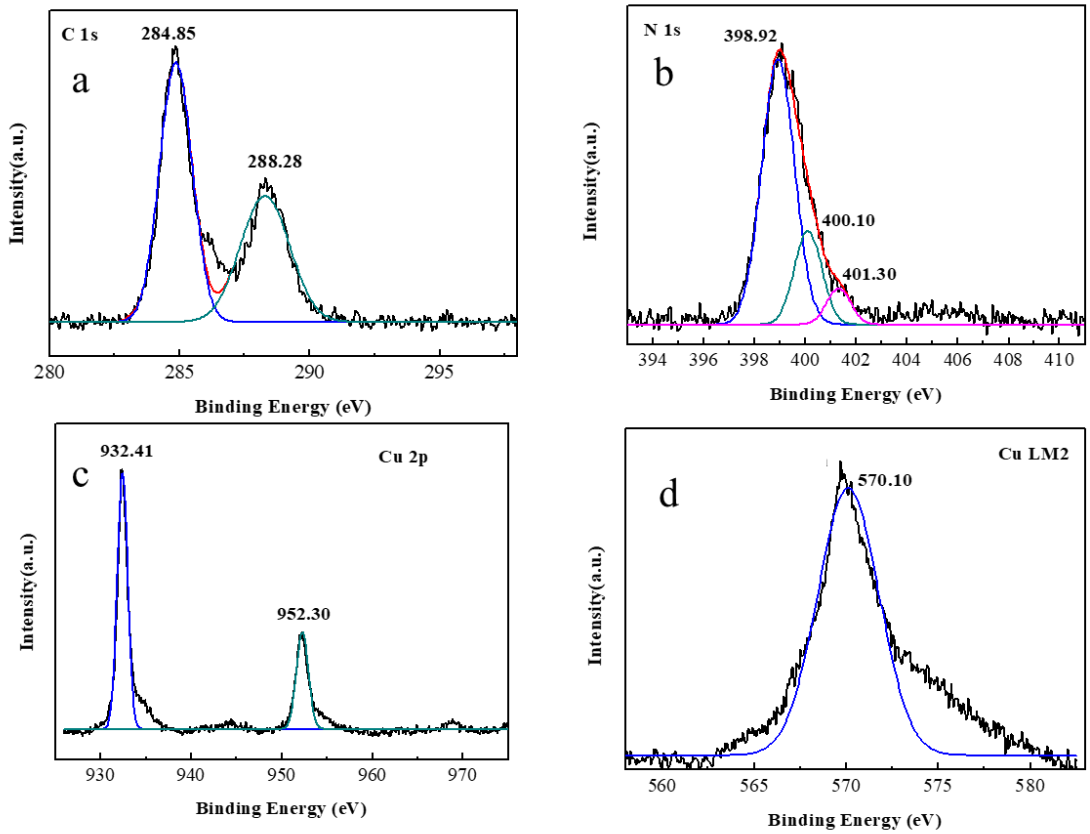

Figure 4.8 XPS analyses of 30 % g-C_3N_4 nanosheets /Cu_2O composite. (a) C1s XPS spectrum; (b) N 1s XPS spectrum; (c) Cu 2p XPS spectrum; (d) Cu LMM spectrum.

Fig. 4. 8a shows the XPS spectrum of C1s. One can see that there were two peaks, one is at 284.8 corresponded to C=C in adventitious carbon and the other is at 288.2 eV corresponded to C−N=C in the heterocycle rings. For the N1s spectrum (**Fig. 4. 8b**), the binding energies at 398.9, 400.10, and 401.3 eV were ascribed to g-C_3N_4 [31], which evidence the existence of g-C_3N_4 in the composite. For the Cu 2p spectrum (Fig. 4. 8c), the characteristic peaks at 952.3 and 932.4 eV were assigned to the binding energies of Cu $2p_{1/2}$ and Cu $2p_{3/2}$, respectively [35]. Because the binding energies of Cu^+ and Cu^0 in the Cu 2p XPS are very close, it is difficult to differentiate them. It is reported that the Cu LMM spectrum could provide a way to recognize them [9]. In Fig. 4. 8d, the peak at 571.2 eV for Cu^0 species was not observed in the sample, implying that Cu^0 was not produced in the photocatalyst. In addition, the peak appeared at 570.10 eV

indicated the existence of Cu_2O. Thus, Cu_2O was the only reduced species from Cu^{2+} in the fresh catalyst.

4.3.2 Photocatalytic performance

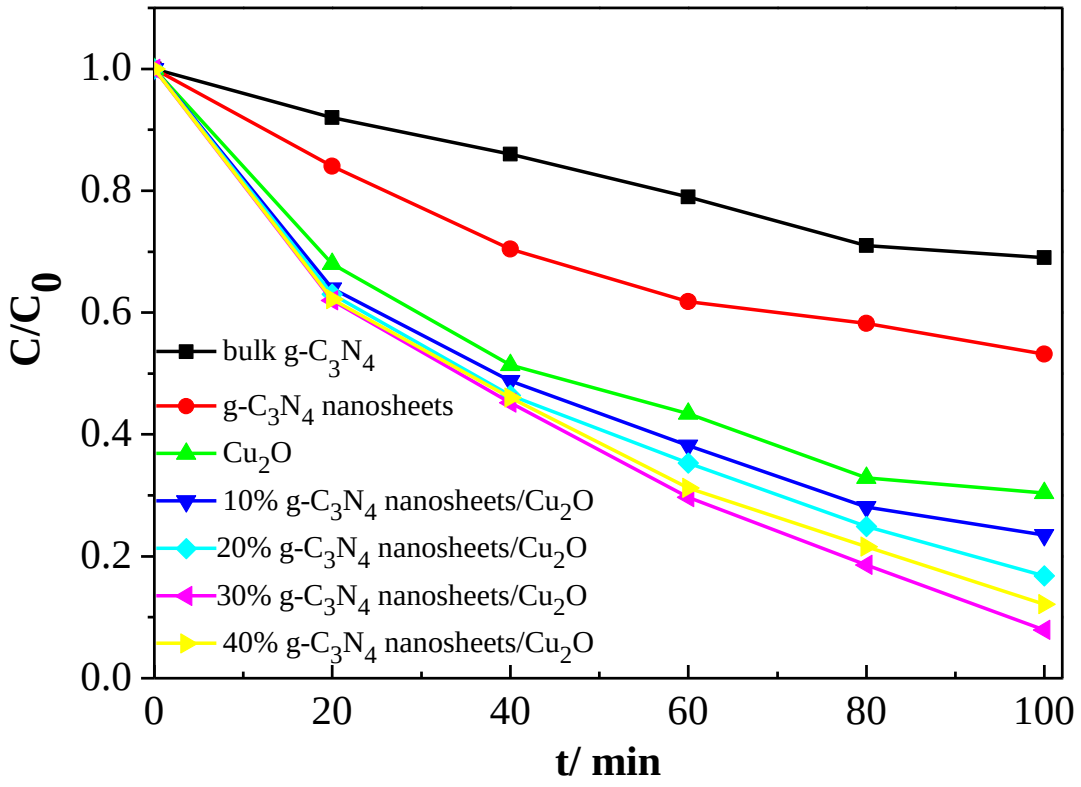

Figure 4.9 Photocatalytic degradation curves for decomposition of TC

Fig. 4. 9 shows the photocatalytic performances for TC degradation. One can see that the photocatalytic activity of 30 % g-C_3N_4 nanosheets /Cu_2O composite was much higher than those of other samples, and approximately 92.1% of TC was decomposed after 100 min, which should be attributed to its higher surface area, more effective separation ability for the photoinduced e^--h^+ pairs and the faster interfacial charge transfer rate as indicated above. However, further increasing the content of g-C_3N_4 could cause incomplete construction of heterojunction with Cu_2O, which is not beneficial to charge separation. So, the effective heterojunction structure can be formed only at a suitable mass ratio between the two catalysts.

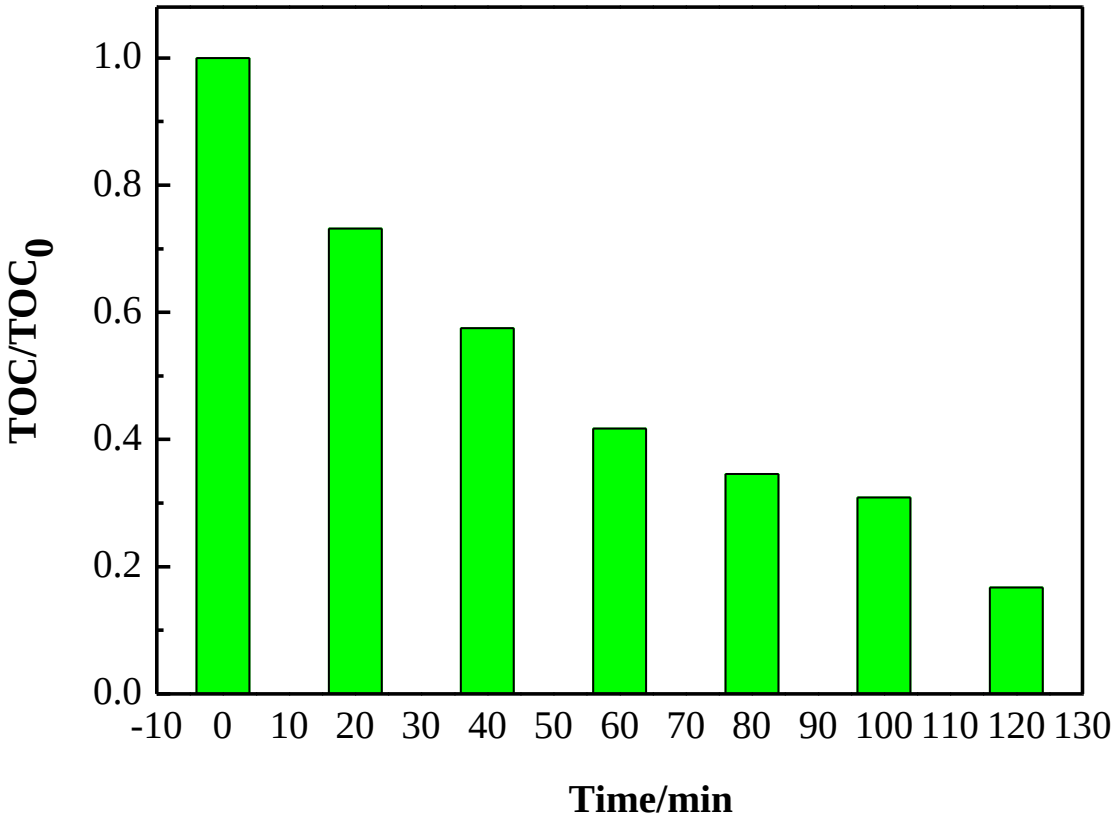

Figure 4.10 Removal of TOC over 30 % g-C_3N_4 nanosheets /Cu_2O composite photocatalyst under visible light irradiation.

The mineralization ratio of TC aqueous solution over g-C_3N_4 nanosheets/Cu_2O was assessed by the TOC analysis. As illustrated in Fig. 4. 10, 83.3% of TOC was removed after the reaction for 120 min, suggesting that most of TC was effectively mineralized by the g-C_3N_4 nanosheets/Cu_2O composite photocatalyst.

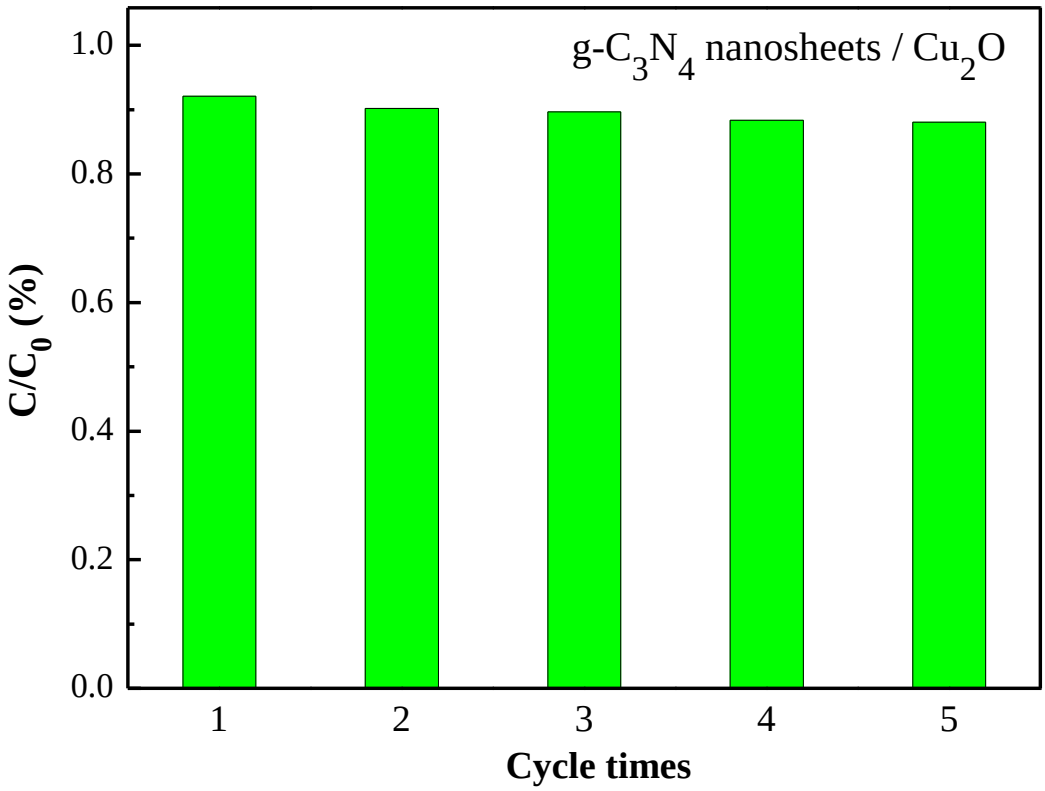

Figure 4.11 Repeated photocatalytic degradation of TC solution over 30 % g-C_3N_4 nanosheets /Cu_2O composite.

The degradation of TC by reusing the spent g-C_3N_4 nanosheets/Cu_2O composite photocatalyst for 5 cycles were also conducted. As seen in Fig. 4. 11, the catalytic activity of 30 % g-C_3N_4 nanosheets/Cu_2O composite was maintained at approximately 88.1% even after five cycles, revealing the excellent stability of g-C_3N_4 nanosheets/Cu_2O composite photocatalyst.

4.3.3 Photocatalytic mechanism

Fig. 4.12 shows the results in the active species trapping experiments using the g-C_3N_4 nanosheets /Cu_2O composite photocatalyst. One can see that the TC degradation rate did not obviously change after adding the IPA (•HO scavengers), implying that •HO should not be the major species in the process. In comparison, the photocatalytic activity decreased obviously and only a small amount of TC were degraded after

introducing AO (h^+ scavengers), implying that the h^+ was also the important species involved in the process. Meanwhile, the photocatalytic activity also decreased obviously under N_2 atmosphere, indicating that during the photocatalytic degrading process, O_2 turned into $\bullet O^{2-}$ by the photo-induced e^- on the g-C_3N_4 nanosheets /Cu_2O and the $\bullet O^{2-}$should be also the major active species in the g-C_3N_4 nanosheets /Cu_2O composite photocatalysts.

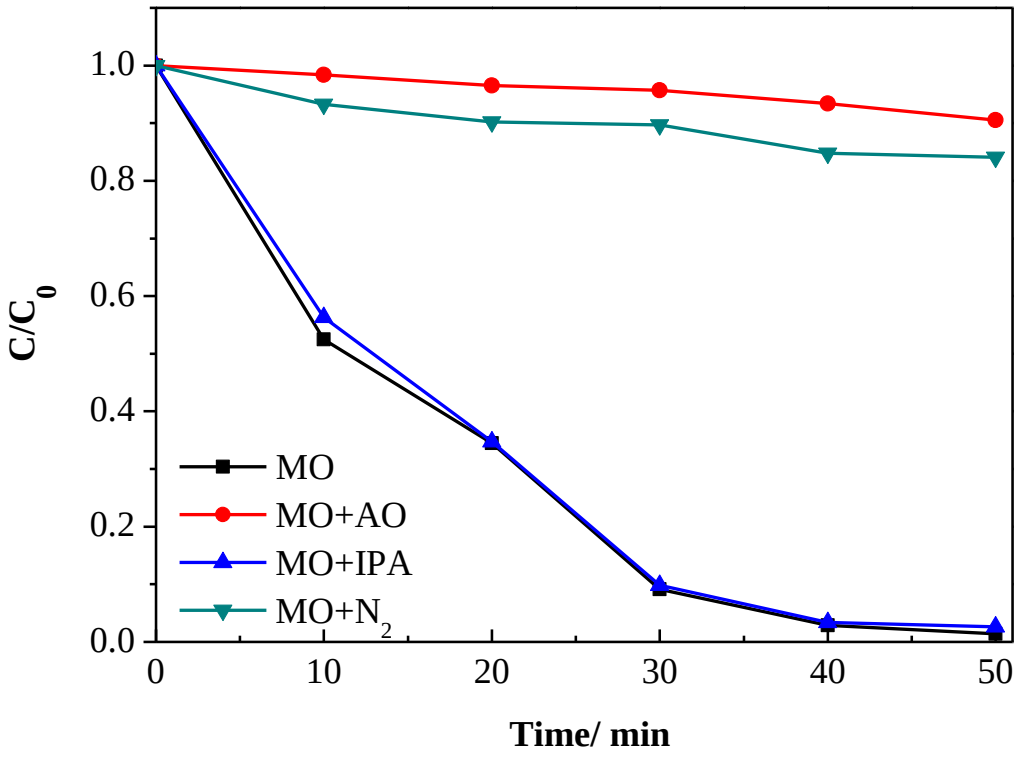

Figure 4.12 Active species trapping experiments with 30 % g-C_3N_4 nanosheets /Cu_2O composite photocatalyst.

The possible mechanism for the photocatalytic degradation of TC over the g-C_3N_4 nanosheets/Cu_2O composite photocatalyst was illustrated in Fig. 4. 13. Herein, when the Cu_2O was combined with g-C_3N_4, the p-n type heterostructure could be formed. Under the visible light irradiation, both of p-type Cu_2O and n-type g-C_3N_4 can be excited to yield e^--h^+ pairs. Under the action of internal electric filed, the photoinduced

e^- in CB of Cu_2O could be delivered to the CB of g-C_3N_4 [33] whereas the excited h^+ on the VB of g-C_3N_4 could be delivered to the VB of the Cu_2O [34]. Meanwhile, the e^- on the g-C_3N_4 can reduce the O_2 to yield the $\bullet O^{2-}$, which is the main active species for the TC degradation and the h^+ enriched on the Cu_2O would also quickly react with the TC. As a consequence, in this p-n type heterostructure, e^--h^+ pairs in two catalyst can be transferred and separated effectively, resulting in obviously enhanced photocatalytic efficiency and stability.

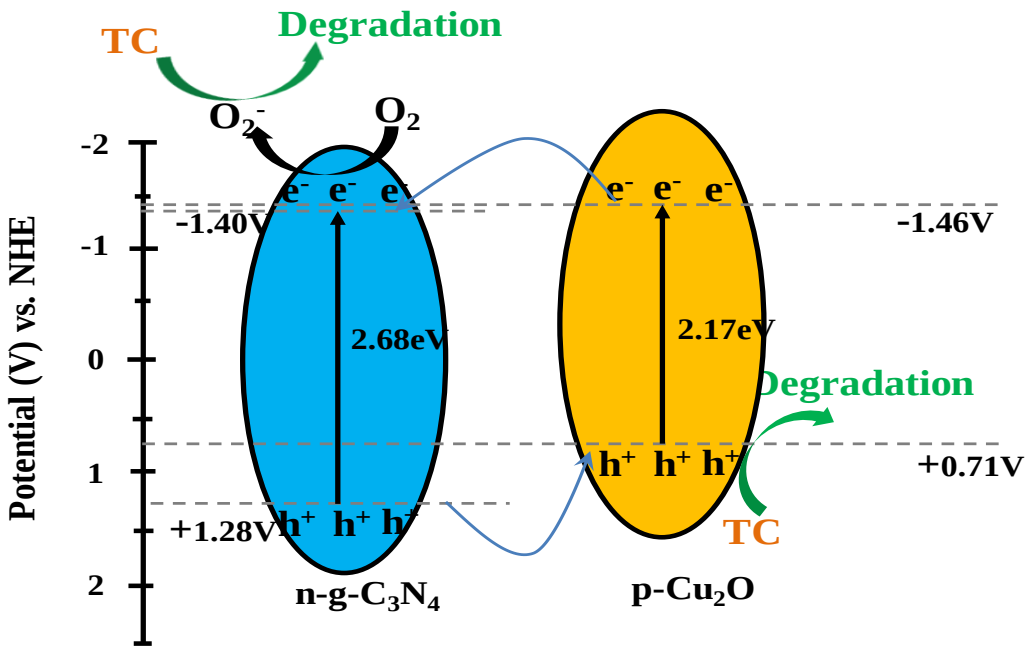

Figure 4.13 Proposed mechanism for the degradation of TC over g-C_3N_4 nanosheets /Cu_2O composite photocatalyst under visible light irradiation.

4.4 Conclusions

The g-C_3N_4 nanosheets with a high surface area were obtained by an expansion method, which were successfully combined with cubic Cu_2O particles to form a g-C_3N_4 nanosheets /Cu_2O composite, and used for the photocatalytic degradation of TC solution under visible light irradiation. As a result, approximately 92.1% of TC was decomposed in 100 min, and 83.3% of TOC was removed after the reaction for 120 min by using this photocatalyst. Also, the catalytic activity maintained at approximately

88.1% even after five cycles, revealing the excellent stability of g-C_3N_4 nanosheets /Cu_2O composite photocatalyst. Furthermore, the results showed that the h^+ and O^{2-}• were the major active species in the photocatalytic degradation of TC over g-C_3N_4 nanosheets/Cu_2O composite photocatalysts. The excellent photocatalytic performance should be ascribed to its higher surface area, more effective separation ability for the photogenerated e^--h^+ pairs and the faster interfacial charge transfer rate with a p-n type heterostructure.

References

[1]. F. Deng, L. N. Zhao, X. B. Luo, S. L. Luo, D. D. Dionysiou, Highly efficient visible-light photocatalytic performance of Ag/$AgIn_5S_8$ for degradation of tetracycline hydrochloride and treatment of real pharmaceutical industry wastewater. Chem. Eng. J. 333 (2018) 423-433.

[2]. R. Li, F. Zhang, D. Wang, J. Yang, M. Li, J. Zhu, C. Li, Spatial separation of photogenerated electrons and holes among {010} and {110} crystal facets of $BiVO_4$. Nat. commun. 4 (2013) 1-7.

[3]. J. Zhang, H. Ma, Z. Liu, Highly efficient photocatalyst based on all oxides WO_3/Cu_2O heterojunction for photoelectrochemical water splitting. Appl. Catal. B. 201 (2017) 84-91.

[4]. H. Dong, G. Chen, J. Sun, C. Li, Y. Yu, D. Chen, A novel high-efficiency visible-light sensitive Ag_2CO_3 photocatalyst with universal photodegradation performances: simple synthesis, reaction mechanism and first-principles study. Appl. Catal. B. 134 (2013) 46-54.

[5]. H. Wang, Y. Bai, J. Yang, X. Lang, J. Li, L. Guo, A facile way to rejuvenate Ag_3PO_4 as a recyclable highly efficient photocatalyst. Chem. Eur. J. 18 (2012) 5524-5529.

[6]. W. C. Huang, L. M. Lyu, Y. C. Yang, M. H. Huang, Synthesis of Cu_2O nanocrystals from cubic to rhombic dodecahedral structures and their comparative

photocatalytic activity. J. Am. Chem. Soc. 134(2011) 1261-1267.

[7]. Q. Zhao, K. Wang, J. Wang, Y. Guo, A. Yoshida, A. Abudula, G. Guan, Cu_2O Nanoparticle Hyper-cross-linked polymer composites for the visible-light photocatalytic degradation of methyl orange. ACS Appl. Nano. Mater. 2 (2019) 2706-2712.

[8]. S. Gao, J. Zhang, W. Li, S. Jiao, Y. Nie, H. Fan, X. Zhang, Near room temperature and large-area synthesis of ZnO/Cu_2O heterojunction for photocatalytic properties. Chem. Phys. Lett. 692(2018) 14-18.

[9]. C. Y. Toe, Z. Zheng, H. Wu, Photocorrosion of cuprous oxide in hydrogen production: rationalising self-oxidation or self-reduction. Angew. Chem. 130(2018) 13801-13805.

[10]. J. Y. Huang, P. L. Hsieh, G. Naresh, H. Y. Tsai, M. H. Huang, Photocatalytic activity suppression of CdS nanoparticle-decorated Cu_2O octahedra and rhombic dodecahedra. J. Phys. Chem. C. 122(2018) 12944-12950.

[11]. M. Li, Y. Li, Q. Zhang, C. Qin, W. Zhao, Z. Wang, A. Inoue, Ultrafine Cu_2O/CuO nanosheet arrays integrated with NPC/BMG composite rod for photocatalytic degradation. Appl. Surf. Sci. 483(2019) 285-293.

[12]. Wu, Z. Cheung, G. Wang, J. Zhao, Z. Osterloh, F. E. Wavelength dependent photochemical charge transfer at the $Cu_2O/BiVO_4$ particle interface-evidence for tandem excitation. Chem. Commun. 54 (2018) 9023-9026.

[13]. Q. Zhao, J. Wang, Z. Li, Y. Qiao, C. Jin, Y. Guo. Preparation of Cu_2O/exfoliated graphite composites with high visible light photocatalytic performance and stability. Ceram. Int. 42(2016) 13273-13277.

[14]. K. Tu, Q. Wang, A. Lu, L. Zhang, Portable Visible-light photocatalysts constructed from Cu_2O nanoparticles and graphene oxide in cellulose matrix, J. Phys. Chem. C. 118(2014) 7202-7210.

[15]. Dong, H.; Guo, X.; Yang, C.; Ouyang, Z. Synthesis of g-C_3N_4 by different precursors under burning explosion effect and its photocatalytic degradation for

tylosin. Appl. Catal. B. 230 (2018) 65-76.

[16]. X. Wang, K. Maeda, X. Chen, K. Takanabe, K. Domen, Y. Hou, M Antonietti, Polymer semiconductors for artificial photosynthesis: hydrogen evolution by mesoporous graphitic carbon nitride with visible light. J. Am. Chem. Soc.131 (2009) 1680-1681.

[17]. J. Liu, Y. Liu, N.Y. Liu, Y.Z. Han, X. Zhang, H. Huang, Y. Lifshitz, S.T. Lee, J. Zhong, Z.H. Kang, Metal-free efficient photocatalyst for stable visible water splitting via a two-electron pathway, Science 347 (2015) 970-974.

[18]. X.D. Zhang, X. Xie, H. Wang, J.J. Zhang, B.C. Pan, Y. Xie, Enhanced photoresponsive ultrathin graphitic-phase C_3N_4 nanosheets for bioimaging J. Am. Chem. Soc. 135(2013) 18-21.

[19]. P. Niu, L. Zhang, G. Liu, H. M. Cheng, Graphene-like carbon nitride nanosheets for improved photocatalytic activities. Adv. Funct. Mater. 22 (2012) 4763-4770.

[20]. H. Shao, X. Zhao, Y. Wang, R. Mao, Y. Wang, M Qiao, Y. Zhu, Synergetic activation of peroxymonosulfate by Co_3O_4 modified g-C_3N_4 for enhanced degradation of diclofenac sodium under visible light irradiation. Appl. Catal. B 218 (2017)810-818.

[21]. Y. Hong, C. Li, B. Yin, D. Li, Z. Zhang, B. Mao, W. Fan, W. Gu, W. Shi, Promoting visible-light-induced photocatalytic degradation of tetracycline by an efficient and stable beta-Bi_2O_3@g-C_3N_4 core/shell nanocomposite. Chem. Eng. J. 338 (2018) 137-146.

[22]. K. Santosh, T. Surendar, B. Arabinda, S. Vishnu, Synthesis of a novel and stable g-C_3N_4-Ag_3PO_4 hybrid nanocomposite photocatalyst and study of the photocatalytic activity under visible light irradiation, J. Mater. Chem. A 1 (2013) 5333-5340.

[23]. X. J. Wang, W. Y. Yang, F. T. Li, Y. B. Xue, R. H. Liu, Y. J. Hao, In situ microwave-assisted synthesis of porous N-TiO_2/g-C_3N_4 heterojunctions with

enhanced visible-light photocatalytic properties, Ind. Eng. Chem. Res. 52 (2013) 17140-17150.

[24]. Y. Tian, B. Chang, J. Fu, B. Zhou, J. Liu, F. Xi, X. Dong, Graphitic carbon nitride/Cu_2O heterojunctions: Preparation, characterization, and enhanced photocatalytic activity under visible light. J. Colloid. Interf. Sci. 212 (2014) 1-6.

[25]. D. Li, J. Zan, L. Wu, S. Zuo, H. Xu, D. Xia, Heterojunction tuning and catalytic efficiency of g-C_3N_4–Cu_2O with glutamate. Ind. Eng. Chem. Res. 58 (2019) 4000-4009.

[26]. L. Liu, Y. Qi, J. Hu, W. An, S. Lin, Y. Liang, W. Cui, Stable Cu_2O@ g-C_3N_4 core@ shell nanostructures: Efficient visible-light photocatalytic hydrogen evolution. Mater. Lett. 158 (2015) 278-281.

[27]. J. Wang, Z. Yang, W. Yao, X. Gao, D. Tao, Defects modified in the exfoliation of g-C_3N_4 nanosheets via a self-assembly process for improved hydrogen evolution performance. Appl. Catal. B. 238(2018) 629-637.

[28]. S. Meng, D. Li, M. Sun, Sonochemical synthesis, characterization and photocatalytic properties of a novel cube-shaped $CaSn(OH)_6$. Catal. Commun. 12(2011) 972-975.

[29]. L. Ye, J. Liu, Z. Jiang, Facets coupling of BiOBr-g-C_3N_4 composite photocatalyst for enhanced visible-light-driven photocatalytic activity. Appl. Catal. B. 142(2013) 1-7.

[30]. J. Xu, L. Zhang, R. Shi, Y. Zhu, Chemical exfoliation of graphitic carbon nitride for efficient heterogeneous photocatalysis. J. Mater. Chem. A 1 (2013) 14766-14772.

[31]. J. Y. Huang, P. L. Hsieh, G. Naresh, H. Y. Tsai, M. H. Huang, Photocatalytic Activity Suppression of CdS Nanoparticle-Decorated Cu_2O Octahedra and Rhombic Dodecahedra. The J. Phys. Chem. C. 122(2018) 12944-12950.

[32]. J. Wang, Z. Yang, X. Gao, W. Yao, W. Wei, X. Chen, Y. Zhu, Core-shell g-C_3N_4@ ZnO composites as photoanodes with double synergistic effects for

enhanced visible-light photoelectrocatalytic activities. Appl. Catal. B. 217 (2017) 169-180.

[33]. Y. Su, D. Ao, H. Liu, MOF-derived yolk-shell CdS microcubes with enhanced visible-light photocatalytic activity and stability for hydrogen evolution. J, Mater. Chem. A. 5(2017) 8680-8689.

[34]. W. Zou, L. Zhang, L. Liu, Engineering the Cu_2O-reduced graphene oxide interface to enhance photocatalytic degradation of organic pollutants under visible light. Appl. Catal. B. 181(2016) 495-5.

CHAPTER 5

Conclusions and Prospects

5.1 Conclusions

Cu_2O based photocatalysts is considered as one of the prospective material in the photocatalytic degradation of organic pollutants, because of its low price, non -toxicity and no secondary pollution. To improve the performance of Cu_2O based photocatalysts under visible light, the key is to effectively suppress the recombination of photo-generated electrons and holes in the catalyst. In this study, a series of Cu_2O based photocatalysts with excellent performance were developed by loading it on the conductive carriers or coupling it with other semiconductors to form heterostructured composites. In addition, the related photocatalytic mechanism was also discussed. The following results were obtained:

- The visible-light-induced KAPs-B/Cu_2O photocatalysts, in which KAPs-B with high specific surface area dispersed over the rhombic dodecahedral Cu_2O particles, were successfully synthesized. The average particle size of Cu_2O was about 200-250nm. The obtained KAPs-B/Cu_2O photocatalysts showed an obviously improved photocatalytic activity and stability under visible light for the MO degradation when compared with the bare Cu_2O. The KAPs-B/Cu_2O photocatalyst with 7.0% KAPs-B exhibited the highest photocatalytic performance, by which approximately 92% of MO was decomposed within 60 minutes. The active species trapping experiments indicated that O_2^{-}• and h^+ could be the major active species in the KAPs-B/Cu_2O photocatalyst system.
- In order to build the Z-scheme heterojunction to further improve its performance, the UiO-66-NH_2 which have high surface area, good chemical durability and also adsorption ability for visible light was used. By using a facile impregnation way, the UiO-66-NH_2/Cu_2O composite catalysts were successfully prepared and used

for the MO photocatalytic degradation process. The as-prepared composites presented higher photocatalytic performances than the Cu_2O. Specially, the UiO-66-NH_2/Cu_2O composite with 20% of UiO-66-NH_2 exhibited the excellent photocatalytic activity, 98.6% of MO was decomposed within 50 minutes. The improved photocatalytic performance could be ascribed to the efficient separation of photoinduced e^--h^+ pairs within the Z-scheme heterojunction and the synergistic effect between Cu_2O and UiO-66-NH_2. The photo-generated h^+ and $\bullet O_2^-$ were the crucial species during this process.

- In practical applications, the dispersity of Cu_2O based photocatalysts in the organic pollution is also important. The cubic Cu_2O particles have smaller particle size, which is beneficial to disperse in water. The g-C_3N_4 nanosheets not only have larger specific surface area, but also show excellent electrical conductivity and good water dispersibility. Thus, a g-C_3N_4 nanosheets /Cu_2O composite were successfully prepared in the following part. Especially, the specific surface area of g-C_3N_4 used in our study was increased by using the expansion method. Tetracycline (TC) antibiotics was used as the degradation target. As a result, under visible light irradiation, approximately 92.1% of TC was decomposed in 100 min, and 83.3% of TOC was removed after the reaction for 120 min by using this photocatalyst. Also, the catalytic activity maintained at approximately 88.1% even after five cycles, revealing the excellent stability of g-C_3N_4 nanosheets /Cu_2O composite photocatalyst. Furthermore, the results showed that the h^+ and $O_2^-\bullet$ were the major active species in the photocatalytic degradation of TC over g-C_3N_4 nanosheets/Cu_2O composite photocatalysts. The excellent photocatalytic performance should be ascribed to its higher surface area, more effective separation ability for the photogenerated e^--h^+ pairs and the faster interfacial charge transfer rate with a p-n type heterostructure.

- The above Cu_2O-based photocatalysts prepared in this work all showed higher catalytic activity and stability than the previously reported visible-light photocatalysts in recent years, which can be seen in Table 5.1 .

Table 5.1 Comparison of the degradation efficiency and Stability of various reported visible photocatalysts with the present work

Catalysts	Band gap (eV)	Model organic pollutant and light power	Experimental condition	Degradation efficiency	Stability (Run Times)	Ref
Ag_2S/ $BiVO_4$	2.30	TC 500W	20mg、50 mL、20 mg/L、150 min	90.2%	8	[1]
SDBS–Bi_2WO_6	2.45	TC 500W	50mg、50 mL、50 mg/L、90 min	90.39%	5	[2]
$FeWO_4$/CNN	2.1	TC 500W	50mg、50 mL、20 mg/L、90 min	88%	4	[3]
g-C_3N_4 /Cu_2O	**2.0**	**TC 500W**	**100mg、90 mL、30 mg/L、100 min**	**92.1%**	**5**	**This work**
Ag_3PO_4/Ti_3C_2	2.22	MO 300W	20mg、50 mL、20 mg/L、50 min	92.2%	8	[4]
Ti_3C_2-OH /ln_2S_3/CdS	1.6	MO 300W	10mg、50 mL、20 mg/L、30 min	96%	3	[5]
a-Fe_2O_3/Cu_2O	1.75	MO 300W	30mg、30 mL、10 mg/L、60 min	95%	5	[6]
Cu_2O-rGO	2.15	MO 500W	40 mg、20 mL、8 mg/L、120 min	98%	3	[7]
KAPs-B/Cu_2O	**2.17**	**MO 500W**	**30mg、90 mL、30 mg/L、60 min**	**92%**	**10**	**This work**
UiO-66-NH_2/Cu_2O	**1.96**	**MO 500W**	**30mg、90 mL、30 mg/L、60 min**	**98.6%**	**5**	**This work**

5.2 Prospects

In this study, the photocatalytic performance of Cu_2O was improved by loading it on the KAPs-B carriers, coupling it with UiO-66-NH_2 semiconductors to form the Z-scheme heterojunction and with g-C_3N_4 nanosheets to form the p-n type heterostructure. Despite progress in the catalyst construction and photocatalytic mechanism for the

Cu_2O based photocatalysts, the following works which should be done in the future are suggested in the following:

- The electronic structure and interface properties of Cu_2O based photocatalysts should be studied theoretically and experimentally in order to better understand the structure-related properties and further develop interface-dependent applications.
- Selective doping and the formation of heterogeneous structures on specific surfaces of Cu_2O is important for improving electron conductivity and charge separation, which could lead to new directions for designing new structures required for applications.
- Reasonable design and selection of the composition and thickness on the Cu_2O surface can effectively improve the structural stability of the composite. In addition, new CuO or Cu should be formed *in situ* on the surface structure of Cu_2O under oxidation or reduction conditions to optimize the energy conversion of Cu_2O based photocatalysts.
- The synthesis of low cost, uniform size, good shape, good dispersion and high purity nanoparticles of Cu_2O in composite systems is still an obstacle. Therefore, new synthetic routes should be systematically explored to prepare the required Cu_2O nanoparticles.

References

[1] Z. Wei.T. Xinyue. W. Xiaomeng. D. Benlin. Z. Lili. X. Jiming. Z. Fengxia, Novel pn heterojunction photocatalyst fabricated by flower-like $BiVO_4$ and Ag_2S nanoparticles: Simple synthesis and excellent photocatalytic performance. Chem Eng J, 2019, 361,1173-1181.

[2] S. Zhong. C. Lv. M. Shen. L. Wu. C. Li, Synthesis of Bi_2WO_6 photocatalyst modified by SDBS and photocatalytic performance under visible light. J. Mater Sci -Mater EL, 2019, 30, 4152-4163

[3] R. Dadigala. R. Bandi. B. R. Gangapuram. V. Guttena, Construction of in situ self-assembled $FeWO_4$/g-C_3N_4 nanosheet heterostructured Z-scheme photocatalysts for enhanced photocatalytic degradation of rhodamine B and tetracycline. Nano Adv, 2019, 1, 322-333.

[4] T. Cai. L. Wang. Y. Liu. S. Zhang. W. Dong. H. Chen. S. Luo, Ag_3PO_4/Ti_3C_2 MXene interface materials as a Schottky catalyst with enhanced photocatalytic activities and anti-photocorrosion performance. Appl. Catal. B, 2018, 239, 545-554

[5] H. Fang. Y. Pan. M. Yin. L. Xu. Y. Zhu. C. Pan. Facile synthesis of ternary Ti_3C_2-OH/ln_2S_3/CdS composite with efficient adsorption and photocatalytic performance towards organic dyes. J. Solid State Chem, 2019,*280*, 120981.

[6] S. K. Lakhera, A. Watts, H. Y. Hafeez, B. Neppolian, Interparticle double charge transfer mechanism of heterojunction α-Fe_2O_3/Cu_2O mixed oxide catalysts and its visible light photocatalytic activity, Catal. Today, 2018, 300: 58-70.

[7] W. Zou, L. Zhang, L. Liu, X. Wang, J. Sun, S. Wu, L. Dong, Engineering the Cu_2O-reduced graphene oxide interface to enhance photocatalytic degradation of organic pollutants under visible light, Appl. Catal. B, 2016, 181, 495-503

List of publications and presentations

Publications

1) **Qiang Zhao,** Kewei Wang, Junli Wang, Yong Guo, Akihiro Yoshida, Abuliti Abudula, Guoqing Guan Cu_2O Nanoparticle Hyper-cross-linked polymer composites for the visible-light photocatalytic degradation of methyl orange, ACS ACS Applied Nano Materials, 10 April, 2019, Volume 2, pages:2706-2712.

2) **Qiang Zhao,** Junli Wang, Zuopeng Li, Yong Guo, Jing Wang, Bing Tang, Abuliti Abudula,Guoqing Guan Heterostructured graphitic-carbon-nitride-nanosheets/copper(I) oxide composite as an enhanced visible light photocatalyst for decomposition of tetracycline antibiotics. Separation and Purification Technology, 12 June, 2020, Volume 250, pages: 117238-117245.

3) **Qiang Zhao**, Junli Wang, Zuopeng Li, Yong Guo， Guoqing Guan. UiO-66-NH_2/Cu_2O composite as an enhanced visible light photocatalyst fordeco mposition of organic pollutants. Journal of Photochemistry & Photobiology A: Chemistry, 22 May, 2020, Volume 399, pages: 112625 -112632.

4) Jing Wang, Peifen Wang, Akihiro Yoshida, **Qiang Zhao,** Shasha Li, Xiaogang Hao, Abuliti Abudula, Guangwen Xu, Guoqing Guan, Mn-Co oxide decorated on Cu nanowires as efficient catalysts for catalytic oxidation of toluene. Carbon Resources Conversion, 13 February, 2020, Volume 3, pages:36-45.

5) Jing Wang, Peifen Wang, **Qiang Zhao,** Tao Yu, Xiao Du, Xiaogang Hao , Abuliti Abudula, Guoqing Guan, Highly dispersed Ag nanoparticles embedded on the surface of CeO_2/CF nanowires derived from three-dimensional structured Cu foam for toluene catalytic oxidation. Molecular Catalysis, 7 March, 2020, Volume 486, pages:110879.

Conference presentation papers

1) **Qiang Zhao**, Junli Wang, Zuopeng Li, Yong Guo, Akihiro Yoshida, Abuliti Abudula, Guoqing Guan, "Enhanced visible light photocatalytic performance and stability of Cu_2O/ UiO-66-NH_2 composites". The 19th National Congress on Catalysis of China, Chongqing, China, Oct. 13-17, 2019.

2) **Qiang Zhao**, KeweiWang, Junli Wang, Akihiro Yoshida, Abuliti Abudula, Guoqing Guan Enhancement of visible light photocatalytic performance of Cu_2O by hypercrosslinked polymers doping. The 10th International Conference on Environmental Catalysis, Tianjin, China, Sep. 22-26, 2018

3) 安 小偉, 郝 晓琼, 謝 正坤, **趙 強**, 吉田 曉弘, 阿布 里提, **官** 国清, "Effect of F doping on the In-based catalysts for the promoting of electrochemical reduction of CO_2 to formic acid," 化学工学会第51回秋季大会、岩手大学、2020年9月24-26日(On line).

4) Jing Wang, Peifen Wang, **Qiang Zhao**, Jin Shi, Akihiro Yoshida, Tao Yu, Abuliti Abudula, and Guoqing Guan, "Cubic structured MnOx incorporated by Co-Fe nanowires for the low temperature catalytic oxidation of toluene," 令和2年度化学系学協会東北大会, 八戸, 2020年9月26-27日（On-line）.

5) 王 ジン, 王 佩芬, **趙 強**, 張 夢娟, 吉田 曉弘, 阿布 里提, **官** 国清, "**S**ynthesis of MnO_x dominated catalysts with cubic structure and its application in the catalytic combustion of volatile organic compounds," 化学工学会第51回秋季大会、岩手大学、2020年9月24-26日(On line).

6) Peifen Wang, Jing Wang, **Qiang Zhao**, Tao Yu, Akihiro Yoshida, Abuliti Abudula, Guoqing Guan, "Low-temperature catalytic combustion of toluene over Mn-Co oxides prepared by one-step agar-gel method," ４校交流会in一関工業高等専門学校, 2019年10月29日